Dissertation

Submitted to the
Combined Faculty of Natural Sciences and Mathematics
of the Ruperto Carola University Heidelberg, Germany
for the degree of
Doctor of Natural Sciences

Presented by
Rebekka Renate Weber (M. Sc.)
born in Mannheim, Germany
Oral examination: 20.01.2020

Regulation of CCR5 expression and immunosuppressive phenotype of MDSC in melanoma

Referees:

apl. Prof. Dr. Viktor Umansky

Prof. Dr. Adelheid Cerwenka

Summary

MDSC play a major role in immunosuppression and tumor progression in melanoma. Their recruitment to the tumor is mediated by chemokine receptors and their ligands, in particular by chemokine receptor CCR5. The aims of this thesis were to study the mechanisms of CCR5 upregulation on murine MDSC in melanoma and of the previously observed stronger immunosuppressive phenotype of $CCR5^+$ MDSC as compared to their $CCR5^-$ counterparts. IL-6, GM-CSF and IFN-γ upregulated *Ccr5* mRNA expression in murine myeloid cells, whereas the CCR5 ligands, tumor-derived extracellular vesicles, toll-like receptor ligands and IL-1β failed to affect *Ccr5* expression. IL-6 and GM-CSF were able to induce CCR5 surface expression during MDSC *in vitro* differentiation for four days by a STAT3 dependent mechanism. Importantly, we found four putative STAT3 binding sites in the murine *Ccr5* promoters. In addition, the STAT3 inhibitor Stattic abrogated *Ccr5* upregulation induced by IL-6 and GM-CSF. In the *RET* transgenic mouse model of malignant melanoma, IL-6 levels in the tumors correlated with the frequency of tumor-infiltrating $CCR5^+$ MDSC. $CCR5^+$ MDSC showed increased phosphorylated STAT3 levels. In addition to the upregulation of CCR5, IL-6 was responsible for stimulation of Arginase (Arg)1 activity and ROS production upon MDSC *in vitro* differentiation, inducing increased capacity of MDSC to suppress $CD8^+$ T cell proliferation in a co-culture assay. The upregulation of *Arg1* by IL-6 was also STAT3 dependent. In contrast to IL-6, CCR5 ligands failed to induce increased immunosuppressive capacity of MDSC. Altogether, IL-6 upregulated CCR5 and immunosuppressive capacity of MDSC *in vitro* in parallel, which could explain the elevated expression of immunosuppressive factors Arg1 and ROS on $CCR5^+$ MDSC and their increased ability to suppress $CD8^+$ T cell proliferation. However, we found only a slight increase in tumor-infiltrating MDSC and no increase in CCR5 expression or immunosuppressive factors detectable upon s.c. injection of IL-6 overexpressing Ret cells into wild type mice. In the same model, the tumor growth and mouse survival remained unaltered. Finally, we blocked IL-6 *in vivo* in *RET* transgenic melanoma-bearing mice by an anti-IL-6 antibody to decrease $CCR5^+$ MDSC recruitment to the tumor and to inhibit IL-6-induced increase in MDSC immunosuppressive capacity, thereby neutralizing the immunosuppression in the tumor and preventing melanoma progression. Unexpectedly, the anti-IL-6 therapy resulted in accelerated tumor progression and earlier death of mice, which was most likely due to the negative effect of anti-IL-6 on T cell activation which was reflected by decreased $CD4^+$ conventional T cells in the tumor. Altogether, we found IL-6 to upregulate CCR5 and immunosuppressive capacity of MDSC *in vitro* making this cytokine an interesting target for immunotherapy. However, further research should be performed to understand the delicate balance of IL-6 signaling in melanoma immunity *in vivo* and the challenges of IL-6 blocking immunotherapy for melanoma treatment.

Zusammenfassung

Myeloide suppressorische Zellen (MDSC) vermitteln Immunsuppression, die zum Tumorfortschreiten beim Melanom beiträgt. Diese Zellen werden durch die Aktivierung von Chemokinrezeptoren, darunter CCR5, zum Tumor rekrutiert. Ziel dieser Arbeit war es, die Mechanismen der CCR5-Hochregulation und den stärkeren immunsuppressiven Phänotyp von $CCR5^+$ MDSC im murinen Melanom zu untersuchen. IL-6, GM-CSF und IFN-γ konnten die *Ccr5*-mRNA-Expression in murinen myeloiden Zellen hochregulieren, wohingegen CCR5-Liganden, extrazelluläre Vesikel des Tumors, Toll-like-Rezeptor-Liganden und IL-1β keine Wirkung auf die *Ccr5*-Expression zeigten. IL-6 und GM-CSF haben die CCR5-Oberflächenexpression, während der MDSC *in vitro* Differenzierung für vier Tage, durch einen STAT3-abhängigen Mechanismus induziert. Wir fanden vier mutmaßliche STAT3-Bindestellen in den murinen *Ccr5*-Promotoren, und der STAT3-Inhibitor Stattic verhinderte die IL-6 und GM-CSF induzierte *Ccr5*-Hochregulation. Im *RET*-transgenen Melanom-Mausmodell korrelierte die IL-6 Konzentration mit der Frequenz der Tumor-infiltrierenden $CCR5^+$ MDSC, die außerdem mehr phosphoryliertes STAT3 zeigten. Zusätzlich zur Hochregulation von CCR5 konnte IL-6 die Arginase (Arg)1-Aktivität und die Produktion von reaktiven Sauerstoffspezies (ROS) während der MDSC *in vitro* Differenzierung induzieren, wodurch die MDSC in der Lage waren, die Proliferation von $CD8^+$ T-Zellen stärker zu unterdrücken. Die Hochregulation von *Arg1* durch IL-6 war ebenfalls STAT3-abhängig. Im Gegensatz zu IL-6 konnten die CCR5-Liganden keine erhöhte Immunsuppression bei MDSC induzieren. IL-6 konnte sowohl CCR5 als auch die immunsuppressive Kapazität von MDSC *in vitro* parallel stimulieren, was die erhöhte Expression der immunsuppressiven Faktoren Arg1 und ROS auf $CCR5^+$ MDSC und deren erhöhte Fähigkeit zur Unterdrückung der $CD8^+$ T-Zell-Proliferation erklären kann. Wir fanden jedoch nur einen geringen Anstieg der Tumor-infiltrierenden MDSC und keinen Anstieg der CCR5-Expression oder der immunsuppressiven Faktoren auf MDSC in IL-6 überexprimierenden Tumoren. Im gleichen Modell blieben das Tumorwachstum und das Mausüberleben unter IL-6 Überexpression unverändert. Schließlich haben wir IL-6 *in vivo* in Melanom-tragenden *RET*-transgenen Mäusen mit einem anti-IL-6-Antikörper blockiert. Die anti-IL-6-Therapie führte nicht zu einer Unterdrückung der immunsuppressiven MDSC im Tumor, sondern zu einem beschleunigten Tumorwachstum und einem früheren Tod der Mäuse, was auf den negativen Effekt von anti-IL-6 auf die T-Zell-Aktivierung zurückzuführen war. Zusammenfassend konnte IL-6 sowohl CCR5 als auch die immunsuppressive Kapazität von MDSC *in vitro* hochregulieren, was dieses Zytokin zu einem interessanten Angriffspunkt für Immuntherapien macht. Weitere Nachforschungen müssen jedoch dazu beitragen, das empfindliche Gleichgewicht der IL-6-Signalübertragung im Melanom *in vivo* und die Herausforderungen der IL-6-blockierenden Immuntherapie bei der Melanom Behandlung zu verstehen.

Table of contents

List of abbreviations

AMP	adenosine monophosphate
APC	antigen-presenting cell
APS	ammonium persulfate
Arg1	arginase 1
ATP	adenosine triphosphate
ATRA	all-trans retinoic acid
B-Raf	B-rapidly accelerated fibrosarcoma
BCG	Bacillus Calmette-Guerin
Bcl-xL	B cell lymphoma extra large
BF	band forms
CCL	CC chemokine ligand
CCR	CC chemokine receptor
CD	cluster of differentiation
CFSE	carboxyfluorescein succinimidyl ester
CMP	common myeloid progenitors
CTLA-4	cytotoxic T-lymphocyte-associated protein 4
CXCL	CXC chemokine ligand
CXCR	CXC chemokine receptor
DAMP	damage-associated molecular pattern
DAPI	4',6-diamidine-2'-phenylindole dihydrochloride
DC	dendritic cell
DKFZ	German cancer research center
DMSO	dimethyl sulfoxide
DNA	deoxyribonucleic acid
DPBS	Dulbecco's phosphate-buffered saline
E-NTPDase1	ectonucleoside triphosphate diphosphohydrolase 1, CD39
EC	endothelial cell
Ecto5’NTase	ecto-5’-nucleotidase, CD73
EDTA	ethylendiamintetraacetat
eMDSC	early stage MDSC
ERK	extracellular signal-regulated kinase

EV	empty vector
EV	extracellular vesicles
FasL	Fas ligand
FATP2	fatty acid transport protein 2
FBS	fetal bovine serum
FMO	fluorescence minus one
FoxP3	forkhead box P3
GM-CSF	granulocyte-macrophage colony-stimulating factor
GMP	granulocyte-macrophage progenitors
gp	glycoprotein
GTPase	guanosine triphosphatase
HEPES	2-(4-(2-Hydroxyethyl)-1-piperazinyl)-ethansulfonsäure
HIF	hypoxia-inducible factor
HPC	hematopoietic progenitor cells
i.d.	intradermal
IDO	indoleamine 2,3-dioxygenase
IFN	interferon
IL	interleukin
infl DC	inflammatory dendritic cells
iNOS	inducible nitric oxide synthase, NOS2
i.p	intraperitoneal
JAK	Janus kinase
LOX1	lectin-type oxidized low-density lipoprotein receptor 1
LPS	lipopolysaccharide
M-MDSC	monocytic-MDSC
MAPK	mitogen-activated protein kinase
MB	myeloblasts
MC	myelocytes
MCA	methylchloranthrene
MDP	dendritic cell precursors
MDSC	myeloid-derived suppressor cells
MEK	MAPK kinase
MHC	major histocompatibility complex

MM	metamyelocytes
MMP	matrix metalloproteinase
MyD88	myeloid differentiation primary response 88
N-Ras	neuroblastoma RAS viral oncogene homolog
NADPH	nicotinamide adenosine dinucleotide phosphate
NF-κB	nuclear factor 'kappa-light-chain-enhancer' of activated B-cells
NK cell	natural killer cell
NO	nitric oxide
NOS2	nitric oxide synthase 2, iNOS
NOX	NADPH oxidases
NSCLC	non-small cell lung cancer
OE	overexpression, overexpressing
P/S	penicillin/streptomycin
PBS	phosphate-buffered saline
PD-1	programmed cell death protein 1
PD-L1	programmed death-ligand 1
PFS	progression-free survival
PGE2	prostaglandin E2
PMN-MDSC	polymorphonuclear-MDSC
PRR	pattern recognition receptor
RAG	recombination activating gene
RNS	reactive nitrogen species
ROS	reactive oxygen species
s.c.	subcutaneous
SDS	sodium dodecyl sulfate
SOCS	suppressor of cytokine signaling
STAT	signal transducer and activator of transcription
T-VEC	talimogen laherparevec
TACE	tumor necrosis factor-α-converting enzyme
TAM	tumor-associated macrophages
TBS	tris-buffered saline
TCR	T cell receptor
TEMED	N,N,N',N'-tetramethyl ethylenediamine

TGF	transforming growth factor
TIL	tumor-infiltrating leukocytes
TLR	Toll-like receptor
TME	tumor microenvironment
TRAIL	tumor necrosis factor-related apoptosis-inducing ligand
Treg	regulatory T cells
Tris	Tris(hydroxymethyl)-aminomethan
TRP	tyrosinase-related protein
UV	ultraviolet
VEGF	vascular endothelial growth factor

List of tables

List of figures

List of own publications during the thesis work

Blattner C, Fleming V, **Weber R**, Himmelhan B, Altevogt P, Gebhardt C, Schulze TJ, Razon H, Hawila E, Wildbaum G, et al. CCR5 + Myeloid-Derived Suppressor Cells Are Enriched and Activated in Melanoma Lesions. *Cancer Res* (2018) 78:157–167. doi:10.1158/0008-5472.CAN-17-0348

Fleming V, Hu X, **Weber R**, Nagibin V, Groth C, Altevogt P, Utikal J, Umansky V. Targeting Myeloid-Derived Suppressor Cells to Bypass Tumor-Induced Immunosuppression. *Front Immunol* (2018) 9:398. doi:10.3389/fimmu.2018.00398

Weber R, Fleming V, Hu X, Nagibin V, Groth C, Altevogt P, Utikal J, Umansky V. Myeloid-Derived Suppressor Cells Hinder the Anti-Cancer Activity of Immune Checkpoint Inhibitors. *Front Immunol* (2018) 9:1310. doi:10.3389/fimmu.2018.01310

Groth C, Hu X, **Weber R**, Fleming V, Altevogt P, Utikal J, Umansky V. Immunosuppression mediated by myeloid-derived suppressor cells (MDSCs) during tumour progression. *Br J Cancer* (2019) 120:16–25. doi:10.1038/s41416-018-0333-1

Fleming V, Hu X, Weller C, **Weber R**, Groth C, Riester Z, Hüser L, Sun Q, Nagibin V, Kirschning C, et al. Melanoma Extracellular Vesicles Generate Immunosuppressive Myeloid Cells by Upregulating PD-L1 via TLR4 Signaling. *Cancer Res* (2019) 79:4715–4728. doi:10.1158/0008-5472.CAN-19-0053

Weber R, Umansky V. Fighting infant infections with myeloid-derived suppressor cells. *J Clin Invest* (2019) 129:4080–4082. doi:10.1172/JCI131649

1 Introduction

1.1 The immune system and cancer

In 1909, Paul Ehrlich was the first to propose the idea that the immune system is controlling the development of cancer by recognizing and eliminating malignantly transformed cells (Ehrlich, 1909). In the 1950s, the first experiments with transplantable tumors in mice were performed that could confirm an involvement of the immune system in the recognition of tumor cells (Green, 1954). Finally, Mac Farlane Burnet proposed the concept of immunological surveillance in cancer, where one major function of the immune system was suggested to be the elimination of cells that show foreign patterns due to somatic mutations (Burnet, 1970). Recently, the concept has changed from cancer immune surveillance to cancer immunoediting (Dunn *et al.*, 2002). Moreover, “tumor-promoting inflammation” and “avoiding immune destruction” were added to the hallmarks of cancer (Hanahan and Weinberg, 2011).

While the concept of cancer immune surveillance was only describing the protective actions of the immune system in the very early steps of cancer development, the new concept of cancer immunoediting suggests a more detailed view on the complex interplay between the tumor and the immune system from both sides (Dunn *et al.*, 2002). The development of the tumor can activate the immune system and lead to a protective immune response; however, the activation of the immune system can lead to a shift in the immunogenicity of the cancer cells by selecting for non-immunogenic cells, thereby promoting tumor development. Furthermore, the chronic inflammation in the tumor can in turn shift the immune system towards a more immunosuppressive state that finally leads to tumor escape from the immune response. This concept of cancer immunoediting comprises three main steps: elimination, equilibrium and escape (Dunn *et al.*, 2004). The concept of cancer immunoediting was visualized by Robert Schreiber (Figure 1).

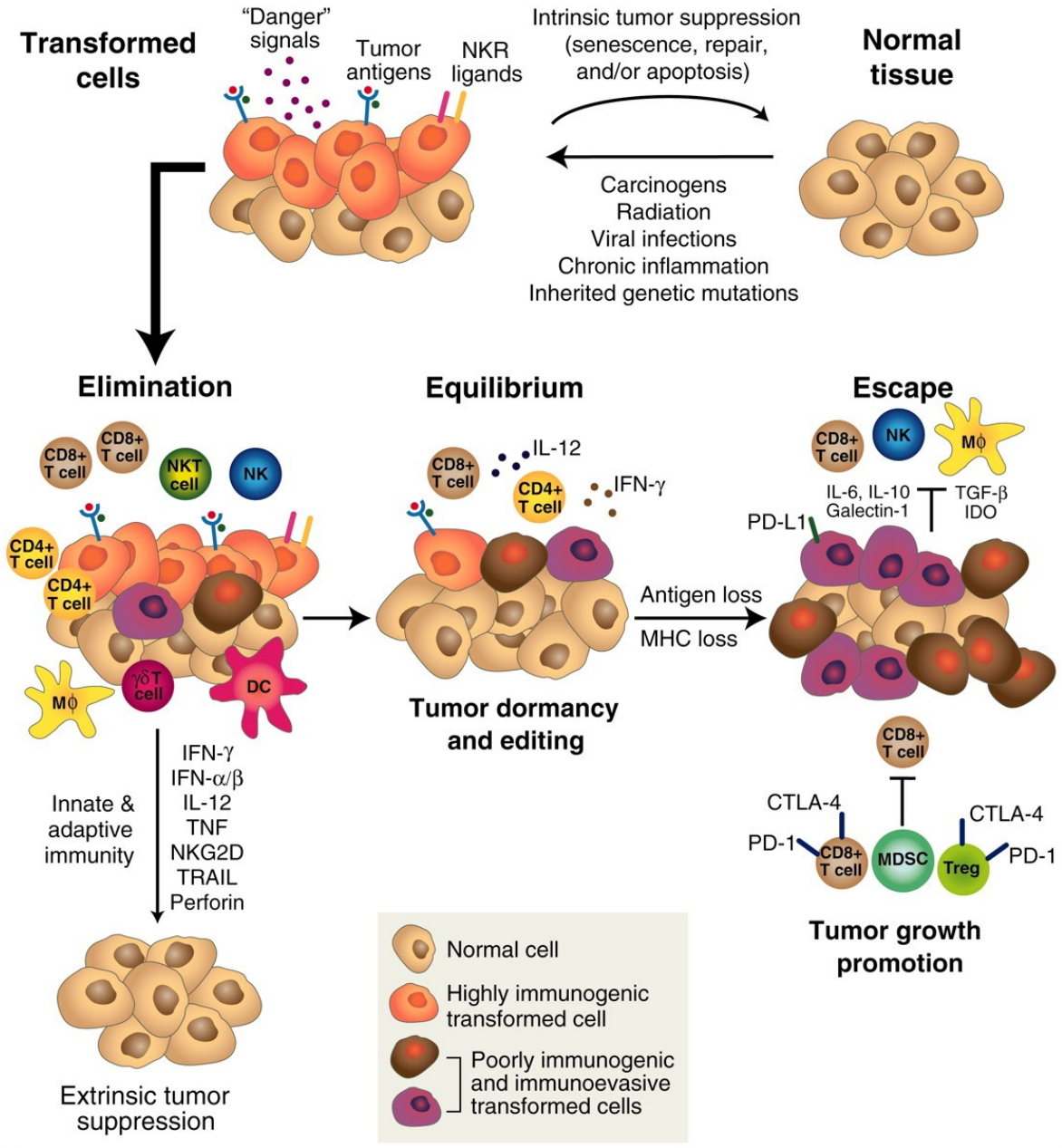

Figure 1. The phases of cancer immunoediting.
Upon failure of intrinsic tumor suppressor mechanisms normal cells can transform and develop into tumor cells. The transformed cells can be recognized by the immune system due to the expression of tumor antigens and the production of cytokines that occurs during tissue remodeling. During the elimination phase innate and adaptive immune cells are recruited and activated to kill the tumor cells. If not all tumor cells are killed by the immune system, the remaining malignant cells can change during the equilibrium phase to be able to finally escape from the immune system, grow and become a clinically detectable tumor. The escape from the immune system can be mediated by antigen and major histocompatibility complex (MHC) expression loss and the generation of an immunosuppressive tumor microenvironment (TME), where immunosuppressive immune cells like regulatory T cells (Treg) and myeloid-derived suppressor cells (MDSC) play a major role. Figure taken from (Schreiber *et al.*, 2011).

1.1.1 Cancer immune surveillance and elimination

Already during the 20th century, a lot of evidence was collected that immune surveillance in tumors does exist, and in the immunoediting concept, this is described as the elimination phase. The cytokine interferon-γ (IFN-γ) was shown to play an important role in the protective immune response against tumors as the blockade of IFN-γ resulted in a decreased rejection of transplanted tumors in mice (Dighe *et al.*, 1994). Furthermore, mice lacking parts of the IFN-γ signaling pathway or IFN-γ itself showed increased development of chemically-induced tumors by methylcholanthrene (MCA) (Kaplan *et al.*, 1998; Street *et al.*, 2001) and an increase in the incidence of spontaneous lung adenocarcinoma (Street *et al.*, 2002). IFN-γ was suggested to have an influence on both tumor and host cells. Tumor cells lacking the IFN-γ receptor were shown to grow more aggressively, were not rejected and failed to induce immunity (Dighe *et al.*, 1993, 1994). It was proposed that IFN-γ could induce an upregulation of major histocompatibility complex (MHC) class I on tumor cells, thereby increasing immunogenicity, and it could have an anti-proliferative and pro-apoptotic impact on tumor cells (Dunn *et al.*, 2004). Moreover, IFN-γ has important effects on host immune cells by polarizing T cells, and signal transducer and activator of transcription (STAT)1 knockout mice lacking this major transcription factor downstream of IFN-γ in host cells failed to reject even highly immunogenic tumors (Fallarino and Gajewski, 1999).

The importance of different immune cell subsets was also shown by various studies. The protein perforin is a component of the cytolytic granules of T and natural killer (NK) cells and is indispensable for lymphocyte-mediated killing of target cells (Russell and Ley, 2002). Interestingly, perforin knockout mice are more susceptible to MCA-induced as well as spontaneous carcinogenesis (Street *et al.*, 2001, 2002). Moreover, recombination activating gene (RAG)2 knockout mice who cannot rearrange lymphocyte antigen receptors and are, therefore, deficient for T, B and NK cells (Shinkai *et al.*, 1992) also developed MCA-induced and spontaneous tumors with increased frequency and progression speed (Shankaran *et al.*, 2001; Smyth *et al.*, 2001). αβ and γδ T cells play an important role in tumor immune surveillance supported by the observation that T cell receptor (TCR) β knockout and TCR δ knockout mice showed an increased development of MCA-induced tumors (Girardi *et al.*, 2001). The same is true for mice upon blockade of NK and NKT cells through injection of NK1.1 murine antibody (Smyth *et al.*, 2001) as well as blockade of tumor necrosis factor-related apoptosis-inducing ligand (TRAIL), which is important for tumor cell killing by myeloid and NK cells (Takeda *et al.*, 2002). These findings suggest that innate and adaptive immune cells play a major role in the control of cancer.

To show that the immune system is also an important player in human cancer, various studies with cancer patients have been conducted. For example, transplant recipients that are under immunosuppressive medication were observed to display an increased risk of malignancies, including malignant melanoma (Sheil, 1986; Penn, 1996). Moreover, specific antibodies to tumor antigens (Carey *et al.*, 1976; Ueda *et al.*, 1979) and tumor specific cluster of differentiation (CD)8^+ and $CD4^+$ T cells (Knuth *et al.*, 1984; Wang and Rosenberg, 1999) were shown in cancer patients. Furthermore, a strong correlation between the abundance of tumor-infiltrating leukocytes (TIL) and patient survival was observed for different cancer types, including malignant melanoma (Clark *et al.*, 1989; Clemente *et al.*, 1996; Mihm *et al.*, 1996).

Altogether, these studies have shown the involvement of the immune system in cancer, and that there is immune surveillance and protective immunity described as elimination phase (Dunn *et al.*, 2002, 2004). First, innate immune cells like NK, NKT and γδ T cells are recruited to the tumor microenvironment (TME) and activated by inflammatory cytokines secreted in the tumor due to the remodeling of the tissue. The activated innate immune cells can then produce cytokines like interleukin (IL)-12 and IFN-γ, which further promote the immune response. Destruction of tumor cells by IFN-γ and NK cells leads to the release of tumor antigens that can be presented by dendritic cells (DC) and macrophages as well as damage-associated molecular pattern (DAMP) factors that further activate innate immune cells expressing pattern recognition receptors (PRR). Then, antigen-presenting cells (APC) activate naïve $CD4^+$ and $CD8^+$ T cells in the tumor draining lymph nodes inducing the adaptive immune response. The mature T cells home to the tumor site where $CD8^+$ T cells selectively kill the malignant cells supported by IL-2 production of $CD4^+$ T cells and IFN-γ secretion.

However, also immunocompetent individuals can develop cancer, suggesting mechanisms of tumors to avoid the protective immune response.

1.1.2 Tumor immune escape

If not all tumor cells have been eradicated by the immune system, it could come to the equilibrium phase (Dunn *et al.*, 2004). Tumor cells that are resistant to the immune system are present and can outgrow, which leads to the clinical detectability of the tumor. The equilibrium phase can last up to 20 years in humans (Loeb *et al.*, 2003). The outgrowth of the tumor is called the immune escape phase in the concept of cancer immunoediting (Dunn *et al.*, 2004). The tumor cells have developed various resistance mechanisms to escape from the immune system in this phase.

It is believed that the selective pressure of the immune system in combination with the high genomic instability of the tumor cells leads to the selection of tumor cells with reduced immu-

nogenicity and increased escape mechanisms which makes the tumor progression possible (Dunn *et al.*, 2004). This is supported by the fact that tumors grown in mice that have no intact immune system get rejected when transplanted into immunocompetent mice because these tumors are highly immunogenic (Svane *et al.*, 1996; Engel *et al.*, 1997). Furthermore, tumor cells from immunocompetent mice are less sensitive to TRAIL-mediated killing compared to tumor cells from mice in which the TRAIL-pathway was inhibited during tumor development (Takeda *et al.*, 2002).

To date, several escape mechanisms of tumor cells have been described. Tumor cells, showing lower antigen expression and, therefore, less intrinsic immunogenicity are selected during the escape phase (Dunn *et al.*, 2004). Furthermore, tumor cells can loose parts of the antigen presenting pathway (Campoli and Ferrone, 2008; Seliger and Ferrone, 2020). The loss of MHC class I proteins in human tumors is well known (Marincola *et al.*, 2000; Garrido, 2019).

Tumor cells also frequently shed NKG2D ligands which interferes with the recognition and killing of tumor cells by NK cells, T cells and macrophages (Groh *et al.*, 2002). By the overexpression of proteinase inhibitor-9 tumor cells can escape from T cell-mediated killing by the perforin/granzyme pathway (Soriano *et al.*, 2012). Tumor cells can become resistant to immune cell-mediated killing by defects in death receptor signaling pathways (Takeda *et al.*, 2002) or the expression of anti-apoptotic signals, e.g. by the constitutive activation of STAT3 (Catlett-Falcone *et al.*, 1999). Furthermore, IFN-γ insensitivity has been observed in tumor cell lines (Kaplan *et al.*, 1998).

Tumor cells can express the programmed death-ligand 1 (PD-L1) in response to IFN-γ (Taube *et al.*, 2012) which leads to T cell anergy by the interaction with programmed cell death protein 1 (PD-1) receptor on T cells.

Interestingly, the chronic inflammation in the TME leads to the accumulation of immunosuppressive immune cells, like regulatory T cells (Treg), tumor-associated macrophages (TAM) and myeloid-derived suppressor cells (MDSC) (Zamarron and Chen, 2011). Under physiological conditions these cells prevent an excessive immune response, an auto-reaction of the immune system and tissue destruction. However, in cancer they can mediate tumor-progression by inhibiting the anti-cancer immune response.

$CD4^+$ Treg are characterized by the expression of CD25 and the transcription factor forkhead box P3 (FoxP3); their physiological function is to mediate self-tolerance by suppressing self-antigen reactive T cells (Lindau *et al.*, 2013). Treg levels were described to be increased in patients with malignant melanoma and other malignancies where they contribute to the immunosuppressive TME by inhibiting T cells, B cells, DC and NK cells (Ouyang *et al.*, 2016). Treg secrete immunosuppressive cytokines like transforming growth factor (TGF)-β and

IL-10, and directly kill T cells and APC in a perforin/granzyme B-dependent manner, as well as compete for IL-2 by CD25 expression (Ouyang *et al.*, 2016).

TAM contribute to the immunosuppressive TME by producing the immunosuppressive factors IL-10, TGF-β and prostaglandin E2 (PGE2), recruiting Treg by secretion of CC chemokine ligand (CCL)22 and down-regulating IL-12 production (Noy and Pollard, 2014).

The third subset of immunosuppressive immune cells that plays a major role in tumor progression is MDSC, that will be described in detail below.

1.2 Malignant melanoma

Malignant melanoma is a form of skin cancer that arises from the melanin-producing cells, melanocytes that are localized in the basal layer of human epidermis (Gray-Schopfer *et al.*, 2007). It is characterized by its fast progression, invasiveness, high metastatic potential and resistance to conventional therapies like chemo- and radiotherapy (Eggermont *et al.*, 2014).

Early stage melanoma can be cured by surgical resection but as soon as it has metastasized prognoses are very poor (Gray-Schopfer *et al.*, 2007; Tas, 2012). Even though only 5 % of all skin cancer cases can be attributed to malignant melanoma, it still is responsible for 90 % of skin cancer related deaths (Garbe *et al.*, 2016).

Importantly, melanoma incidence rates have increased in different populations over the last decades and were predicted to increase even more until the year 2031, which makes the development of strategies for melanoma control and therapy highly important (Whiteman *et al.*, 2016).

One main reason for the development of malignant melanoma is the accumulation of deoxyribonucleic acid (DNA) mutations due to ultraviolet (UV) light exposure (Cust *et al.*, 2018). The two most common mutations in malignant melanoma are in the genes for neuroblastoma RAS viral oncogene homolog (N-Ras) and B-rapidly accelerated fibrosarcoma (B-Raf). About 15 to 20 % of melanoma patients show a mutation in the codons 12, 13 or 61 of the N-Ras gene leading to the constitutive activation of this guanosine triphosphatase (GTPase) (Johnson and Puzanov, 2015). More than 50 % of all melanoma patients have the B-Raf^{V600E} mutation that leads to constitutive activation of this serine/threonine-kinase downstream of N-Ras (Cust *et al.*, 2018). Both of these mutations induce an activation of the mitogen-activated protein kinase (MAPK) pathway, involving the kinases mitogen-activated protein kinase kinase (MEK) and extracellular signal-regulated kinase (ERK) leading to aberrant cell proliferation (Shtivelman *et al.*, 2014). Importantly, the discovery of these mutations has led to the development of inhibitors of this pathway for targeted therapy.

1.2.1 Targeted therapy for melanoma

Two tyrosine kinase inhibitors that inhibit the active form of B-Raf with the V600E mutation are highly effective in B-Raf^{V600E}-mutant metastatic melanoma patients: vemurafenib and dabrafenib (Wong and Ribas, 2016). Clinical studies could report an overall response rate of 50 % using the B-Raf inhibitor vemurafenib in advanced unresectable melanoma with a median progression-free survival (PFS) between 5.3 and 7.3 months (Young *et al.*, 2012).

However, resistance occurs in the majority of patients, and a combination with MEK inhibitors such as trametinib can delay the development of resistance (Wong and Ribas, 2016). Improved clinical response rates were shown for the combination of B-Raf and MEK inhibitors (dabrafenib and trametinib) compared to monotherapy (Robert *et al.*, 2015).

1.2.2 Melanoma immunotherapy

Immunotherapy of cancer has revolutionized the therapy options for cancer patients in the last couple of years (Farkona *et al.*, 2016). Immune checkpoint inhibition was proved to be very promising (Domingues *et al.*, 2018). Under physiological conditions, immune checkpoint pathways prevent an excessive immune response (Nirschl and Drake, 2013). Signals transmitted to T cells via cytotoxic T-lymphocyte-associated protein 4 (CTLA-4) or PD-1 receptors lead to T cell anergy and thereby diminish the immune response. In cancer, these pathways can be exploited in the TME to promote tumor progression, tumor cells themselves can express the inhibitory ligands PD-L1/PD-L2 or CD80/CD86 or they are expressed by immunosuppressive cells in the TME, both leading to a T cell arrest and immunosuppression (Nirschl and Drake, 2013). In 2011, a monoclonal antibody against CTLA-4, ipilimumab, was approved for melanoma therapy. Ipilimumab could increase the overall survival of patients to 10.1 months in a clinical trial (Hodi *et al.*, 2010).

Furthermore, in 2014 nivolumab and pembrolizumab, that block PD-1, were approved. Nivolumab alone was able to achieve a PFS of 6.9 months in melanoma patients, which was increased to 11.4 months in combination with ipilimumab (Raedler, 2015). Pembrolizumab could even reach a PFS of over 24 months with a response rate of 33 % in a clinical trial, whereas ipilimumab alone had a response rate of 12 % in the same trial (Schachter *et al.*, 2017).

In 2015, a drug consisting of a modified oncolytic herpes virus that only replicates in melanoma cells, called talimogen laherparevec (T-VEC), was approved for intratumoral injection in non-resectable skin melanoma lesions (Pol *et al.*, 2015). The virus leads to the lysis of melanoma cells and in addition induces the expression and secretion of granulocyte-macrophage colony-stimulating factor (GM-CSF) by melanoma cells to stimulate the host

immune system (Pol *et al.*, 2015). The median overall survival could be increased to 23.3 months by T-VEC with an overall response rate of 26.4 % in a clinical trial (Andtbacka *et al.*, 2015).

1.2.3 The *RET* transgenic mouse model of malignant melanoma

Different mouse models can be used to study malignant melanoma. Cell-line xenograft models and patient-derived xenograft models mimic the genetic heterogeneity of human cancer and can be used to predict the response of (human) tumor cells itself to drugs, however, these models lack the component of the immune system (Saleh, 2018). Induction of melanoma by UV irradiation or chemicals can be useful to study the carcinogenesis by these risk factors that are also true for human melanoma (Saleh, 2018). Orthotopic or ectopic transplantation of syngeneic tumor cells into mice are fast and easy model systems; however, they are artificial as they do not reflect the human genetics, pathology and natural interaction with the immune system due to their extremely fast progression (Saleh, 2018).

Genetically engineered mouse models of melanoma have the advantages that common human mutations can be introduced to mimic the pathogenesis of human melanoma, the initiation and progression of the tumor can be studied with a time course that resembles more the clinical situation and the new therapies can be tested (Pérez-Guijarro *et al.*, 2017).

The *RET* transgenic mouse model belongs to the genetically engineered mouse models of melanoma and was established in 1998 (Kato *et al.*, 1998). The mice overexpress the human *RET* oncogene under a metallothioneine-I promoter enhancer in melanocytes. The expression of the Ret tyrosine kinase stimulates the MAPK pathway by activating ERK2 as well as c-Jun and metalloproteinases, leading to the formation of skin melanomas that metastasize to the lymph nodes, the lung, the brain, the kidneys, the liver and the spleen and show high similarity to human melanomas with respect to histopathology and clinical development (Kato *et al.*, 1998; Umansky *et al.*, 2008). Although the activation of the Ret tyrosine kinase was not described in human melanomas the activation of the MAPK pathway is very common (Dantonio *et al.*, 2018).

Interestingly, it has been described that the melanoma lesions of *RET* transgenic mice show a characteristic melanoma morphology and that the melanoma-associated antigens tyrosinase, tyrosinase-related protein (TRP)-1, TRP-2 and glycoprotein (gp)100 are expressed in these lesions (Abschuetz *et al.*, 2012). Furthermore, a melanoma specific T cell response was described in this mouse model (Umansky *et al.*, 2008; Abschuetz *et al.*, 2012). Importantly, the accumulation of immunosuppressive cells like Treg and MDSC and their promoting effect on tumor progression plays a major role in the *RET* model (Kimpfler *et al.*, 2009; Meyer *et al.*, 2011). The depletion of $CD25^+$ $FoxP3^+$ Treg in lymphoid organs could not

stop tumor development (Kimpfler *et al.*, 2009), whereas the inhibition of MDSC had a beneficial effect on mouse survival (Meyer *et al.*, 2011; Sevko *et al.*, 2013).

These findings suggest the *RET* transgenic mouse model, which was used in the following study, as a suitable system to investigate melanoma immunity, especially immunosuppression in the TME, and to test new immunotherapeutic strategies.

1.3 Myeloid-derived suppressor cells (MDSC)

MDSC are a heterogeneous population of myeloid cells that are absent under physiological conditions in adults but accumulate upon chronic inflammation, i.e. chronic infection, trauma or cancer and exhibit strong immunosuppression on T and NK cells (Gabrilovich and Nagaraj, 2009; Gabrilovich *et al.*, 2012).

In 1978, natural suppressor cells were first described to inhibit the formation of cell-mediated immunity in a co-culture of splenocytes and tumor cells and their suppressive effect was even increased upon systemic administration of Bacillus Calmette-Guerin (BCG) to the donor mice (Bennett *et al.*, 1978). Later, it was reported that transplantation of mammary carcinoma into mice resulted in an accumulation of cells devoid of mature leukocyte antigens and granulocytic cells, and that this accumulation was associated with a deletion of effector lymphocytes (Lee and Rosse, 1982). In the following years, two more studies have identified immunosuppressive myeloid cells in murine cancer models (Buessow *et al.*, 1984; Young *et al.*, 1987). In recent years, the term MDSC was introduced (Talmadge and Gabrilovich, 2013; Bronte *et al.*, 2016).

MDSC have been identified to expand and play an important role in the immunosuppressive TME and the clinical outcome of patients with malignant melanoma (Poschke *et al.*, 2010; Jordan *et al.*, 2013; Weide *et al.*, 2014; Jiang *et al.*, 2015; Martens *et al.*, 2016). Furthermore, MDSC have also been described in various other cancer types, such as multiple myeloma (Brimnes *et al.*, 2010), hepatocellular carcinoma (Hoechst *et al.*, 2008), non-small cell lung cancer (NSCLC) (Liu *et al.*, 2010), renal cell carcinoma (van Cruijsen *et al.*, 2008), breast cancer (Danilin *et al.*, 2012), prostate cancer (Vuk-Pavlović *et al.*, 2010) and colorectal cancer (Chun *et al.*, 2015).

However, MDSC play a role not only in cancer but also in various other pathological conditions like chronic inflammation (reviewed in (Mira *et al.*, 2017)), trauma (reviewed in (Marik and Flemmer, 2012)), infection (reviewed in (Medina and Hartl, 2018)), autoimmune diseases (reviewed in (Ma and Xia, 2018)), organ transplantation (reviewed in (Nakamura and Ushigome, 2018)), pregnancy (reviewed in (Zhao *et al.*, 2016)) and neonatal inflammation control (Liu *et al.*, 2019). The following paragraphs will yet mainly focus on the phenotype, generation and role of MDSC in cancer.

1.3.1 MDSC phenotypic characterization

In mice, MDSC were characterized by the expression of CD11b, alias integrin α-M, and the myeloid differentiation antigen Gr1. However, two subpopulations exist that show differential expression of Ly6G and Ly6C, the components of Gr1. In mice, polymorphonuclear (PMN-)MDSC are $CD11b^{+}Ly6G^{high}Ly6C^{low}$ and monocytic (M-)MDSC are $CD11b^{+}Ly6G^{-}Ly6C^{high}$ (Bronte *et al.*, 2016). In humans, M-MDSC are defined as $Lin^{-}CD11b^{+}CD14^{+}CD15^{-}HLA\text{-}DR^{-/low}$ and PMN-MDSC as $Lin^{-}CD11b^{+}CD14^{-}CD15^{+}HLA\text{-}DR^{-}$ or $Lin^{-}CD11b^{+}CD14^{-}CD66b^{+}$ (Solito *et al.*, 2014; Bronte *et al.*, 2016). Furthermore, lectin-type oxidized LDL receptor-1 (LOX-1) has been proposed as a new marker to distinguish human immunosuppressive PMN-MDSC from non-immunosuppressive neutrophils (Condamine *et al.*, 2016). A third subtype of human MDSC, composed of more immature $HLA\text{-}DR^{-}CD33^{+}CD15^{-}CD14^{-}$ MDSC, has been recently proposed and was termed early stage MDSC (eMDSC) (Bronte *et al.*, 2016).

1.3.2 MDSC accumulation and activation

In chronic inflammation and cancer, instead of differentiation of myeloid precursors into neutrophils, monocytes and DC, MDSC are developed from these precursors (Figure 2). The accumulation and activation of MDSC is proposed to be a two-step process, which is mediated by an altered cytokine, growth factor and chemokine environment (Condamine and Gabrilovich, 2011). The chronic production and enrichment of IL-6, IFN-γ, IL-1β, GM-CSF, IL-10, M-CSF, G-CSF and vascular endothelial growth factor (VEGF) as well as Toll-like receptor (TLR) ligands, that belong to DAMP, leads to the accumulation of immature myeloid precursors and their development and activation to become MDSC (Condamine and Gabrilovich, 2011).

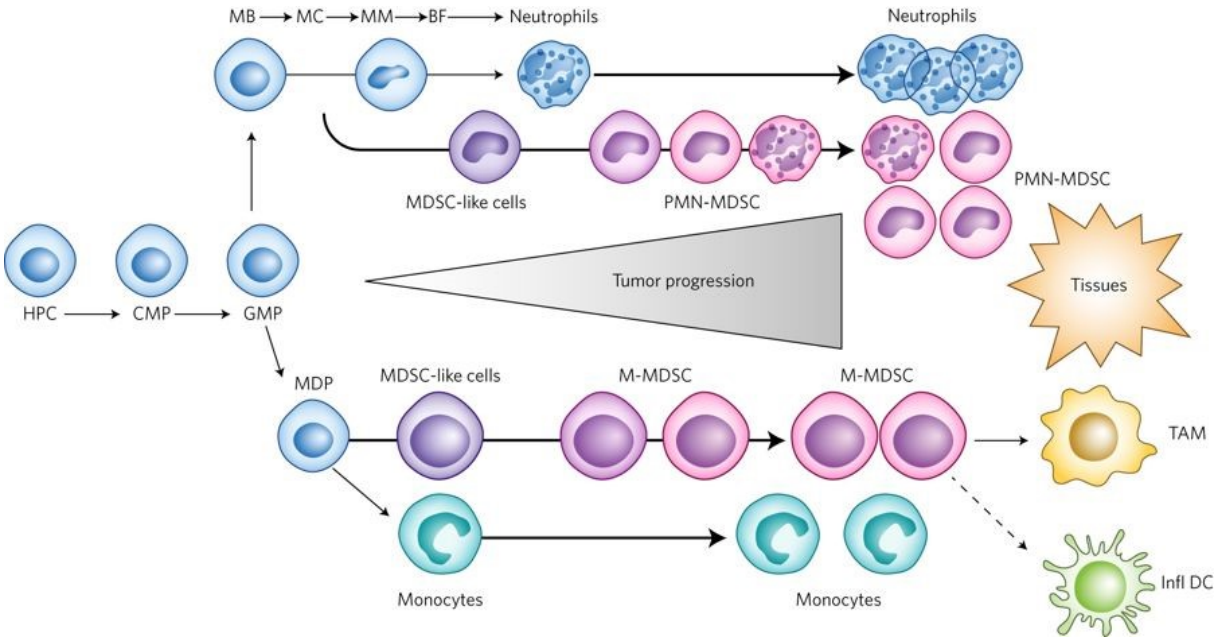

Figure 2. MDSC development by alteration of myelopoiesis.
Upon the chronic inflammation during tumor progression differentiation of hematopoietic progenitor cells (HPC) via common myeloid progenitors (CMP) and granulocyte-macrophage progenitors (GMP) into neutrophils and monocytes is altered. Under physiological conditions, neutrophil differentiation progresses through the precursor stages of myeloblasts (MB), myelocytes (MC), metamyelocytes (MM) and band forms (BF). Monocytes originate from monocyte/macrophage and dendritic cell precursors (MDP). With tumor progression, populations of immature myeloid cells (IMC) are expanded and converted into immunosuppressive MDSC. IMC that share markers with MDSC but have no immunosuppressive activity can be called MDSC-like cells. Immunosuppressive MDSC can be separated into polymorphonuclear (PMN-) and monocytic (M-) MDSC. Neutrophils, monocytes and pathologically activated MDSC are coexisting. In tumors, M-MDSC rapidly differentiate in tumor-associated macrophages (TAM) and inflammatory dendritic cells (infl DC). Figure taken from (Veglia *et al.*, 2018).

GM-CSF, G-CSF, M-CSF, IL-6 and VEGF signaling, through Janus kinase/signal transducer and activator of transcription (JAK/STAT) and MAPK pathways, leads to the expression of anti-apoptotic factors like B cell lymphoma-extra large (Bcl-xL), Cyclin D1, Survivin and c-Myc that lead to the accumulation of MDSC (Condamine and Gabrilovich, 2011). Whereas factors like IFN-γ, IL-1β and TLR ligands, mainly via JAK/STAT and myeloid differentiation primary response 88/nuclear factor 'kappa-light-chain-enhancer' of activated B-cells (MyD88/NF-κB) signal transduction cascades, lead to the expression of immunosuppressive factors and activation of MDSC (Condamine and Gabrilovich, 2011).

In addition, it has been reported that mature normal human monocytes could be converted into MDSC by tumor-derived extracellular vesicles (EV) (Valenti *et al.*, 2006; Fleming *et al.*, 2019). It was also shown that microRNAs located in EV played an important role in this process (Huber *et al.*, 2018). Therefore, MDSC development seems to be also possible by pathological conversion of mature myeloid cells into MDSC in addition to their generation from immature myeloid precursors.

1.3.3 MDSC recruitment

The recruitment of MDSC to the tumor site is mainly mediated by chemokines secreted in the TME and chemokine receptors expressed on MDSC.

M-MDSC have been shown to be CC chemokine receptor (CCR)2 positive in a B16 melanoma mouse model that was proved to be critical for the recruitment of these cells to the TME (Lesokhin *et al.*, 2012). In colorectal cancer patients, high levels of CCL2 are produced in the TME, and its deletion in a colorectal cancer mouse model lead to the decrease in numbers and immunosuppressive capacity of PMN-MDSC (Chun *et al.*, 2015). In a glioblastoma mouse model, M-MDSC and Treg were recruited by CCL2 that negatively correlated with glioblastoma patients' outcome (Chang *et al.*, 2016).

In our lab, it was shown that M- and PMN-MDSC from melanoma bearing *RET* transgenic mice were recruited to the tumor by a CCR5-CCR5 ligand dependent mechanism and that the MDSC of melanoma patients expressed higher levels of CCR5 compared to healthy donor control cells (Blattner *et al.*, 2018).

In human ovarian cancer, MDSC could be recruited via the interaction between CXC chemokine ligand (CXCL)12 and the CXC chemokine receptor (CXCR)4 receptor (Obermajer *et al.*, 2011). Also IL-8 (CXCL8) was able to attract M- and PMN-MDSC from cancer patients *ex vivo* (Alfaro *et al.*, 2016). MDSC expressing CX3CR1 were shown to be attracted by CCL26 produced in hypoxic tumor regions by tumor cells in response to hypoxia-inducible factors (HIF) (Chiu *et al.*, 2016).

1.3.4 MDSC immunosuppressive mechanisms

Activated MDSC can contribute in different ways to the establishment of an immunosuppressive TME (Groth *et al.*, 2019). They can suppress anti-tumor functions of T and NK cells by depletion of essential metabolites, homing prevention and the expression of reactive species as well as immune checkpoint molecules; in addition, they can have promoting effects on other suppressive immune cells like Treg (Figure 3).

Activated MDSC express elevated levels of arginase 1 (Arg1) (Rodriguez *et al.*, 2007) and inducible nitric oxide synthase (iNOS, NOS2) (Raber *et al.*, 2014), that can both lead to the depletion of L-arginine from the microenvironment, inducing a cell cycle arrest in T cells (Rodriguez *et al.*, 2007) and T cell anergy due to the downregulation of TCR ζ-chain expression (Rodriguez *et al.*, 2004). Moreover, by the expression of iNOS (Raber *et al.*, 2014) and nicotinamide adenosine dinucleotide phosphate oxidases (NADPH oxidases, NOX) (Corzo *et al.*, 2009) MDSC produce elevated levels of nitric oxide (NO) and reactive oxygen species (ROS), respectively. The reactive species lead to suppression of T cell proliferation (Corzo *et*

al., 2009) and TCR nitration (Nagaraj *et al.*, 2007). In addition, NO impairs the Fc receptor-mediated functions of NK cells (Stiff *et al.*, 2018).

Furthermore, MDSC express indoleamine 2,3-dioxygenase (IDO) that degrades L-tryptophan into N-formylkynurenine (Yu *et al.*, 2013). This leads to T cell arrest and anergy (Munn *et al.*, 2005). Another mechanism, promoting anergy in T cells, is the interaction of PD-L1 on MDSC with PD-1 receptor on T cells (Bardhan *et al.*, 2016). PD-L1 has been shown to be expressed by MDSC in the hypoxic TME (Noman *et al.*, 2014).

MDSC were shown to be able to decrease the expression of the lymph node homing receptor L-selectin on naïve T and B cells even outside of the TME, which severely restricts antigen driven expansion of T and B cells in lymph nodes (Ku *et al.*, 2016).

It was demonstrated in tumor-bearing mice that MDSC induce T cell tolerance and Treg accumulation by expressing CD40 (Pan *et al.*, 2010). Furthermore, by the secretion of IL-10 and IFN-γ, MDSC could lead to the development of Treg from $CD4^+$ T cells (Huang *et al.*, 2006). In addition to their stimulating effects on Treg, MDSC could induce an M2-like macrophage phenotype with decreased IL-12 production and tumor-promoting effects (Beury *et al.*, 2014).

It is known that extracellular adenosine exerts suppressive effects on T and NK cells (Hoskin *et al.*, 2008). Adenosine was shown to inhibit $CD8^+$ T cell priming by interfering with membrane-proximal TCR signaling (Linnemann *et al.*, 2009). Tumor-derived TGF-β was described to induce the expression of ectonucleoside triphosphate diphosphohydrolase 1 (E-NTPDase1, CD39) and ecto-5'-nucleotidase (Ecto5'NTase, CD73) on MDSC that catalyze the dephosphorylation from adenosine triphosphate (ATP) to adenosine monophosphate (AMP) and thereafter to adenosine (Li *et al.*, 2017). Therefore, MDSC contribute to the generation of extracellular adenosine that inhibits the anti-tumor immune response.

In addition to the immunosuppressive effects, MDSC exert also tumor promoting functions. In particular, they secrete VEGF (Shen *et al.*, 2014) that stimulates tumor angiogenesis. In addition, it was shown that MDSC were recruited to the pre-metastatic niche and suppressed NK cell functions there, creating a microenvironment facilitating metastasis (Sceneay *et al.*, 2012).

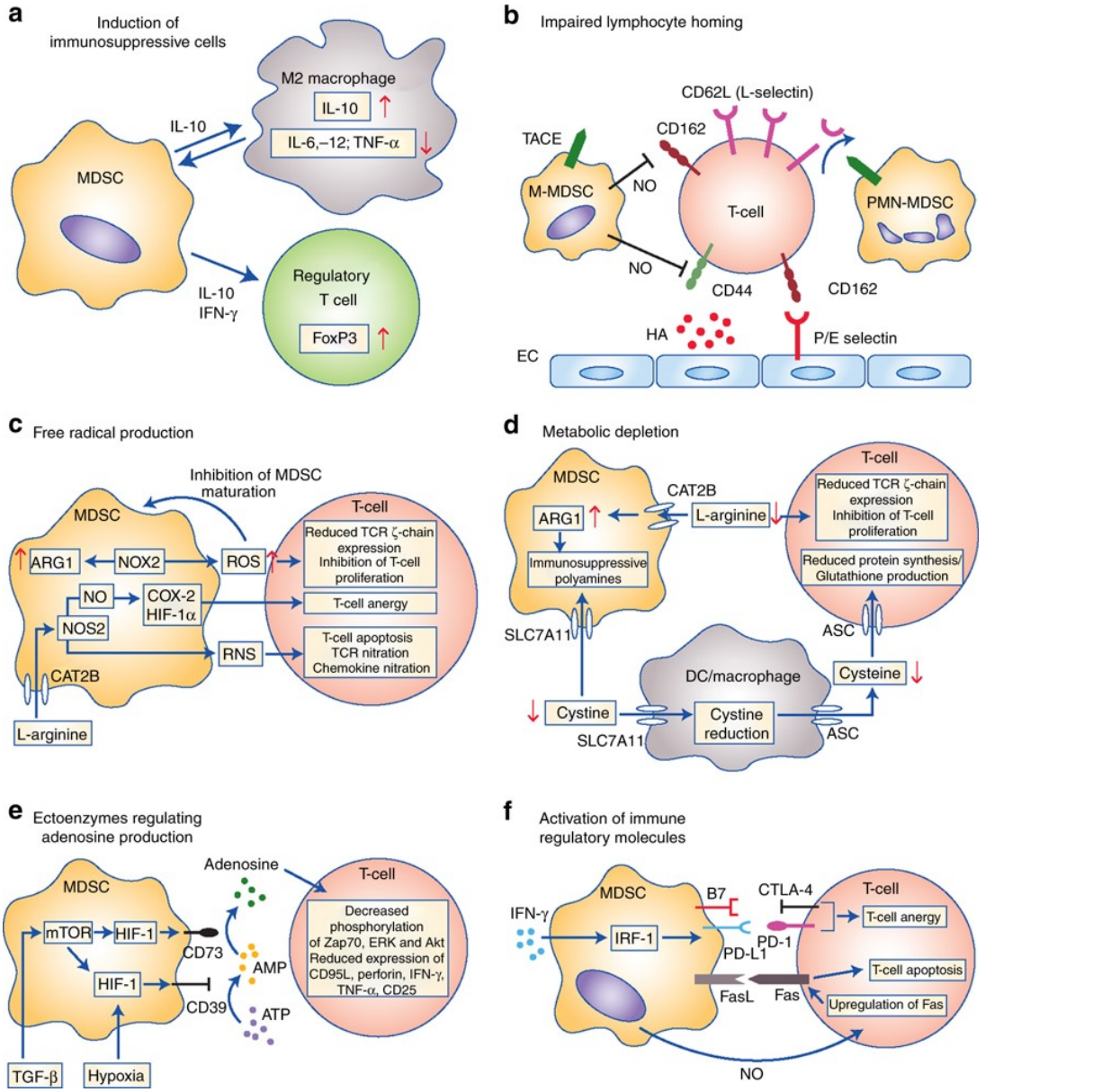

Figure 3. Main mechanisms of MDSC-mediated immunosuppression.
MDSC can promote the generation of M2 macrophages and Treg by interleukin (IL-)10 and interferon (IFN-)γ secretion (a); they can impair lymphocyte adhesion to endothelial cells (EC) and extravasation through nitric oxide (NO-)mediated downregulation of adhesion molecules and tumor necrosis factor-alpha-converting enzyme (TACE)-mediated cleavage of CD62 ligand (L-Selectin) (b); reactive oxygen and reactive nitrogen species (ROS, RNS) are produced by MDSC via NADPH oxidase 2 (NOX2) and nitric oxide synthase 2 (NOS2), leading to increased cyclooxygenase 2 (COX-2), hypoxia-inducible factor 1-alpha (HIF-1α) and arginase 1 (ARG1) inhibiting T cell function (c); MDSC deplete the micro-environment from the amino acids L-arginine and cysteine which leads to a T cell arrest (d); the ecto-enzymes CD39 and CD73 are expressed on MDSC under hypoxic conditions leading to adenosine production and thereby reduced T cell function (e); MDSC express the immune checkpoint ligands B7 (CD80, CD86), programmed death-ligand 1 (PD-L1) and Fas ligand (FasL) causing T cell anergy and apoptosis via binding to their respective receptors (f). Figure taken from (Groth *et al.*, 2019).

1.3.5 MDSC targeting for cancer immunotherapy

As MDSC have strong immunosuppressive and tumor-promoting capacity, they are an important target for cancer immunotherapy (Fleming *et al.*, 2018). There are three different strategies to target MDSC, namely blocking i.) MDSC accumulation, ii.) MDSC recruitment and iii.) MDSC-mediated immunosuppression.

The blockade of MDSC accumulation can be achieved by a normalization of myelopoiesis, which was shown to happen under the therapy with some chemotherapeutic drugs (Fleming *et al.*, 2018). In the *RET* transgenic mouse model of malignant melanoma, ultra-low doses of paclitaxel inhibited MDSC accumulation, inducing anti-tumor effects (Sevko *et al.*, 2013). In patients with pancreatic cancer, gemcitabine led to a decrease in PMN-MDSC frequencies and a restoration of effector T cells (Eriksson *et al.*, 2016). Furthermore, it was discovered that all-trans retinoic acid (ATRA), which blocks retinoic acid signal transduction, has a positive effect on myelopoiesis by promoting the differentiation of DC and macrophages and thereby preventing the accumulation of MDSC in murine and human samples (Nefedova *et al.*, 2007). Therefore, ATRA was successfully used in two clinical trials with patients suffering from metastatic renal cell carcinoma and late stage small cell lung cancer. It was shown that ATRA improved patient survival by a reduction of the MDSC frequency (Mirza *et al.*, 2006; Iclozan *et al.*, 2013). ATRA was also used in combination with ipilimumab in a phase II clinical trial in melanoma patients. It improved the clinical outcome of patients by decreasing MDSC frequencies and leading to an increased antigen-specific T cell response as compared to ipilimumab alone (Tobin *et al.*, 2017).

The blockade of MDSC recruitment can be achieved by blocking the chemokine receptors and ligands that are important for MDSC trafficking to the tumor. In the *RET* transgenic mouse model of malignant melanoma, it could be shown that the blockade of the CCR5 ligands by a murine CCR5-Ig fusion protein prevented MDSC migration to the tumor, leading to an increase in tumor-infiltrating T cells and improved mouse survival (Blattner *et al.*, 2018). Moreover, in a prostate cancer mouse model, MDSC recruitment could be blocked by a CXCR2 antagonist (Di Mitri *et al.*, 2014). One clinical trial with melanoma patients is currently ongoing using SX-682, a small molecule inhibitor of CXCR1 and 2, to block MDSC recruitment in combination with pembrolizumab (trial number NCT03161431).

To neutralize MDSC-mediated immunosuppression phosphodiesterase-5 inhibitor, sildenafil was applied in different transplantable tumor mouse models. It decreased Arg1 and iNOS expression by MDSC, increased tumor-infiltrating T cells and the efficacy of adoptive T cell therapy (Serafini *et al.*, 2006). Sildenafil could likewise prolong mouse survival of melanoma-bearing *RET* transgenic mice by reducing MDSC frequency and activity and restoring $CD8^+$ T cell infiltration and function (Meyer *et al.*, 2011). Tadalafil was applied in clinical trials in

patients with head and neck squamous cell carcinoma and metastatic melanoma showing an improved clinical outcome correlated with the reduction of tumor-infiltrating and peripheral MDSC and increased anti-tumor immune responses (Califano *et al.*, 2015; Weed *et al.*, 2015; Hassel *et al.*, 2017). In a murine model of pancreatic ductal adenocarcinoma, an IDO1 inhibitor diminished MDSC immunosuppressive capacity and increased the efficacy of a cancer vaccine but not anti-PD-1/anti-PD-L1 therapy (Blair *et al.*, 2019). In ovarian cancer patients, metformin reduced the frequency of circulating $CD39^+CD73^+$ MDSC, inducing thereby increased anti-tumor activity of circulating $CD8^+$ T cells and increased overall survival (L. Li *et al.*, 2018).

Altogether, there are various MDSC-targeting strategies that have shown beneficial effects in pre-clinical tumor models and in clinical trials. However, none of the MDSC-targeting approaches is routinely used in the cancer therapy (Weber *et al.*, 2018). Therefore, more research is needed to find the most promising therapeutic approach to really help cancer patients.

1.4 Chemokines and their receptors

Chemokines are small (8 to 17 kDa) chemotactic cytokines that are able to induce the directed mobilization of cells that express the respective chemokine receptors (Lazennec and Richmond, 2010). They are classified by variations of the first two cysteines of a conserved cysteine motif in the mature sequence of the protein (Lazennec and Richmond, 2010). The CC subfamily has 28 and the CXC subfamily has 17 members. There are two more subfamilies with only one member each, the CX3C and the XC subfamiles (Lazennec and Richmond, 2010).

Chemokines are expressed by different cell types like leukocytes, endothelial cells, fibroblasts, epithelial cells and cancer cells and are mainly responsible to attract leukocytes to the site of inflammation and to mediate their homing to lymphatic organs (Thelen and Stein, 2008).

Chemokine receptors are class A G-protein coupled receptors also separated into the four subfamilies (Lazennec and Richmond, 2010). There are ten CCR family members and seven CXCR family members, in addition there are XCR1 and CX3CR1 (Lazennec and Richmond, 2010). The signaling of chemokine receptors is mediated by heterotrimeric G-proteins that regulate a diversity of signal transduction pathways involved not only in migration but also in invasion, cell survival and proliferation (New and Wong, 2003).

Chemokine receptors were first found to be expressed on immune cells to mediate their trafficking through the body. However, they can be also expressed on other cell types, for example cancer cells. In cancer cells, the expression of chemokine receptors can mediate their

survival, proliferation, invasiveness and metastasis formation (Lazennec and Richmond, 2010). Since there are more chemokines than chemokine receptors, most receptors have more than one ligand (Lazennec and Richmond, 2010).

1.4.1 Chemokine receptor CCR5 and its downstream signaling

CCR5 is a seven-transmembrane domain G-protein coupled receptor (Oppermann, 2004) composed of 352 amino acids with a calculated molecular mass of 40.6 kDa (Samson *et al.*, 1996). CCR5 was first described in 1996 as a new chemokine receptor binding to the ligands macrophage inflammatory protein-1 α (MIP-1α/CCL3), macrophage inflammatory protein-1 β (MIP-1β/CCL4) and regulated on activation, normal T cell expressed and secreted (RANTES, CCL5) (Combadiere *et al.*, 1996; Raport *et al.*, 1996; Samson *et al.*, 1996). Later also monocyte chemotactic protein-2 (MCP-2, CCL8) was found to be a ligand of CCR5 (Gong *et al.*, 1998).

The chemokines bind to acidic and tyrosine residues in the N-terminal region of CCR5 and to regions vicinal to the second extracellular loop to initiate signaling by a conformational change (Samson *et al.*, 1996; Blanpain *et al.*, 1999). By the release of the α and $\beta\gamma$ G-protein subunits, adenylyl cyclase and phospholipase Cβ (PLCβ) get activated and lead to the formation of inositol triphosphate (IP3) and the mobilization of intracellular calcium as well as the formation of diacylglycerol (DAG) and the activation of protein kinase C (PKC) (Oppermann, 2004). Furthermore, phosphatidylinositol 3-kinases (PI3K), inducing activation of the MAPK pathway (Oppermann, 2004). Therefore, CCR5 activates transcription, cell proliferation and survival. In addition, the Rho GTPases, RhoA, Rac and Cdc42, are activated by CCR5 downstream signaling to coordinate the reorganization of the actin cytoskeleton and regulate cell polarity, adhesion, and motility (Oppermann, 2004).

CCR5 was shown to be expressed on various cell types, including myeloid cells, dendritic cells, T cells, endothelium cells, epithelium cells, vascular smooth muscle cells and fibroblasts, as well as microglia, neurons, and astrocytes in the central nervous system (Rottman *et al.*, 1997).

Importantly, CCR5 was identified to be a co-receptor for the human immunodeficiency virus (HIV) mediating the entry of the virus into T cells and macrophages where they replicate and can cause the acquired immune deficiency syndrome (AIDS) (Deng *et al.*, 1996; Dragic *et al.*, 1996).

1.4.2 Regulation of CCR5 expression

After ligand binding, CCR5 becomes a subject of desensitization, internalization and recycling to the plasma membrane (Oppermann, 2004). The receptor gets phosphorylated by PKC or G-protein coupled receptor kinases (GRK) at C-terminal serine residues (Oppermann *et al.*, 1999; Pollok-Kopp *et al.*, 2003). The regulatory proteins β-arrestin-1 and -2 bind to the phosphorylated C-terminal serine residues but can also bind phosphorylation-independent, leading to the internalization of CCR5 by clathrin-mediated endocytosis (Kraft *et al.*, 2001; Huttenrauch *et al.*, 2002). Then CCR5 accumulates in endosomes and is recycled to the plasma membrane in a dephosphorylated form (Pollok-Kopp *et al.*, 2003). As CCR5 does not colocalize with late endosomal or lysosomal markers (Signoret *et al.*, 2000), it is suggested that it is not degraded but undergoes several rounds of recycling until the ligand is dissociated and CCR5 is sensitive again (Oppermann, 2004).

Chemokine receptors can either be constitutively expressed on several immune cell subtypes or hematopoietic stem cells, which is important for their homing to lymphatic organs, or their expression is induced by cytokines under inflammatory conditions, to recruit the immune cells to the site of inflammation (Stone *et al.*, 2017). It was shown that CCR5 is abundantly expressed on long-term activated, IL-2 stimulated human T cells *ex vivo* (Wu *et al.*, 1997). In addition, a gradual increase of CCR5 was observed on human PBMC *ex vivo* after 12 days of stimulation with IL-2 (Bleul *et al.*, 1997). Moreover, IL-2, IL-12, TNF-α and IFN-γ led to CCR5 mRNA upregulation after 24 hours in human PBMC *ex vivo*; for IL-2 the upregulation was also confirmed on protein level on $CD4^+$ and $CD8^+$ T cells (Patterson *et al.*, 1999). In the same study, IL-10 and IL-4 were shown to downregulate CCR5 mRNA expression (Patterson *et al.*, 1999) on PBMC *ex vivo*.

The upregulation of CCR5 on T cells upon IL-2 stimulation could be confirmed in another paper (Yang *et al.*, 2001). However, the authors argued that prior anti-CD3/anti-CD28 activation was needed for the IL-12-induced CCR5 upregulation, as the TCR triggering led to upregulation of the IL-12 receptor. Furthermore, CCR5 could also be induced on $CD4^+$ T cells by lipoarabinomannan, a cell wall component and virulence factor of Mycobacterium tuberculosis (Juffermans *et al.*, 2001).

IFN-γ was able to upregulate CCR5 surface expression and increase migration towards the CCR5 ligands in human mononuclear phagocytes isolated from peripheral blood and stimulated *ex vivo* for 12 hours (Hariharan *et al.*, 1999). Contrary to what was shown before for whole PBMC on mRNA level, IL-10 stimulated human monocytes showed an increased CCR5 surface expression and migration towards the CCR5 ligands after 16 hours of stimulation (Sozzani *et al.*, 1998). Moreover, IFN-γ, IL-10, IL-4 and lipopolysaccharide (LPS) could increase CCR5 expression at the mRNA and protein level in murine macrophages, whereas

hypoxia could decrease both constitutive and induced CCR5 expression in the same cells (Bosco *et al.*, 2004).

Altogether, these findings suggest that IL-2, IL-12, TNF-α and IFN-γ upregulate CCR5 on T cells and that IL-4, IL-10, IFN-γ and LPS upregulate CCR5 on myeloid cells. However, different times of stimulation were used in the different studies and not all of them have shown the functional relevance by studying the migration of the cells towards the CCR5 ligands. Moreover, it is not clear in these studies, which molecular mechanisms, signal transduction cascades and transcription factors were responsible for the regulation of CCR5.

As displayed in Figure 4, the human CCR5 gene consist of three exons and two introns; in the 5' region before the first exon the upstream promoter Pu is located and the second more downstream promoter Pd composes the first intro and the second exon (Mummidi *et al.*, 1997). The CCR5 open reading frame is located in the third exon (Mummidi *et al.*, 1997). Interestingly, many transcription factor binding sites were described in the two promoter regions. The promoters contain consensus sequences for AP-1, OCT-1, GATA-1 and Sp-1 (Mummidi *et al.*, 1997). GATA-1 was shown to upregulate the CCR5 promoter activity (Moriuchi *et al.*, 1999). Another study showed consensus sequences for STAT, NF-κB, AP-1, NF-AT and CD28RE in the CCR5 promotor regions with the NF-κB/Rel family member p65 (RelA) being a potent activator of the promoter activity (Liu *et al.*, 1998). Furthermore, it was shown that C/EBPβ can bind to the CCR5 promotor (Rosati *et al.*, 2001), whereas CREB-1 can activate the CCR5 promoter (Wierda and van den Elsen, 2012).

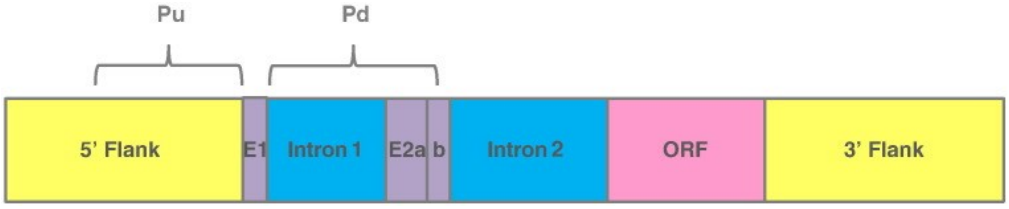

Figure 4. CCR5 gene structure.
The human CCR5 gene consist of three exons and two introns with two identified promotor regions; in the 5' region before the first exon the upstream promoter Pu is located and the second more downstream promoter Pd composes the first intro and the second exon. The CCR5 open reading frame is located in the third exon. The figure was taken from (Barmania and Pepper, 2013).

1.4.3 CCR5 in cancer

In recent years, evidence has been accumulated that CCR5 plays an important role in different types of cancer. On the one hand, it is expressed on cancer cells, promoting their proliferation, invasion and metastasis. On the other hand, it could be responsible for recruiting immunosuppressive immune cells like Treg and MDSC to the tumor.

It was found that the treatment with the CCR5 and CCR1 antagonist Met-CCL5 was able to decrease primary tumor growth in a breast cancer mouse model by inhibiting the infiltration with immunosuppressive leukocytes (Robinson *et al.*, 2003). Furthermore, the CCR5 inhibitors maraviroc and vicriviroc could reduce *in vitro* invasiveness of murine breast cancer cell lines and pulmonary metastasis in a breast cancer mouse model (Velasco-Velázquez *et al.*, 2012). The expression of CCR5 and CCL5 in human breast cancer samples could also be shown by microarray in the same study, highlighting CCR5 blockade as a promising therapy for breast cancer patients. Another study showed that $CCR5^+$ Treg are recruited to the primary tumor and the lungs of breast cancer-bearing mice, and that CCR5 blockade by maraviroc reduces the metastatic tumor burden in the lungs (Halvorsen *et al.*, 2016). In addition, maraviroc was able to decrease proliferation, migration and colony formation of human metastatic breast cancer cells *in vitro* and significantly inhibited bone marrow metastasis in nude rats implanted with these tumor cells (Pervaiz *et al.*, 2019).

It was shown that B16 melanoma growth was decreased in CCR5-deficient mice, and that DC vaccination was more efficient in these mice (Ng-Cashin *et al.*, 2003). In the same mouse model, CCR5 expression on stromal cells was proved to be necessary for the spread of melanoma cells to the lung (van Deventer *et al.*, 2005). The delay of primary melanoma growth in CCR5-deficient mice could also be confirmed by two other groups (Song *et al.*, 2012; Aldinucci and Colombatti, 2014). In human melanoma samples, CCR5 mRNA was detected in primary melanomas as well as some cutaneous metastasis (Seidl *et al.*, 2007).

In the B16 and *RET* transgenic mouse models of malignant melanoma M-MDSC were shown to express the CCR5 ligands and thereby recruit $CCR5^+$ Treg to the TME (Schlecker *et al.*, 2012).

In a mouse model of pancreatic cancer, the CCR5 inhibitor TAL-779 blocked migration of Treg to the TME, reducing thereby tumor growth (Tan *et al.*, 2009). In the CT26 murine colon cancer mouse model, $CCR5^+$ $CD103^+$ effector/memory Treg were observed to be highly immunosuppressive and CCR5-deficiency or CCL5 knockdown prevented the accumulation of these cells in the tumor and impaired their suppression capacity *in vivo* (Chang *et al.*, 2012). However, in colorectal cancer patients, the inhibition of CCR5-CCR5 ligand interaction by maraviroc delayed the tumor growth without reducing Treg numbers (Ward *et al.*, 2015). In a recent clinical trial, it was demonstrated that maraviroc led to the reprogramming of the immune system and thereby to a beneficial outcome in colorectal cancer patients (Halama *et al.*, 2016). Moreover, it could be shown that patients with a functionally mutated CCR5 are resistant to prostate cancer (Balistreri *et al.*, 2009).

Altogether, these studies already suggest CCR5 as a promising target for cancer therapy.

1.4.4 CCR5 on MDSC

In the *RET* transgenic mouse model of malignant melanoma, it was found that CCR5$^+$ PMN- and M-MDSC accumulated in the tumors and metastatic lymph nodes, correlating with an increased concentration of the CCR5 ligands CCL3, -4 and -5 as well as tumor progression (Blattner *et al.*, 2018). Interestingly, CCR5$^+$ MDSC were found to be more immunosuppressive, and the blockade of the CCR5 ligands by a murine CCR5-Ig fusion protein increased mouse survival by blocking MDSC migration to the tumor and thereby increasing tumor-infiltrating T cell numbers (Blattner *et al.*, 2018). Furthermore, the accumulation of CCR5$^+$ MDSC in the tumor and the peripheral blood was demonstrated in melanoma patients indicating that CCR5 targeting might be an interesting strategy for the therapy of these patients (Blattner *et al.*, 2018). In addition, CCR5 and its ligands were described to be important for the mobilization of PMN-MDSC from the bone marrow to the peripheral blood and the CCR5 ligands stimulated proliferation of PMN-MDSC and an upregulation of Arg1 expression in these cells (Hawila *et al.*, 2017).

In line with this, CCL5 was also shown to be important for the generation of MDSC in the bone marrow of breast cancer bearing mice, and the blockade of CCL5 inhibited tumor growth by decreasing MDSC generation and impairing their immunosuppressive function (Zhang *et al.*, 2013). Moreover, in murine breast cancer, the autocrine CCR5-CCL5 interaction was proved to be crucially important for the generation of immunosuppressive myeloid cells like PMN-MDSC and TAM (Ban *et al.*, 2017). The same study showed an inverse correlation between CCR5 expression and the maturation status of tumor-infiltrating neutrophils in breast cancer patient samples as well as the 5 year-survival rates of the breast cancer patients (Ban *et al.*, 2017).

The CCR5-CCL5 axis was also suggested to be responsible for the recruitment of MDSC to the tumor in a mouse model of gastric cancer (Yang *et al.*, 2018). Moreover, the blockade of CCR5 by maraviroc was able to increase the efficacy of anti-PD-1 therapy by decreasing MDSC accumulation and increasing CD4$^+$ and CD8$^+$ T cell numbers in the tumor (Yang *et al.*, 2018).

In patients with resectable non-small-cell lung cancer the frequency of CCR5$^+$ M-MDSC was significantly higher in the circulation compared to healthy donors, and the frequency of CCR5$^+$ M-MDSC in the peripheral blood correlated negatively with recurrence-free survival (Yamauchi *et al.*, 2018).

1.5 IL-6 and its pleiotropic role in cancer

IL-6 is a ~25 kDa cytokine that was first discovered as a factor to induce B cell differentiation and maturation into antibody producing cells (Hirano *et al.*, 1985). Meanwhile, it is known that IL-6 is playing a major role in the homeostasis of hepatocytes, hematopoietic progenitor cells, the skeleton, the placenta, the cardiovascular system and the endocrine as well as nervous systems, besides being an important regulator of the immune response (Kumari *et al.*, 2016). There are two main ways of IL-6 signaling. For the classical signaling, the IL-6 receptor (IL-6R) is expressed on hepatocytes, some epithelial cells and several types of leukocytes. Upon binding of IL-6 to the IL-6R on the plasma membrane, the complex is associated with the signal transducing component gp130. The activated IL-6R complex then induces the JAK/STAT signal transduction via the SHP-2 domain of gp130 (Wolf *et al.*, 2014). The janus-kinase family members become activated and phosphorylate different transcription factors, among them STAT3 that gets phosphorylated at tyrosine 705 (pY705), dimerizes and translocates to the nucleus, inducing the expression of STAT3-target genes. There is also a soluble form of the IL-6R, that can form a complex with IL-6 in the extracellular space and then activate cells that do only express gp130 but not the IL-6R; this second mechanism is called trans-signaling (Wolf *et al.*, 2014). A third form of IL-6-induced signaling was described for DC that trans-present the IL-6 to T cells, which is essential for the generation of T_H17 cells (Heink *et al.*, 2017).

IL-6 is known to have pro- as well as anti-inflammatory properties in infection and cancer (Kumari *et al.*, 2016). During the acute phase of the inflammatory reaction, TNFα and IL-1β induce the expression of IL-6, which in turn leads to the upregulation of more acute phase response factors (Gruys *et al.*, 2005). Moreover, IL-6 signaling leads to the expression of T cell-attracting chemokines (such as CCL4, CCL5, CCL17 and CXCL10), thereby promoting inflammation (McLoughlin *et al.*, 2005). Furthermore, by the STAT3-dependent upregulation of anti-apoptotic factors (such as Bcl-2 and Bcl-xL) and the modulation of the surface expression of Fas receptor, IL-6 can prevent the apoptosis of T cells (Atreya *et al.*, 2000; Curnow *et al.*, 2004). When it comes to the switch between pro- and anti-inflammatory properties, the same pathways are generating negative feedback loops to control inflammation and restrict immune reactions. TNFα and IL-1β then counteract pro-inflammatory IL-6 signaling by enhancing the IL-6-induced expression of suppressor of cytokine signaling (SOCS3), which blocks the expression of pro-inflammatory IL-6 target genes (Bode *et al.*, 1999). Furthermore, IL-6 promotes an anti-inflammatory environment by regulating the differentiation of recruited T cells towards T_H2 phenotype by inducing the expression of IL-4 (Krishnamoorthy *et al.*, 2007). Importantly, IL-6 also plays a major role in the accumulation of MDSC, as described above.

Besides its effects on immune cells, IL-6 exerts important effects on cancer cells. The activation of the IL-6/STAT3 signaling pathway in the cancer cells supports tumorigenesis by inhibiting apoptosis and promoting survival, proliferation, angiogenesis, invasiveness and metastasis (Kumari *et al.*, 2016). Importantly, IL-6 is upregulated in several different types of cancer, including melanoma, where its increased levels correlated with worse patient outcome, progression of the disease and therapy resistance (Hoejberg *et al.*, 2012). Therefore, IL-6 is considered to be an interesting target for cancer therapy (Q. Liu *et al.*, 2017).

2 Aim of the study

The upregulation of CCR5 expression on MDSC and the accumulation of CCR5 ligands in the melanoma microenvironment led to the recruitment of MDSC to melanoma tumor lesions. Importantly, $CCR5^+$ tumor-infiltrating MDSC show increased expression of PD-L1 and Arg1, as well as increased production of ROS and NO as compared to their $CCR5^-$ counterparts (Blattner *et al.*, 2018). Furthermore, the recruitment of MDSC could be successfully blocked by a CCR5-Ig fusion protein that neutralizes the CCR5 ligands, leading to prolongation of survival of melanoma bearing *RET* transgenic mice (Blattner *et al.*, 2018). However, the mechanisms leading to CCR5 upregulation on MDSC and making CCR5-dependend MDSC recruitment possible were poorly studied. In addition, the mechanisms inducing an increased immunosuppressive phenotype in $CCR5^+$ MDSC were not investigated.

Therefore, the aims of this thesis were to study the molecular mechanisms of CCR5 upregulation on MDSC in melanoma, to elucidate the link between CCR5 expression and immunosuppressive capacity of MDSC and to block the factors leading to CCR5 upregulation and increased immunosuppressive potential of MDSC in the *RET* transgenic mouse model of malignant melanoma.

We studied the effect of factors, that are increased in the melanoma microenvironment and are involved in the MDSC differentiation, on CCR5 expression by qRT-PCR, Western blot and flow cytometry. Furthermore, we analyzed the molecular mechanisms of CCR5 upregulation *in vitro*. We also evaluated the activity of these pathways in the *RET* transgenic mouse melanoma model *ex vivo* by flow cytometry and ELISA. We investigated the differences in immunosuppressive capacity between $CCR5^+$ and $CCR5^-$ tumor-infiltrating MDSC using suppression of T cell proliferation assay and microarray analysis and tested the capacity of the CCR5 ligands to stimulate increased immunosuppressive capacity of $CCR5^+$ MDSC. Furthermore, we studied the effect of IL-6 on immunosuppressive capacity of MDSC since IL-6 was the main factor to upregulate CCR5 and to increase immunosuppression. Finally, we investigated the effects of IL-6 *in vivo* by subcutaneous (s.c) injection of IL-6 overexpressing (OE) Ret melanoma cells and by the application of anti-IL-6 monoclonal antibodies in the *RET* transgenic melanoma model.

3 Material

3.1 Technical equipment

Device	Manufacturer
Balance BP 3100P	Sartorius
Cell culture incubator Hera cell 150	Heraeus
Centrifuge Biofuge primo R	Heraeus
Centrifuge Labofuge 400R	Heraeus
Centrifuge MEGAFUGE 40R	Heraeus
Counting chamber Neubauer improoved	Brand
Electrophoresis chamber Mini-PROTEAN® 3 Cell	BioRad
Flow cytometer BD FACSAria™ IIU	Becton Dickinson
Flow cytometer BD FACSLyric™	Becton Dickinson
Fluorescence microscope Eclipse Ti	Nikon
Fridge	Liebherr
Heating Block Thermomixer compact	Eppendorf
Ice machine	Manitowoc
Imaging System Fusion SL	Viber Lourmat
Laminar flow hood Hera safe	Heraeus
Light microscope DM IL	Leica
Magnetic bead column holder MACS® multistand	Miltenyi Biotec
Microplate reader Tecan infinite M200	Tecan
Mr. Frosty™ freezing container	Thermo Fisher
N_2 tank BIOSAFE®	Cryotherm
Pipettes Transferpette	Brand
Power supply PAC HC	BioRad
qPCR cycler MX3005	Stratagene
Refrigerator (-20 °C)	Liebherr
Refrigerator (-80 °C)	Heraeus
Semi dry blotting chamber	BioRad
Thermal Cycler DNA Engine Peltier	BioRad
Vortexer REAX Top	Heidolph

3.2 Computer software

Software	Manufacturer
FACSuite™	Beckton Dickinson
FIJI	SciJava (Schindelin *et al.*, 2012)
FlowJo V10	Becton Dickinson
GraphPad Prism	GraphPad Software
iControl	Tecan
Microsoft Office 365	Microsoft Corporation
MxPro qPCR	Stratagene
TFbind	(Tsunoda and Takagi, 1999)

3.3 Consumables

Consumable	Manufacturer	Order number
15 ml tube	Sarstedt	62.554.502
24-well plate	Sarstedt	83.3922.005
5 ml test tube	Becton Dickinson	352053
50 ml tube	Sarstedt	62.547.254
6 well plate	Sarstedt	83.3920.005
96 well TC plate R	Sarstedt	83.3925
96-well PCR plate	Steinbrenner Laborsysteme	SL-PP96-1
96-well plate F	Sarstedt	82.1581
96-well plate R	Sarstedt	82.1582
Cell culture dish 10x2 cm	Greiner Bio-One	664160
Cell Scraper 25 cm	Sarstedt	83.1830
Cell strainer 100 µm	Neolab	21008-950
Cell strainer 40 µm	Neolab	21008-949
Cryovial 1.8 ml, sterile	Sarstedt	72.379
MACS® LS colums	Miltenyi Biotec	130-042-401
MACS® MS colums	Miltenyi Biotec	130-042-201
Microscopy slides	VWR	48311-703
Needles 27G ¾	Becton Dickinson	302200
Needles 30G ½	Becton Dickinson	305106

Consumable	Manufacturer	Order number
PCR stripes 0,2 ml	Sarstedt	72.991.992
PCR tubes 0,2 ml	Sarstedt	72.737.992
Pipette Filter Tips 10 µl	Sarstedt	70.1116.210
Pipette Filter Tips 1000 µl	Sarstedt	70.762.211
Pipette Filter Tips 200 µl	Sarstedt	70.760.211
Pipette tips 10 µl	Sarstedt	70.1130.600
Pipette tips 1000 µl	Sarstedt	70.760.452
Pipette tips 200 µl	Sarstedt	70.762.100
PVDF Transfer membrane	Thermo Fisher	88520
Reaction tube 1.5 ml	Eppendorf	0030120086
Reaction tube 2.0 ml	Eppendorf	0030120094
Serological pipette 10 ml	Sarstedt	86.1254.001
Serological pipette 25 ml	Sarstedt	86.1685.001
Serological pipette 5 ml	Sarstedt	86.1253.001
Syringe 1 ml	Becton Dickinson	300013
Syringe 10 ml	Becton Dickinson	309110
T75 cell culture flask	Sarstedt	83.3911
ThickBlot Filter Paper	BioRad	1703
Transfer pipette	Sarstedt	86.1171
Transwell inserts 8 µm	Sarstedt	83.3932.800

3.4 Chemicals, solvents and reagents

Reagent	Manufacturer	Order no.
2-propanol	Sigma-Aldrich	I9516
2-β-mercaptoethanol (50 mM)	Thermo Fisher	31350-010
4x Laemmli sample buffer	Bio-Rad	161-0747
7AAD	Becton Dickinson	559925
ACK Lysing Buffer	Thermo Fisher	A1049201
Albumin	Carl Roth	3737.3
Ammonium persulfate (APS)	Bio-Rad	1610700
Carboxyfluorescein succinimidyl ester (CFSE)	Biolegend	423801
CellROX™ Deep Red reagent	Thermo Fisher	C10422

Reagent	Manufacturer	Order no.
Collagenase	Sigma-Aldrich	C0130
DAF-FM DA (NO detection reagent)	Cayman Chemical	18767
DAPI	Thermo Fisher	D1306
Dimethyl sulfoxide (DMSO)	Carl Roth	A994.1
DMEM medium	Thermo Fisher	12491015
DNase	Siga-Aldrich	D5025
Dulbecco's phosphate-buffered saline (DPBS)	Thermo Fisher	14190250
Dynabeads™ Mouse T-Activator CD3/CD28	Thermo Fisher	11452D
Ethanol	Carl Roth	9065.1
Fetal bovine serum (FBS)	Merck	TMS-013-B
Fixable viability stain 700	Becton Dickinson	564997
Fluorescence mounting medium	Sigma-Aldrich	F4680
Glycin	Carl Roth	3908.1
Heparin-natrium-25000 units	Ratiopharm	N68542.04
HEPES (1 M)	Thermo Fisher	15630080
Histopaque® 1119	Sigma Aldrich	11191
MEM non-essential amino acids	Thermo Fisher	11140050
Methanol	Carl Roth	4627.4
NaCl	Carl Roth	9265.1
NaN_3	Carl Roth	K305.1
Penicillin/streptomycin (P/S)	Thermo Fisher	15140-122
Protease inhibitor cocktail 50x	Promega	G6521
Puromycin	Thermo Fisher	A11138-03
RIPA Lysis Buffer 10x	Merck	20-188
RNase out	Thermo Fisher	10777019
RPMI 1640 medium	Thermo Fisher	11875101
Sodium dodecyl sulfate (SDS)	Carl Roth	3029.1
Sodium pyruvate	Thermo Fisher	11360-03
Stattic	Sigma-Aldrich	S7947
TEMED	Bio-Rad	1610800
Tris(hydroxymethyl)-aminomethan (Tris)	Carl Roth	0188.3
Trypan blue solution	Sigma-Aldrich	T8154

Reagent	Manufacturer	Order no.
Trypsin	Thermo Fisher	15400054
Tween 20	Sigma-Aldrich	P9416
UltraPure™ 0.5 M EDTA	Thermo Fisher	15575020
X-tremeGENE™ solution	Sigma-Aldrich	636624400

3.5 Anti-mouse antibodies

3.5.1 Unconjugated antibodies

Specificity	Clone	Manufacturer	Order no.	Dilution
CCR5	645807	RnD Systems	MAB6138	1:1000
CD28	37.51	eBioscience	553294	1:10000
CD3	17A2	eBioscience	100201	1:10000
GAPDH	1D4	BioLegend	919501	1:2000
pSTAT3	polyclonal	Cell signaling technology	9131	1:500

3.5.2 Conjugated antibodies

Specificity	Conjugate	Clone	Manufacturer	Order no.	Dilution
Arg1	APC	polyclonal	RnD Systems	IC5868A	1:100
CCR5	Ax488	HM-CCR5	BioLegend	107008	1:100
CCR5	BB515	C34-3448	Becton Dickinson	565093	1:100
CCR5	BV605	C34-3448	Becton Dickinson	743697	1:100
CD11b	APC-Cy™ 7	M1/70 BD	Becton Dickinson	557657	1:200
CD11c	APC	HL3	Becton Dickinson	561119	1:50
CD25	BB515	PC61	Becton Dickinson	564458	1:50
CD3	PerCP-Cy5.5	145-2C11	Becton Dickinson	551163	1:100
CD4	PE-Cy™ 7	RM4-5	Becton Dickinson	552775	1:100
CD45	V500	30-F11	Becton Dickinson	561487	1:100
CD69	PE	H1.2F3	Becton Dickinson	561932	1:100
CD8a	APC-Cy™ 7	53-6.7	Becton Dickinson	557654	1:100
CD8a	eFluor450	53-6.7	Thermo Fisher	48-0081-82	1:100
F4/80	APC-R700	T45-2342	Becton Dickinson	565787	1:50
FoxP3	Ax647	MF23	Becton Dickinson	560402	1:100

Specificity	Conjugate	Clone	Manufacturer	Order no.	Dilution
gp130	PE	4H1B35	BioLegend	149403	1:50
Gr1	PE-Cy™ 7	RB6-8C5	Becton Dickinson	565033	1:800
IL-6R	APC	D7715A7	BioLegend	115811	1:50
Ly6C	PE	AL-21	Becton Dickinson	560592	1:100
Mouse IgG	HRP	polyclonal	Sigma-Aldrich	A9044	1:10000
p-p38 MAPK	PE	36/p38	Becton Dickinson	562065	1:30
pCD247	PE	K25-407.69	Becton Dickinson	558448	1:100
PD-1	BV421	EH12.1	Becton Dickinson	562584	1:100
PD-L1	BV421	MIH5	Becton Dickinson	564716	1:100
pNFκB	PE	K10-895.12.50	Becton Dickinson	558423	1:30
pSTAT3	PE	4/P-STAT3	Becton Dickinson	562072	1:30
Rat IgG	Ax488	polyclonal	Dianova	711545152	1:500
Rat IgG	HRP	polyclonal	Sigma-Aldrich	919501	1:2000

3.5.3 Therapeutic antibodies for mice

Name	Clone	Company	Order no.	Concentration
Anti-PD-1	RMP1-14	BioXcell	BE0146	12,5 mg/kg
Rat IgG2A	2A3	BioXcell	BE0089	12,5 mg/kg
Anti-IL-6	MP5-20F3	BioXcell	BE0046	10 mg/kg
Rat IgG1	HRPN	BioXcell	BE088	10 mg/kg

3.6 TLR ligands

All TLR ligands were ordered at InvivoGen.

Ligand	Order no.	Final concentration
LPS	tlrl-epelps	5 µg/ml
Pam3CSK3	tlrl-pms	1 µg/ml
R848	tlrl-r848	1 µg/ml

3.7 Cytokines, chemokines and growth factors

All cytokines, chemokines and growth factors were ordered at PeproTech and were murine recombinant proteins.

Factor	Order no.	Final concentration
CCL3	250-09	20 ng/ml
CCL4	250-32	20 ng/ml
CCL5	250-07	20 ng/ml
GM-CSF	315-03	40 ng/ml
IFN-γ	315-05	10 ng/ml
IL-1β	211-11B	40 ng/ml
IL-6	216-16	40 ng/ml

3.8 Commercial kits

Kit	Manufacturer	Order no.
$CD8a^+$ T cell isolation Kit, mouse	Miltenyi Biotec	130-104-075
ELISA MAX™ Deluxe Set Mouse IL-6	BioLegend	431304
FoxP3/Transcription Factor Fixation/Permeabilization Kit	eBioscience	00-5512-00
Myeloid-Derived Suppressor Cell Isolation Kit, mouse	Miltenyi Biotec	130-094-538
Pierce® BCA Protein Assay Kit	Thermo Fisher	23225
Pierce® ECL Western Blotting Substrate	Thermo Fisher	32106
RNase-Free DNase Set	QIAGEN	79254
RNeasy Mini Kit	QIAGEN	74104
SensiFAST™ cDNA Synthesis Kit	Bioline	BIO-65053
SensiFAST™ SYBR® No-ROX Kit	Bioline	BIO-98005
Bio-Plex® Cell Lysis Kit	BioRad	171-304011
Pierce™ BCA Protein Assay Kit	Thermo Fisher	23225
Arginase Activity Assay Kit	Sigma-Aldrich	MAK112

3.9 Buffers and media

Buffer/medium	Composition
10 x Running buffer	30 g Tris base
	144 g Glycine
	10 g SDS
	1 l H_2O

Buffer/medium	**Composition**
10 x Phosphate-buffered saline (PBS)	80 g NaCl 2 g of KCl 14.4 g Na_2HPO_4 2.4 g KH_2PO_4 1 l H_2O Adjusted to pH 7.4.
10 x Tris-buffered saline (TBS)	24 g Tris base 88 g NaCl 1 l H_2O
10 x Transfer buffer	30 g Tris base 144 g Glycine 1 l H_2O
10 % Polyacrylamide separating gel	21.3 ml H2O 13.3 ml 30 % Acrylamide solution 5.3 ml 3 M Tris/HCl 400 µl 10 % SDS 133 µl 10 % APS 10 µl TEMED
MSC medium	500 ml RPMI Medium 10 % heat inactivated FBS 1 % P/S 10 mM Sodium Pyruvate

Buffer/medium	Composition
MDSC medium	500 ml RPMI Medium 10 % heat inactivated FBS 1 % P/S 10 mM HEPES 1 mM Sodium Pyruvate 50 µM β-mercaptoethanol 1 mM MEM non-essential amino acids
FACS buffer	1x PBS 2 % heat inactivated FBS 0.2 % NaN_3
MACS buffer	1x PBS 0,5 % BSA 2 mM EDTA
Polyacrylamide stacking gel	6 ml H_2O 1.32 ml 30 % Acrylamide solution 2.5 ml 0.5 M Tris/Hcl 100 µl 10 % SDS 100 µl 10 % APS 10 µl TEMED
TBS-T	100 ml 10 x TBS 900 ml H_2O 1 ml Tween 20

3.10 Mouse primers

All primers were ordered as oligonucleotides from Metabion.

Gene	Forward primer	Reverse Primer
Arg1	GCTGTCTTCCCAAGAGTTGGG	ATGGAAGAGACCTTCAGCTAC
Ccr5	TGGGCTCACTATGCTGCAAA	TCACCCCAAAGTTGACCGTT

Gene	Forward primer	Reverse Primer
Cox2	TCTGGAACATTGTGAACAACATC	AAGCTCCTTATTTCCCTTCACAC
Ido1	AGGATCCTTGAAGACCACCA	CCAATAGAGAGACGAGGAAG
Il10	ATAACTGCACCCACTTCCCA	GGGCATCACTTCTACCAGGT
Il6	TTCCATCCAGTTGCCTTCTTG	GAAGGCCGTGGTTGTCACC
Nos2	TTGGGTCTTGTTAGCCTAGTC	TGTGCAGTCCCAGTGAGGAAC
Pdl1	TGGACAAACAGTGACCACCAA	CCCCTCTGTCCGGGAAGT
Rn18s	CGCGGTTCTATTTTGTTGGT	AGTCGGCATCGTTTATGGTC
S100a8	GGAAATCACCATGCCCTCTACAA	ATGCCACACCCACTTTTATCACC
S100a9	GGAGCGCAGCATAACCACCATC	GCCATCAGCATCATACACTCCTCA
Tgfb1	GGATACCAACTATTGCTTCAGCTCC	AGGCTCCAAATATAGGGGCAGGGTC

3.11 Plasmids

pLenti-GIII-CMV-C-term-HA IL-6 overexpression (OE) plasmid

pLenti-GIII-CMV-C-term-HA empty vector (EV)

pCMV-VSV-G

pCMV-dR 8.91

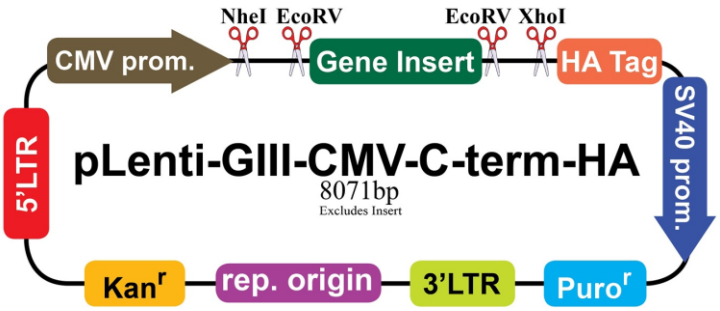

Figure 5. Vector map of pLenti-GIII-CMV-C-term-HA used for IL-6 overexpression (OE).
The gene insert (IL-6, accession number: NM_031168) is expressed under the CMV promoter and the vector contains a Kanamycin and a Puromycin resistance for selection of bacteria and mammalian cells (source: www.abmgood.com).

3.12 Mice and cell lines

RET transgenic mice with C57BL/6 background were provided by Dr. I. Nakashima (Chubu University, Aichi, Japan) (Kato *et al.*, 1998) and bred at the animal facility of the German Cancer Research Center (DKFZ) in Heidelberg. C57BL/6 wild type mice were provided by the DKFZ animal facility (non-transgenic litter mates) or Janvier Labs. Murine Ret melanoma cell line was established from skin melanomas isolated from *RET* transgenic mice (Zhao *et al.*, 2009). Furthermore, immortalized myeloid suppressor cell line (MSC-)2 was kindly provided by Dr. S. Ugel (University of Verona, Verona, Italy) (Apolloni *et al.*, 2000).

4 Methods

4.1 *In silico* analysis of the *Ccr5* and *Arg1* promoters

The murine *Ccr5* and *Arg1* gene sequences were extracted from the NCBI database (Gene-ID: 12774 (*Ccr5*) and 11846 (*Arg1*)) and the TFbind online tool was used to search for STAT3 binding sites in the two *Ccr5* promoters that are located upstream of the transcription start site and in the first intron (Mummidi *et al.*, 1997), as well as in the *Arg1* promoter/enhancer that is located upstream of the transcription start site (Pauleau *et al.*, 2004).

4.2 Cell counting

For determination of the cell number, 10 µl of single cell suspension were diluted 1:10 in Trypan blue. Cells were counted after transferring 10 µl of the solution into a Neubauer chamber. Only alive cells, that were Trypan blue negative, were counted. Total number of alive cells per ml was calculated by the following formula.

$$alive\ cell\ number\ per\ ml = \frac{counted\ number\ of\ Trypan\ blue\ negative\ cells}{number\ of\ counted\ squares} * 10^4 * dilution\ factor$$

4.3 Expansion of cell lines

MSC-2 and Ret cells were cultured in T75 flasks at 37 °C and 5 % CO_2 in MSC medium or RPMI 1640 containing 10 % FBS and 1 % P/S, respectively. Before reaching 100 % confluency, cells were passaged. MSC-2 cells grow partly in suspension and partly adherent, resembling the heterogeneous MDSC population. The cells growing in suspension were collected in a 50 ml tube and adherent cells were detached with a cell scraper in 10 ml sterile PBS. Subsequently, both cell populations were combined again. After removing the culture medium, Ret cells were detached by incubating them for 5 min at 37 °C in 2 ml 1x Trypsin containing 5 mM EDTA. Trypsinization was stopped by addition of 10 ml RPMI 1640 medium and cells were transferred into a 50 ml tube. Cells were pelleted by centrifugation at 300 g for 5 min, supernatant was discarded, and cells were resuspended in 10 ml of the respective medium. Cells were split 1:10 into a new T75 flask in 20 ml medium for further cultivation, while the rest of the cells was counted and used for stimulation and further downstream analysis.

4.4 Cell line freezing and thawing

For cryopreservation of cell lines, cells from one 80 to 90 % confluent T75 flask were harvested and resuspended in 2.5 ml of the respective medium. 2.5 ml of freezing solution (20 % DMSO, 80 % FBS) were added to the cells and mixed gently. 1 ml each was immediately distributed to five freezing tubes and frozen to -80 °C in a Mr. Frosty™ freezing container filled with isopropanol. After 24 h, cryovials were transferred to the liquid nitrogen tank for long term storage.

Frozen cells were thawed quickly in the 37 °C water bath and immediately transferred into a T75 flask containing 20 ml of respective medium for culture at 37 °C and 5 % CO_2. Cells were used for *in vitro* experiments between passage 2 and passage 10 after thawing and for *in vivo* experiments between passage 2 and 3 after thawing.

4.5 Lentiviral transduction of Ret melanoma cells

HEK293T cells were used for lentiviral particle production at the DKFZ Heidelberg by Dr. L. Hüser. For transfection, the OE plasmid containing the IL-6 sequence (11 µg) was incubated with the packaging plasmids pCMV-VSV-G (5.5 µg) and pCMV-dR 8.91 (8.25 µg) in DMEM and X-tremeGENE™ solution for 30 min and added to HEK293T producer cells. The respective EV, without the IL-6 sequence, was transfected as a control. After incubation for 12 h, the supernatant was discarded. After further 12, 24 and 36 h the supernatant was collected, and virus particles were concentrated by ultracentrifugation. Then, murine Ret melanoma cells were incubated with concentrated virus for 24 h. After the first infection, Ret cells were re-infected with the same virus in fresh medium. After 48 h of transduction, the cells were washed twice with PBS and cultured at 37 °C and 5 % CO_2. To select transduced cells, 2 µg/ml puromycin were added for 3 days. After 3 days, cells were expanded and cryopreserved. Furthermore, the overexpression of IL-6 was validated by qRT-PCR and ELISA.

4.6 Isolation of primary murine cells

4.6.1 Mouse breeding and keeping

All mouse work was performed according to German legal and ethical standards and approved by or reported to the local authorities (Regierungspräsidium Karlsruhe). *RET* transgenic mice were bred at the animal facility of the DKFZ in Heidelberg under specified pathogen free (SPF) conditions (approval numbers G-4/14 and G-40/19). *RET* transgenic mice and wild type litter mates were then transported to and kept under SPF conditions at the animal facility of the Zentrum für Medizinische Forschung (ZMF) Mannheim and monitored two

to three times per week. For organ preparation, mice were sacrificed by cervical dislocation or by asphyxiation with CO_2 (internal approval number I-17/20).

4.6.2 Bone marrow cell isolation

Femur and tibiae were isolated by surgical cutlery, cleaned with an ethanol wetted tissue and cut at both ends under sterile conditions. Bone marrow was flushed out with PBS using a 10 ml syringe with a 27G needle. Cells were filtered through a 100 µm cell strainer and washed with PBS at 300 g for 5 min. Red blood cells were lysed with 1 ml ACK lysis buffer for 4 min at room temperature (RT). PBS was used to stop the reaction and cells were washed at 300 g for 5 min. The pellet was resuspended in appropriate buffer for further analysis.

4.6.3 Splenocyte isolation

Mouse spleen was isolated by surgical cutlery and collected in a tube with PBS. Spleen was washed once with sterile PBS and single cell suspension was obtained by cutting the spleen in small pieces and smashing it with a plunger through a 100 µm cell strainer. Cells were washed with PBS at 300 g for 5 min. Red blood cells were lysed with 2 ml ACK lysis buffer for 4 min at RT. PBS was used to stop the reaction and cells were washed at 300 g for 5 min. The pellet was resuspended in appropriate buffer for further analysis.

4.6.4 Metastatic lymph node preparation

In *RET* transgenic mice all lymph nodes (LN) are black, contain melanin producing tumor cells and are therefore metastatic LN by definition. LN from the inguinal, axillary and head region were extracted and smashed with a plunger through a 100 µm cell strainer. The strainer was then washed with PBS to collect all cells. The cells were washed with PBS at 300 g for 5 min and resuspended in appropriate buffer for further analysis.

4.6.5 Skin tumor preparation

Skin tumors from melanoma bearing mice were excised, weighed and smashed through a 100 µm cell strainer by a plunger into a 50 ml falcon tube for FACS analysis. For FACS sorting and intracellular pSTAT3 staining, the tumors were first digested for 30 min at 37 °C and 5 % CO_2 with 1 mg/ml collagenase and 10 µg/ml DNase in PBS before smashing them through a 100 µm cell strainer. After the depletion of the erythrocytes with 1 to 5 ml of ACK lysis buffer for 5 min at RT, cells were washed with PBS at 300 g for 5 min and resuspended in an appropriate buffer for further analysis.

4.6.6 Cryopreservation of murine tumor and serum

Skin tumors from melanoma bearing mice were excised, weighed and an approximately 0.5 cm big piece was put in a 1.5 ml tube, immediately snap frozen in liquid nitrogen and stored at -80 °C. Peripheral blood was obtained by cardiac puncture with a heparin-wetted syringe. Per mouse, 0.2 to 0.8 ml of blood was collected. Whole blood was centrifuged at 1200 g for 10 min, serum was collected in a new 1.5 ml tube, immediately snap frozen in liquid nitrogen and stored at -80 °C.

4.6.7 Lysis of murine tumor for protein analysis

For the lysis of murine tumor samples for protein analysis the Bio-Plex® cell lysis kit was used according to the manufacturer's instructions. Briefly, 4 µl factor 1, 2 µl factor 2 and 4 µl phenylmethylsulfonylfluoride (PMSF, 500 mM stock) were added to 1 ml lysis buffer. 250 µl of lysis buffer were added to the tumor sample, which was thawed on ice before, and the tissue was disrupted with a pestel. After 5 min of incubation on ice and 10 min incubation at -80 °C the sample was again thawed on ice and subsequently sonicated for 10 min. After centrifugation at 4500 g for 4 min the supernatant was directly used for protein analysis or stored again at -80 °C.

4.7 MDSC *in vitro* differentiation

The protocol for MDSC *in vitro* differentiation was established as published (Marigo *et al.*, 2010). Briefly, bone marrow cells were isolated and $2.5x10^6$ cells were cultured in 10 ml MDSC medium supplemented with 40 ng/ml GM-CSF plus 40 ng/ml IL-6 (for MDSC differentiation) or 40 ng/ml GM-CSF only (as a control) for four days in a 10 cm cell culture dish at 37 °C and 5 % CO_2. At day 4, the cells were harvested. The *in vitro* differentiated MDSC grow partly in suspension and partly adherent, resembling the heterogeneous MDSC population. The cells growing in suspension were collected in a 50 ml tube and adherent cells were detached in 10 ml sterile PBS using a cell scraper. Subsequently, the two cell populations were combined, washed once with PBS, centrifuged for 5 min at 300 g and resuspended in the respective medium or buffer for downstream analysis.

4.8 Magnetic-activated cell sorting (MACS)

4.8.1 MACS of $CD8^+$ splenic T cells

Murine splenocytes were isolated and $CD8^+$ T cells were isolated by the $CD8a^+$ T cell isolation Kit (mouse) from Miltenyi Biotec according to the manufacturer's instructions. With this kit, the $CD8^+$ T cells are isolated by negative selection.

4.8.2 MACS of $Gr1^+$ IMC

Murine bone marrow cells were isolated and the Myeloid-Derived Suppressor Cell Isolation Kit (mouse) from Miltenyi Biotec was used according to the manufacturer's instructions to isolate $Gr1^+$ cells. With this kit, the immature myeloid cells (IMC) are isolated from wild type bone marrow by two rounds of positive selection, first for $Ly6C^+$ and then for $Gr1^+$. At the end, these monocytic and polymorphonuclear populations were combined to further analyze the mixed IMC population as a whole.

4.9 Isolation of tumor-infiltrating MDSC

4.9.1 Isolation of TIL

Single cell suspension was obtained from murine melanoma tumor including the collagenase/DNase digest. Cells were resuspended in 6 ml of PBS per 200 mg tumor and put in a 15 ml falcon. The 6 ml were underlaid with 4 ml of Histopaque® 1119 and centrifuged at 400 g for 30 min at RT without break. The leukocytes assembled as a white ring at the interface between Histopaque® 1119 and PBS and were collected by a plastic Pasteur pipette, washed with PBS and resuspended in 50 µl FACS buffer per $1x10^6$ cells.

4.9.2 FACS sorting of tumor-infiltrating MDSC

Cells were subjected to Fc block and FACS staining as described later and then resuspended in 1 ml of FACS buffer. $CCR5^+$ and $CCR5^-CD45^+CD11b^+Gr1^+$ MDSC were sorted at the BD FACSAria™ IIU cell sorter at the FlowCore Mannheim. Importantly, sorting was performed at room temperature and cells were collected into 10 ml prewarmed MDSC medium supplied with 20 % FBS. Sorted cells were centrifuged at 300 g for 5 min and resuspended in medium or buffer for further analysis.

4.10 RNA isolation

Total RNA was isolated from $2x10^6$ (MSC-2, *in vitro* differentiated MDSC), $3x10^6$ (IMC) or about $1x10^6$ (FACS sorted tumor-infiltrating MDSC) cells using the RNeasy Mini kit from Qiagen. DNA digest was performed using the on-column RNase-free DNase set from Qiagen according to manufacturer's instructions. RNA was eluted in 25 µl of RNase-free water. After RNA isolation, RNA concentration was determined with the microplate reader Tecan Infinite M200 using a Nanoquant plate. RNA was stored at -80 °C until further use.

4.11 cDNA synthesis and qRT-PCR

RNA concentrations were adjusted to be the same and up to 1 µg of RNA was used for cDNA synthesis using the SensiFAST cDNA synthesis kit from Bioline according to the manufacturer's instructions. A noRT control, containing RNA but no reverse transcriptase, and a H_2O control, containing reverse transcriptase but no RNA, were included, to exclude genomic DNA contamination in the RNA preparation or contamination of the reagents.

Working on ice, cDNA and controls were diluted 1:55 in RNase-free water. Forward and reverse primers (2 µM) were mixed in equal parts. A master mix was prepared, containing 10 µl diluted cDNA, 7 µl primer mix and 17 µl SensiFAST™ SYBR® Lo-ROX Kit from Bioline. 10 µl of this master mix were applied to three wells of a 96-well qPCR plate in triplicates. The plate was sealed, and samples were analyzed by the Stratagene MX3005P qPCR machine using the temperature conditions displayed in Table 1. To allow normalization, mRNA levels for the gene of interest and a house keeping gene were quantified for each sample.

Step	Temperature	Time	Cycles
1	50 °C	2 min	1
2	95 °C	10 min	1
3	95 °C 59 °C	30 s 1 min	42
4	95 °C	1 min	1
5	65 °C	30s	1
6	95 °C	30 s	1

Table 1. Thermocycler program for qRT-PCR.
During steps 1 to 3, the cDNA was amplified and SYBR green fluorescence was measured. After the additional denaturation step 4, the samples were heated from 65 °C to 95 °C in steps 5 and 6 and the denaturation curve for the respective primers was recorded.

4.12 Microarray

RNA was isolated and 1 µl of RNAse out was added after elution in 25 µl RNase-free water. RNA was submitted to the genomics and proteomics core facility of the DKFZ Heidelberg for

microarray. The Affymetrix GeneChip™ Mouse Gene 2.0 ST Array from Thermo Fisher was used according to the manufacturer's instructions.

The data were submitted to Dr. Carsten Sticht (ZMF Mannheim) for bioinformatics and statistics. A Custom CDF Version 22 with ENTREZ based gene definitions was used to annotate the arrays (Dai *et al.*, 2005). The raw fluorescence intensity values were normalized applying quantile normalization and robust multiarray analysis (RMA) background correction. Before performing the ANOVA, a batch normalization was used to remove the individual mouse variations. An ANOVA was performed to identify differentially expressed genes using a commercial software package SAS JMP Genomics, version 7, from SAS (SAS Institute, Cary, NC, USA). A false positive rate of a=0.05 with false discovery rate (FDR) correction was taken as the level of significance.

Gene Set Enrichment Analysis (GSEA) was used to determine whether defined lists (or sets) of genes exhibit a statistically significant bias in their distribution within a ranked gene list using the software GSEA (Subramanian *et al.*, 2005). Pathways belonging to various cell functions such as cell cycle or apoptosis were obtained from public external databases (KEGG, http://www.genome.jp/kegg).

4.13 Protein isolation

$5x10^6$ MSC-2 cells were seeded in 3 ml MSC medium into a 6-well plate and stimulated or left untreated. Cells were detached using a cell scraper and transferred to two 2 ml reaction tubes. Wells were washed with 1 ml sterile PBS. The cell suspension was centrifuged at 300 g for 5 min. Afterwards, the cell pellet was resuspended in 300 µl RIPA buffer containing 1x protease inhibitor cocktail. Cells were lysed for 30 min at 4 °C under continuous rotation. Lysates were centrifuged at 16000 g for 10 min at 4 °C. The supernatant was transferred to new 1.5 ml reaction tubes and stored at -20 °C.

4.14 Bicinchoninic acid (BCA) assay

For determining protein concentration, the Pierce® BCA Protein Assay Kit was used. The albumin standard was diluted in PBS to final concentrations of 2000 µg/ml, 1500 µg/ml, 1000 µg/ml, 750 µg/ml, 250 µg/ml, 125 µg/ml and 25 µg/ml protein. To measure protein concentration, 10 µl of each sample, each standard dilution and a blank was pipetted into a flat bottom 96-well plate in duplicates. To each well 200 µl of a 1:50 dilution of BCA reagent B in BCA reagent A was added, and the plate was incubated in the dark for 30 min at 37 °C, shaking. After incubation, the absorbance at 562 nm was measured using the Tecan Infinite M200 microplate reader.

4.15 Gel electrophoresis

After determining the protein concentration, concentrations of samples were equalized and samples were mixed 1:4 with 4x Lämmli buffer and boiled at 95 °C for 5 min. Samples were loaded on a 10 % sodium dodecylsulphate-polyacrylamide gel electrophoresis (SDS-PAGE) gel, mounted in a gel electrophoresis tank containing 1x running buffer. Electrophoresis was performed at 70 V for approximately 15 min, until the proteins passed the stacking gel. Then, voltage was increased to 100 V and the gel was run until the solvent front reached the lower end of the gel.

4.16 Western blot and immunostaining

After SDS-PAGE, the separated proteins were transferred to a polyvinylidene-difluoride (PVDF) membrane via electroblotting. The membrane was cut to size and activated for 1 min in 100 % methanol. Electroblotting in a semi-dry blotting chamber was performed for 90 min at 60 mA with the gel put onto the membrane and surrounded by filter paper. To block unspecific binding sites, the membrane was incubated for 30 min in 3 % BSA in TBS-T at RT, shaking. Subsequently, the membrane was incubated with the primary antibody diluted in 10 ml 3 % BSA in TBS-T overnight at 4 °C. The membrane was washed three times for 10 min in TBS-T before addition of the corresponding horseradish peroxidase (HRP)-conjugated secondary antibody diluted in 10 ml 3 % BSA in TBS-T. The membrane was incubated for 1 h at RT, shaking. After washing for three times in TBS-T for 10 min, the membrane was incubated for 1 min in Pierce® ECL Western Blotting Substrate at RT. Chemiluminescence was detected using the Fusion SL detection device.

4.17 Flow cytometry analysis

4.17.1 Extracellular staining

Between $2x10^5$ and $2x10^6$ cells were put per well into a 96 well plate with round bottom. Cells were washed (300 g, 5 min, 4 °C) with PBS and the pellet was resuspended in 50 µl PBS containing 1:100 7AAD, if cells were only extracellularly stained, or 1:200 fixable viability dye (FVD) 700, if subsequent intracellular staining was planned. Cells were incubated for 15 min at 4 °C in the dark before washing with 150 µl of PBS. The cell pellet was then resuspended in 50 µl FACS buffer containing 1:200 Fc block, to block unspecific binding of antibodies via the Fc receptors on cells. Fc block was incubated for 15 min at 4 °C in the dark. After washing, cells were resuspended in the master mix containing the conjugated antibodies for extracellular staining and incubated for 30 min at 4 °C in the dark. After washing, the pellet was

resuspended in 100 µl of FACS buffer for subsequent analysis on the BD FACSLyric™ flow cytometer or intracellular staining was performed.

4.17.2 ROS and NO detection by flow cytometry

For the detection of ROS, the CellROX™ Deep Red reagent was diluted 1:500 in PBS and for the detection of NO, the DAF-FM DA reagent was diluted 1:200 in PBS. The cell pellet was resuspended in 50 µl of this mix and incubated for 30 min at 4 °C in the dark. Afterwards the cells were washed with 150 µl of PBS and resuspended in 100 µl PBS. The staining of ROS and NO was always performed after the live/dead staining and the Fc block and in parallel to the extracellular antibody staining. After ROS and NO staining, cells were measured immediately, the latest within one hour, at the BD FACSLyric™ flow cytometer.

4.17.3 Intracellular staining

The FoxP3/Transcription Factor Fixation/Permeabilization kit was used for the fixation and permeabilization of cells for intracellular staining. After extracellular staining was completed, the cell pellet was resuspended in 50 µl of Fix/Perm solution (Fixation/Permeabilization Concentrate 1:4 diluted in Fixation/Permeabilization Diluent) and incubated for 30 min at 4 °C in the dark. After washing the cells with 150 µl of PermWash (10x Permeabilization Buffer diluted 1:10 in ddH_2O), the pellet was resuspended in 50 µl of PermWash containing the antibodies for intracellular staining and cells were incubated for 30 min at RT in the dark. Subsequently, cells were washed with 150 µl of PermWash and resuspended in 100 µl of PermWash for analysis at the BD FACSLyric™ flow cytometer.

4.18 Enzyme-linked immunosorbent assay (ELISA)

The ELISA MAX™ Deluxe Set Mouse IL-6 from BioLegend was used according to the manufacturer's instructions, except for the fact, that all the volumes were divided by two. 50 µl of undiluted murine serum were used as samples, as well as 50 µl of lysate from tumor preparation or different dilutions of cell culture supernatant. For the lysate of the tumor preparation, protein concentration was measured by BCA assay in parallel, to calculate pg IL-6/mg protein.

4.19 Arginase activity assay

To determine arginase activity, $1x10^6$ cells were used per sample and processed according to the manufacturer's instructions of the Arginase Activity Assay Kit from Sigma-Aldrich.

Briefly, cells were washed with PBS and afterwards lysed with 100 µl of 10 mM Tris-HCl (pH 7.4) containing 1x protease inhibitor cocktail. 40 µl of the lysate were incubated together with arginine and manganese in a 96 well flat bottom plate for 2 h at 37 °C and 5 % CO_2, where the arginase in the sample catalyzes the conversion of arginine to urea and ornithine. The produced urea was then detected by the color development reagent that generates a colored product upon the reaction with urea, proportional to the arginase activity present. A urea standard with known concentration, as well as a H_2O control and a blank for each sample were included. After measuring the absorbance at 430 nm at the Tecan Infinite M200 micro-plate reader, the arginase activity was calculated according to the following formula.

$$arginase\ activity\ (units/l) = \frac{A430\ (sample) - A430\ (blank)}{A430\ (standard) - A430\ (water)} * \frac{1\ mM * 50 * 10^3}{40\ \mu l * 120\ min}$$

4.20 Suppression of T cell proliferation assay

$CD8^+$ splenic T cells from normal mice were isolated by MACS. T cells from one spleen were resuspended in 2 ml PBS containing 2 nM of the cell proliferation dye CFSE and incubated for 5 min at 37 °C. T cells were washed with 10 ml MDSC medium at 300 g for 5 min and resuspended in MDSC medium for counting. 80000 T cells were subsequently co-cultured with 80000 stimulated or unstimulated IMC or *in vitro* differentiated MDSC for a 1:1 ratio and with 40000 stimulated or unstimulated IMC or *in vitro* differentiated MDSC for a 1:2 ratio. The co-culture was performed for 72 h at 37 °C and 5 % CO_2 in 200 µl of MDSC medium in a 96 well round bottom plate coated before for 3 h with anti-CD3 and anti-CD8 antibodies (both 1:10000 diluted). After 72 h the cells were stained for CD8 and the proliferation of $CD8^+$ T cells was assessed by measuring the dilution of CFSE staining at the BD FACSLyric™ flow cytometer.

4.21 Migration assay

A transwell assay was applied to determine chemotactic migration capacity of IMC and *in vitro* differentiated MDSC. The transwell system was composed of an insert for a 24-well cell culture plate and thereby creates two chambers separated by a permeable membrane with a pore size of 8 µm. The cells were resuspended in FBS-free MDSC medium and $0.75x10^6$ cells in 200 µl medium were seeded in the upper chamber of the transwell. The lower chamber was filled with 500 µl of FBS-free MDSC medium containing CCL3, -4 and -5 (100 ng/ml each). In a control well, the lower chamber was filled with FBS-free MDSC medium without CCL. After 16 h of incubation at 37 °C and 5 % CO_2, the transwell was removed and the cell number in the lower chamber was determined by the BD FACSLyric™ flow cytometer.

4.22 *In vivo* mouse experiments

4.22.1 Mouse therapy

All mouse work was performed according to German legal and ethical standards and approved by the local authorities (Regierungspräsidium Karlsruhe). *RET* transgenic mice were bred at the animal facility of the DKFZ in Heidelberg under SPF conditions (approval numbers G-4/14 and G-40/19). *RET* transgenic mice and wild type littermates were then transported to and kept under SPF conditions at the animal facility of the ZMF Mannheim and monitored two to three times per week. The first tumors started to develop in week 5 after birth. Upon the first signs of tumors mice were classified and separated into four equal groups containing equal numbers of male and female mice. One group was receiving the isotype control antibodies, the second group was receiving anti-PD-1 therapeutic antibodies, the third group was receiving anti-IL-6 therapeutic antibodies and the fourth group was receiving the combination therapy of anti-PD-1 and anti-IL-6 (approval number G-73/18). Antibodies were injected intraperitoneally (i.p.) in 100 µl of PBS using a 1 ml syringe and a 30G ½ needle. Mice were weighed once per week. Anti-PD-1 was given 12.5 mg/kg mouse and anti-IL-6 was given 10 mg/kg mouse for four weeks, twice per week. Mice were monitored two to three times per week until 100 days after therapy initiation. Mice who displayed one of the termination criteria were sacrificed and recorded as “died”. Survival curves of mice are therefore showing survival until reaching the termination criterion. A second cohort of mice was treated similar, but all mice were sacrificed after four weeks of therapy, and organs and tumors were taken for FACS analysis.

4.22.2 Subcutaneous injection of melanoma cells in mice

C57BL/6 wild type mice were subcutaneously (s.c.) injected with $5x10^5$ Ret cells overexpressing IL-6 or not (approval number G-73/18), using a 1 ml syringe and a 27G ¾ needle. Tumor size of mice was measured by a caliper and recorded three times per week. Upon a tumor length or width of 1.5 cm or another termination criterion, mice were sacrificed and recorded as “died”. Here as well, survival curves of mice are showing survival until reaching the termination criterion. Tumor volume was calculated according to the following formula (Faustino-Rocha *et al.*, 2013).

$$volume = \frac{width^2 * length}{2}$$

4.23 Statistical analysis

Statistical analysis of data was performed using the GraphPad Prism software on at least three biological replicates (different mice) or at least three independent experiments (cell lines). Two groups were compared with the paired or unpaired (depending on the data) two-tailed Student's t test assuming a Gaussian distribution of the data. Survival curves were generated using the Kaplan-Meier method and statistical comparison was done by the Log-rank (Mantel-Cox) test. Bioinformatics and statistics for the microarray analysis were done as described in before (chapter 4.12). For qRT-PCR results, statistics were performed on the ΔCT values and 2^-ΔΔCT values are shown in the graphs.

5 Results

5.1 Molecular mechanisms of CCR5 upregulation on MDSC

5.1.1 *Ccr5* regulation by inflammatory mediators *in vitro*

We used inflammatory mediators, that are known to be increased in the melanoma microenvironment and to play an important role in MDSC development, to stimulate the MSC-2 cell line and $CD11b^+Gr1^+$ IMC isolated by MACS to test the effect on *Ccr5* mRNA expression *in vitro*. We chose the CCR5 ligands CCL3, -4 and -5, the cytokines IFN-γ, IL-6 and IL-1β and the growth factor GM-CSF. In addition, we applied the synthetic TLR ligands LPS (TLR4 ligand), Pam3CSK4 (TLR1/2 ligand) and R848 (TLR7/8 ligand) and tumor-derived extracellular vesicles (EV) isolated from the murine Ret melanoma cell line.

MSC-2 is a murine myeloid suppressor cell line that can be used as a model for MDSC. IMC are the primary cells that can be seen as a precursor of MDSC since the latter cells can develop by pathologic accumulation and activation of IMC.

We observed a significant upregulation of *Ccr5* for MSC-2 stimulation with IFN-γ, GM-CSF and IL-6 (Figure 6A). However, using IL-1β and the CCR5 ligands, CCL3, -4 and -5, we did not detect an upregulation (Figure 6A). Furthermore, no significant upregulation was seen upon stimulation of MSC-2 cells with tumor-derived EV (Figure 6B) or TLR ligands (Figure 6C). Importantly, we were able to reproduce the upregulation of *Ccr5* seen with IFN-γ, IL-6 and GM-CSF in primary IMC (Figure 6D).

Taken together, we could show that *Ccr5* expression can be induced *in vitro* in myeloid cells by stimulation with IL-6, GM-CSF and IFN-γ, which play an important role in MDSC development in the melanoma microenvironment.

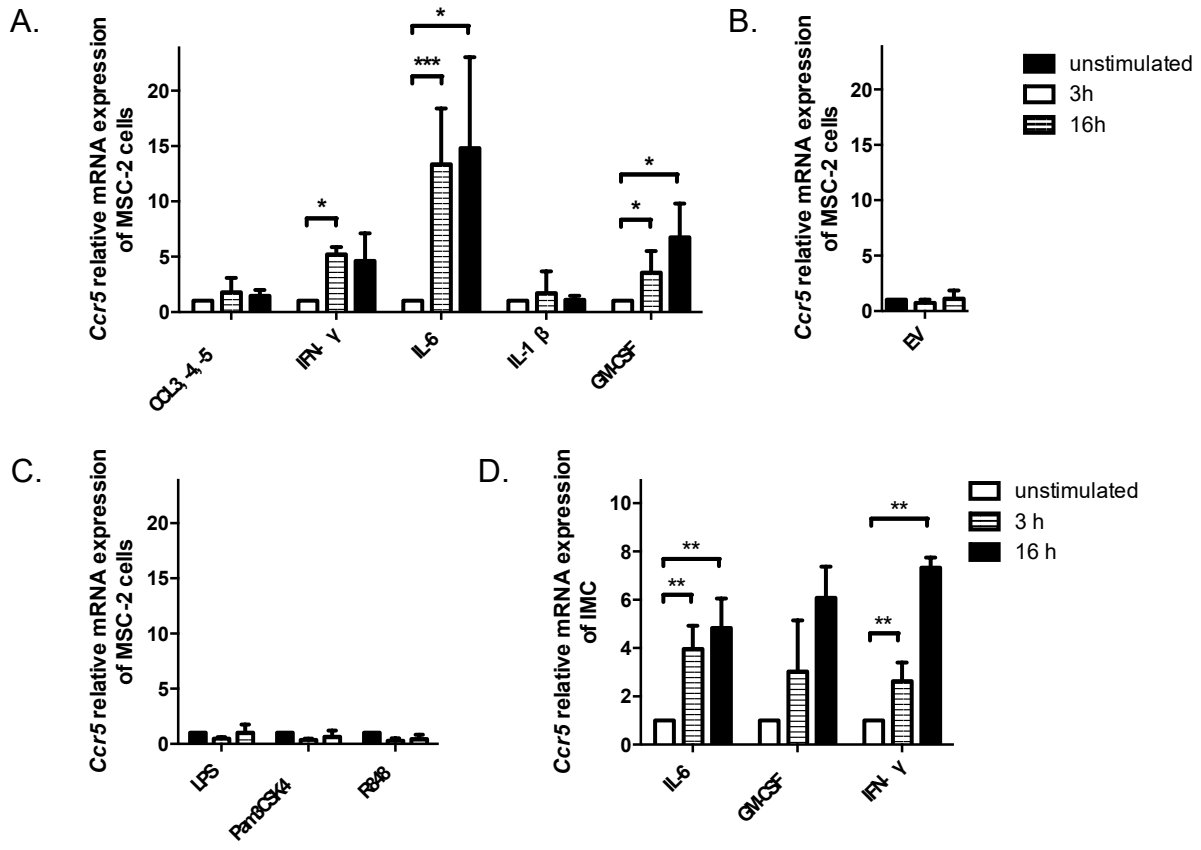

Figure 6. *Ccr5* regulation by factors from the melanoma microenvironment.
MSC-2 cells or immature myeloid cells (IMC) were stimulated for 3 h and 16 h with the inflammatory factors indicated on the x-axis, including the CCR5 ligands, cytokines and growth factors (A. and D.), tumor derived extracellular vesicles (EV) (B.) as well as Toll-like receptor (TLR) ligands (C.) and *Ccr5* mRNA expression was measured by qRT-PCR. Relative expression calculated by the 2^-ΔΔCT method, normalized to the housekeeping gene *Rn18S* and expressed as fold change towards the unstimulated control is shown. Statistics were performed on ΔCT values (mean with SEM, n=3-5, *p<0.05, **p<0.01, ***p<0.001).

5.1.2 Mechanism of IL-6-induced *Ccr5* upregulation

Since IL-6 induced a strong and stable upregulation of *Ccr5*, we aimed at further investigating the molecular mechanism of IL-6-induced *Ccr5* upregulation. As described above (chapter 1.5), the IL-6 signaling is mediated by either soluble or membrane bound IL-6R that binds to IL-6 and forms a complex with homodimerized gp130, which initiates further downstream signaling. To test if the IL-6R and gp130 are expressed by the MSC-2 cell line, we performed a FACS analysis.

After excluding doublets and debris, we gated on the alive cells, composing nearly 90 % of the population, and on $CD11b^+$ cells to verify the myeloid character of the cell line (Figure 7A). As expected, nearly all cells were $CD11b^+$ (Figure 7A). Furthermore, we found a shift of the entire population in comparison to the fluorescence minus one control (FMO) when

stained for IL-6R (Figure 7B) or gp130 (Figure 7C), indicating that all cells express the receptor and the signal transduction component of the IL-6 signaling pathway.

The complex formed by IL-6, IL-6R and the gp130 homodimer, stimulates the activation of JAK family kinases that phosphorylate the transcription factor STAT3. Upon homodimerization, STAT3 then translocates to the nucleus where it can activate target gene expression (Hillmer *et al.*, 2016). Therefore, we hypothesized that the IL-6-induced *Ccr5* upregulation is STAT3 dependent.

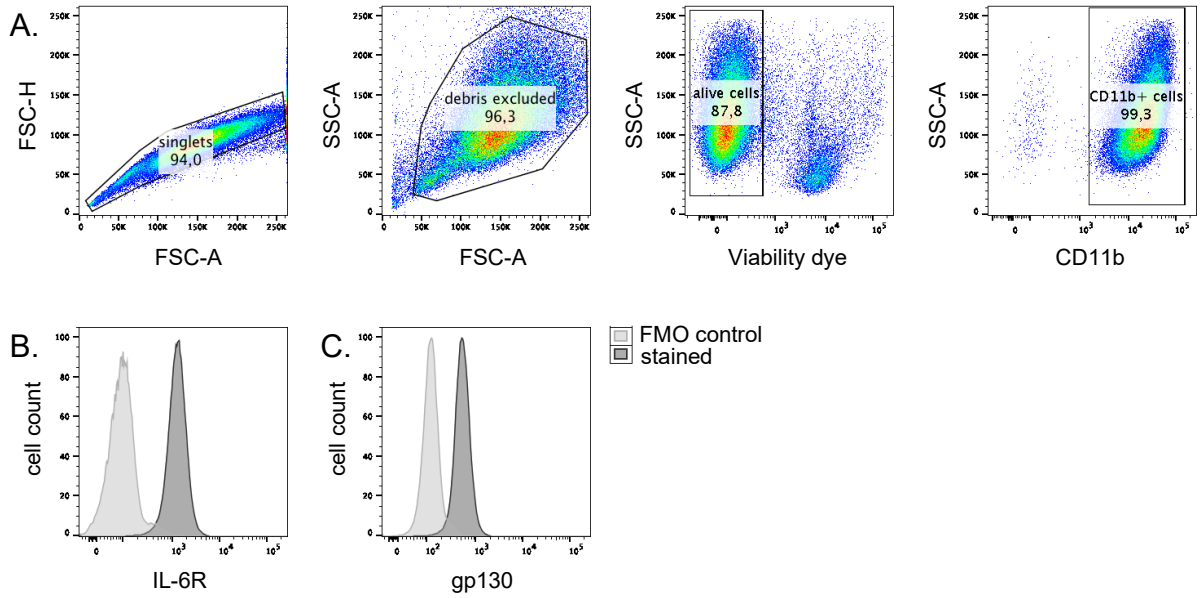

Figure 7. Expression of IL-6R and gp130 by MSC-2 cells.
MSC-2 cells were stained with Fixable viability dye, as well as fluorescently labelled antibodies against CD11b, IL-6R and gp130 and analyzed by flow cytometry. The gating strategy for MSC-2 cells is shown (A.). The expression of IL-6R (B.) and gp130 (C.) are shown as representative histograms in comparison to the fluorescence minus one (FMO) control.

To test this hypothesis, we performed *in silico* analysis for putative STAT3 binding sites in the two murine *Ccr5* promoters located upstream of the transcription start site and in the first intron (Mummidi *et al.*, 1997). Indeed, we found four predicted STAT3 binding sites in the *Ccr5* gene promoters, suggesting that STAT3 could be responsible for IL-6-induced *Ccr5* upregulation (Figure 8A). Moreover, we performed a Western blot with lysates from MSC-2 cells unstimulated or stimulated with IL-6 to analyze phosphorylation of STAT3 upon IL-6 stimulation. We detected increased phosphorylation of STAT3 with IL-6 stimulation, whereas the CCR5 protein level remained unchanged until 24 h of stimulation (Figure 8B).

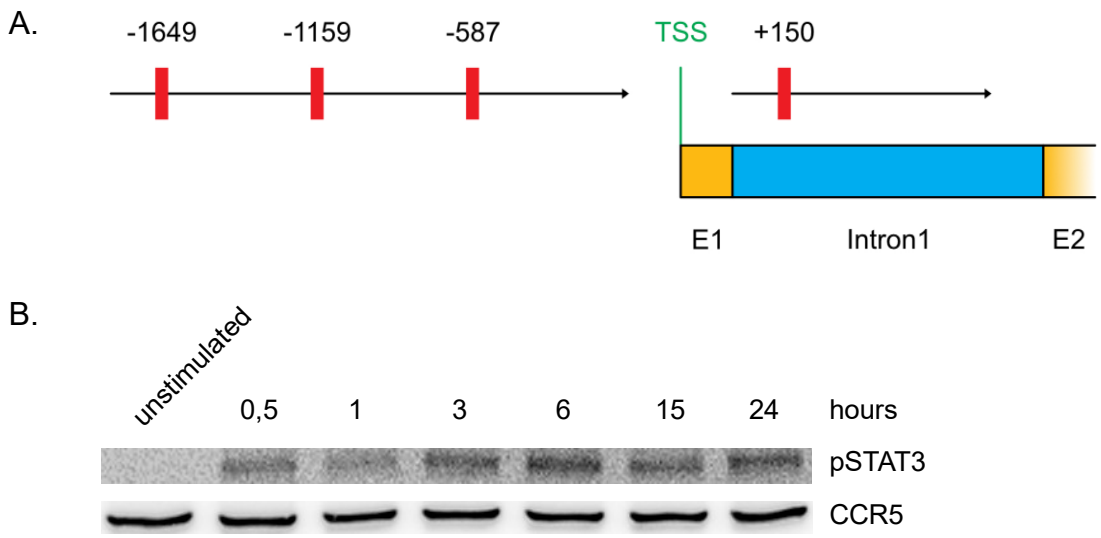

Figure 8. Potential role of STAT3 in IL-6-induced *Ccr5* upregulation.
A.) *In silico* analysis of putative STAT3 binding sites in the murine *Ccr5* promoters was performed using the TFbind online tool. The predicted binding sites are shown in red with their respective position to the transcription start site (TSS). The black arrows represent the two *Ccr5* promoters, exons (E) are orange, introns are blue. B.) Western blot for pSTAT3 and CCR5 of MSC-2 cells unstimulated or stimulated with IL-6.

Next, we used the STAT3 inhibitor Stattic (Schust *et al.*, 2006) to prove that IL-6-induced *Ccr5* upregulation is STAT3 dependent. We stimulated MSC-2 cells and IMC with IL-6 and treated them in parallel with the STAT3 inhibitor. We found that STAT3 inhibition abrogated IL-6-induced *Ccr5* upregulation in MSC-2 cells after 3 h (Figure 9A) and in IMC after 3 and 16 h. In the MSC-2 cells, the abrogation of *Ccr5* upregulation upon STAT3 inhibition was significant after 3 h of stimulation. However, after 16 h of stimulation the effect of the STAT3 inhibitor was not observable anymore, since the metabolism of the immortalized cells might be too fast. For the IMC, we were able to detect significantly less *Ccr5* expression upon STAT3 inhibition in parallel to IL-6 stimulation after 3 h. After 16 h of STAT3 inhibition in parallel to IL-6 stimulation, the expression of *Ccr5* in IMC was even downregulated compared to the unstimulated control and in some cases not detectable anymore. There was no change in the expression of the housekeeping gene *Rn18S*, indicating that the cells are still alive but lost expression of *Ccr5*. Statistics could therefore not be performed since too few values were above the detection limit.

This experiment clearly shows that IL-6-induced *Ccr5* upregulation is dependent on STAT3 activation in myeloid cells *in vitro*.

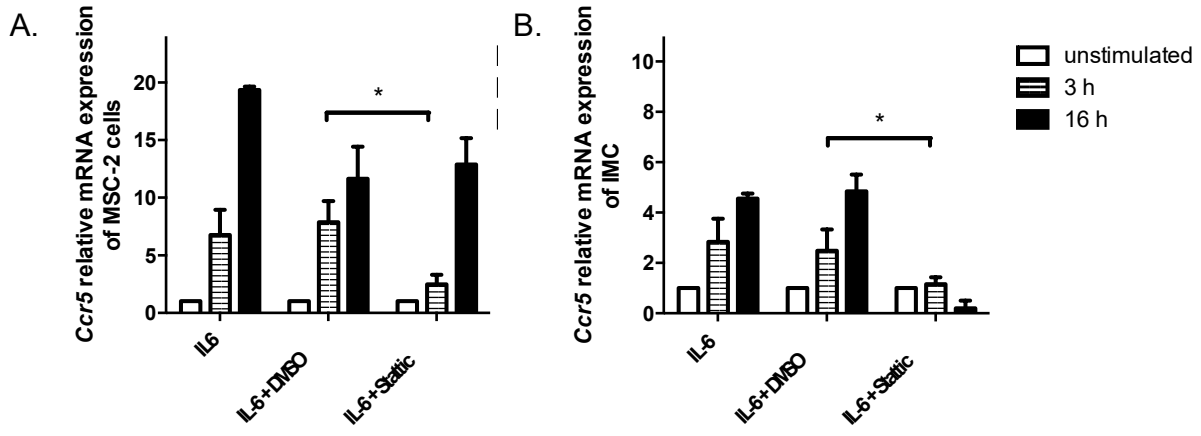

Figure 9. Effect of STAT3 inhibition on IL-6-induced *Ccr5* upregulation.
MSC-2 cells (A.) or IMC (B.) were stimulated for 3 h and 16 h with IL-6 ± DMSO (solvent control) or Stattic and *Ccr5* mRNA expression was measured by qRT-PCR. Relative expression calculated by the 2^-ΔΔCT method, normalized to the housekeeping gene *Rn18S* and expressed as fold change towards the unstimulated control is shown. (mean with SEM, n=3, *p<0.05)

5.1.3 Effect of IL-6 on CCR5 surface expression

So far, our investigations were focused on the upregulation of *Ccr5* at the mRNA level. However, since CCR5 is a surface receptor, it is indispensable to study the protein level and its functional relevance. Therefore, we stimulated MSC-2 cells and IMC with IL-6 and analyzed CCR5 surface expression by flow cytometry. IMC were gated as $CD11b^{+}Gr1^{+}$ alive single cells (Figure 10A). Surprisingly, we did not detect any upregulation of CCR5 on the surface of IMC (Figure 10B) or MSC-2 cells (Figure 10C) after overnight stimulation with IL-6. Independently from IL-6 stimulation, around 4 % of IMC and around 15 % of MSC-2 cells expressed CCR5. The same data were shown by using median fluorescence intensity (MFI) that correlates to the expression level of CCR5. These results go in line with the Western blot for CCR5 that showed no change in CCR5 expression upon IL-6 stimulation (Figure 8B), indicating the absence of changes not only in the surface expression but also in the overall expression.

To check the possibility that the CCR5 upregulation might need longer time than 18 h, we applied the protocol for MDSC *in vitro* differentiation by IL-6 and GM-CSF for four days (Marigo *et al.*, 2010). Since *Ccr5* mRNA expression was upregulated by both IL-6 and GM-CSF, we hypothesized that these two factors could upregulate CCR5 surface expression during the differentiation process of MDSC.

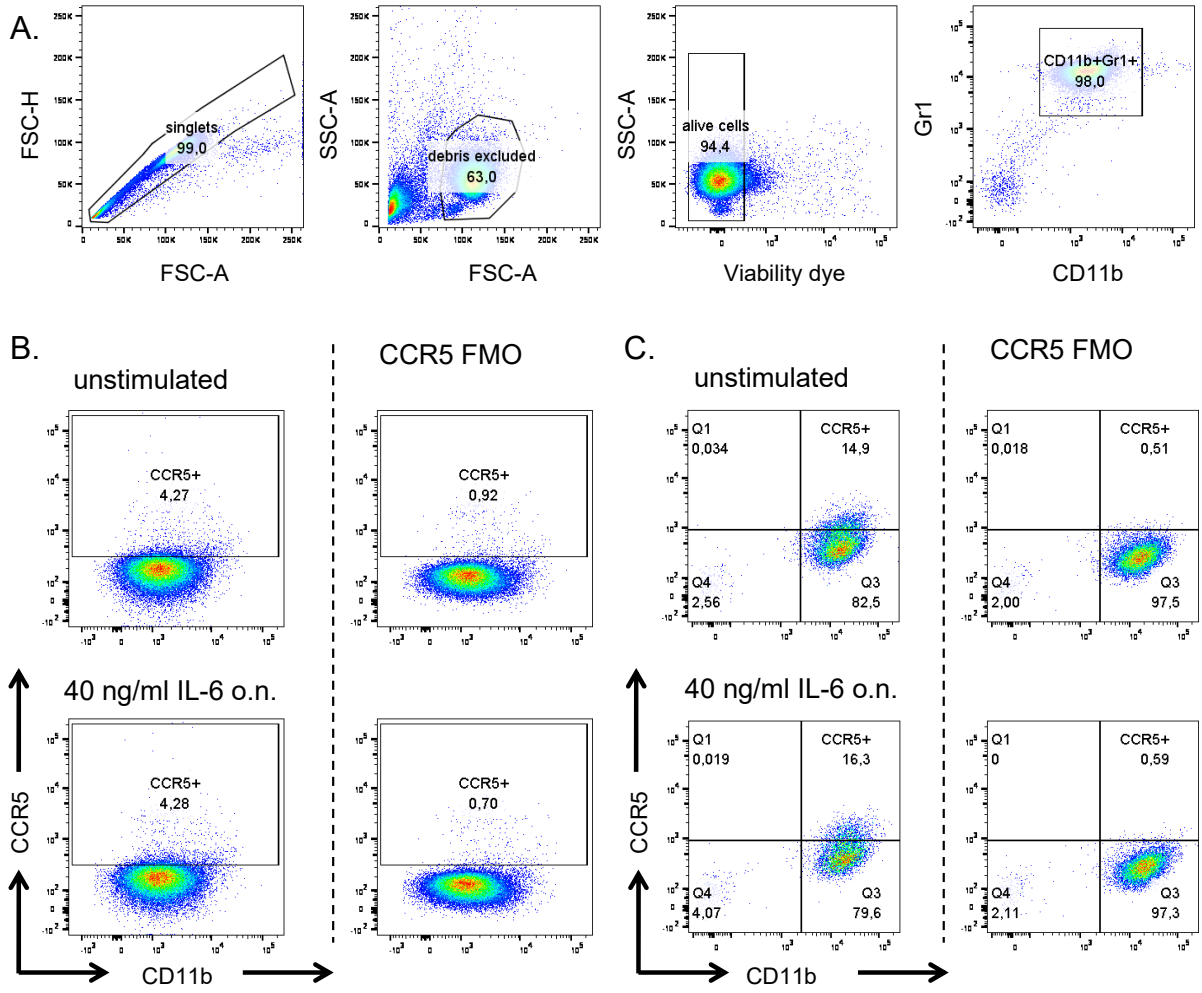

Figure 10. Regulation of CCR5 surface expression by IL-6 on IMC and MSC-2 cells.
A.) Gating strategy for IMC isolated by MACS and incubated overnight (18 h). After gating on singlets and excluding debris and dead cells, IMC were defined by the expression of CD11b and Gr1. IMC were left untreated or incubated for 18 h with IL-6. Representative dot plots for CCR5 surface expression are shown (B.). MSC-2 cells were treated the same and gated as shown in Figure 7A. Representative dot plots for CCR5 expression are shown (C.).

Using the MDSC *in vitro* differentiation 2.5x10^6 bone marrow cells seeded at day 0 were shown to proliferate indicated by a two-fold increase of the mean cell number at day 4 (Figure 11A). In addition, we found a significant accumulation of CD11b$^+$Gr1$^+$ cells when comparing the differentiated MDSC (IL-6, GM-CSF) with the freshly isolated bone marrow cells (Figure 11B). Furthermore, we found that around 40 % of the MDSC (IL-6, GM-CSF) were PD-L1$^+$ as compared to around 5 % PD-L1$^+$CD11b$^+$Gr1$^+$ cells in the freshly isolated bone marrow samples (Figure 11C). In addition, MDSC (IL-6, GM-CSF) displayed an increased production of ROS after the differentiation (Figure 11D).

Finally, we performed a suppression of T cell proliferation assay to test the capacity of the MDSC (IL-6, GM-CSF) to inhibit CD8$^+$ T cell proliferation. For this assay, CD8$^+$ T cells were isolated from murine spleens by MACS, stained with CFSE and activated by anti-CD3 and

anti-CD28 antibodies. After 72 h of co-culture with MDSC or IMC, isolated by MACS from the fresh bone marrow as a control, proliferation of T cells was evaluated by measuring the dilution of CFSE staining by flow cytometry (Figure 11E). As expected, the MDSC were able to significantly suppress proliferation of $CD8^+$ T cells in the 1:1 and 1:2 MDSC:T cell ratio as compared to the co-culture of T cells with IMC (Figure 11F).

Next, we tested if CCR5 could be upregulated during the differentiation by IL-6 and GM-CSF. We measured the CCR5 level on $CD11b^+Gr1^+$ IMC found in freshly isolated bone marrow by flow cytometry (Figure 12A) and compared it to the expression level of CCR5 on *in vitro* differentiated $CD11b^+Gr1^+$ MDSC (Figure 12B). Indeed, we demonstrated a significant upregulation of the frequency of $CCR5^+$ $CD11b^+Gr1^+$ (Figure 12C), whereas the MFI of CCR5 was not significantly changed (Figure 12D).

Therefore, we showed that *Ccr5* can be strongly upregulated at the mRNA level by IL-6 and to a lesser extent by GM-CSF and IFN-γ on MSC-2 cells and IMC. In addition, IL-6 and GM-CSF induced an upregulation of CCR5 at the protein level after four days of MDSC *in vitro* differentiation.

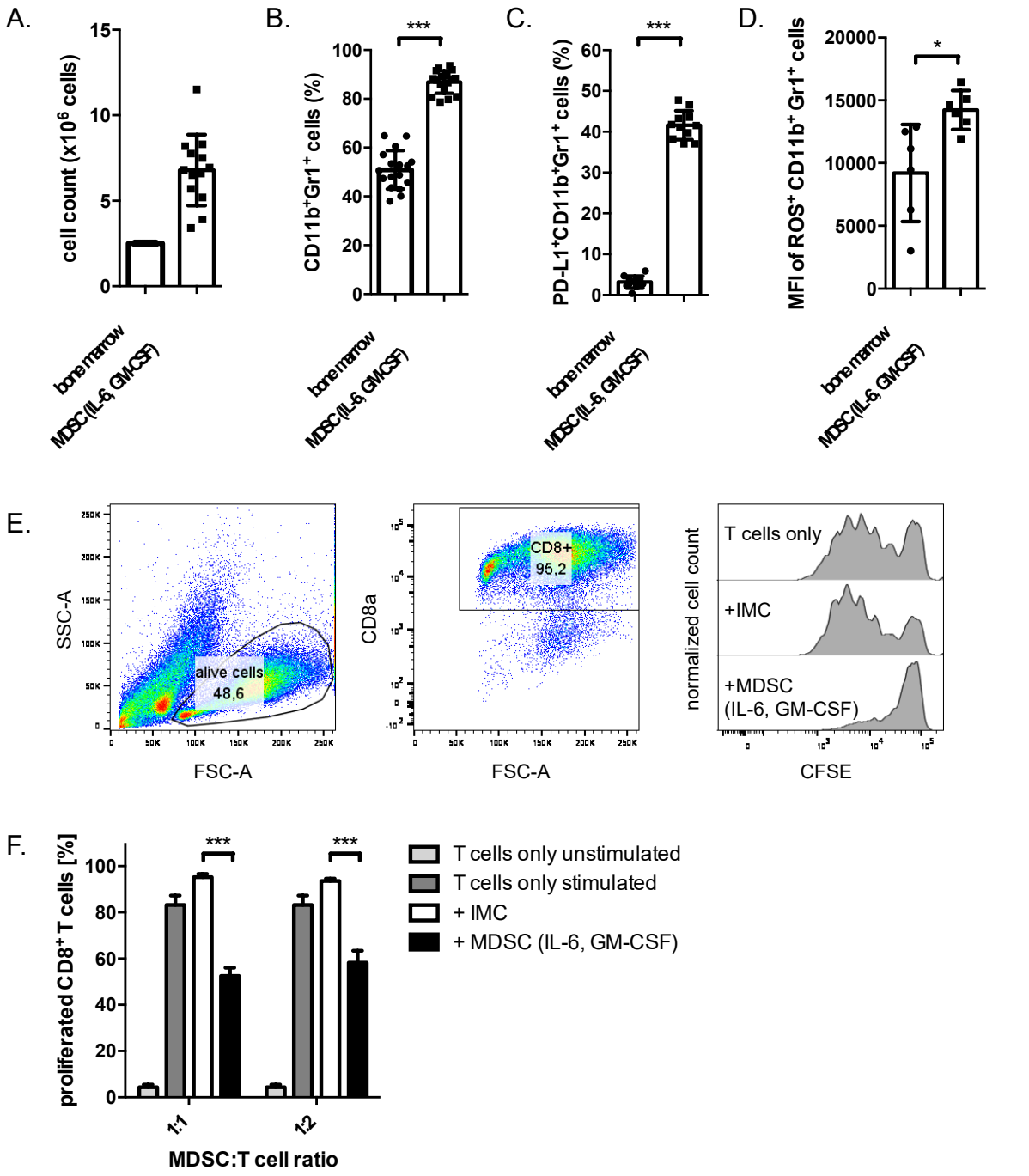

Figure 11. *In vitro* differentiation of MDSC by IL-6 and GM-CSF for four days.
Murine bone marrow was analyzed after isolation or cultured for four days with IL-6 and GM-CSF for MDSC differentiation. Cells were counted by a Neubauer chamber (A., n=13) and analyzed by flow cytometry for the expression of CD11b and Gr1 (B., n=17), PD-L1 (C., n=11) and the production of ROS (D., n=6). For the suppression of T cell proliferation assay, splenic $CD8^+$ T cells were labeled with CFSE, activated with anti-CD3 and anti-CD28 antibodies and co-cultured with IMC or MDSC at the indicated ratios for 72 h. Dilution of CFSE staining in proliferated $CD8^+$ T cells was assessed by flow cytometry. Gating strategy (E.) and quantification of proliferated cells (F., n=5) are shown (mean with SD, *p<0.05, ***p<0.001).

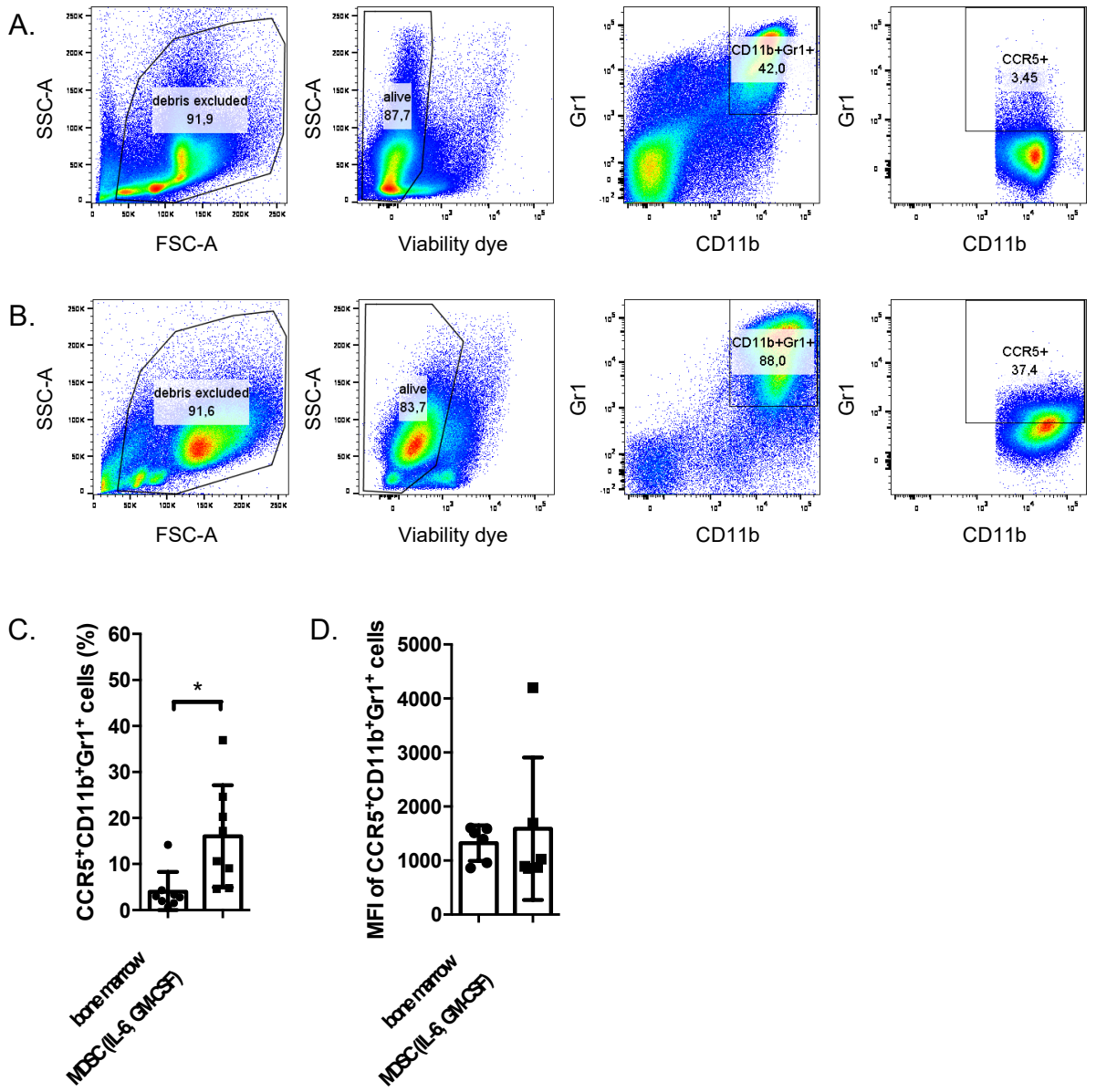

Figure 12. Regulation of CCR5 surface expression during MDSC *in vitro* differentiation.
Murine bone marrow was analyzed directly after isolation or cultured for four days with IL-6 and GM-CSF for MDSC differentiation. Gating strategy for bone marrow (A.) and differentiated MDSC (B.) is shown. Singlets were gated by FSC-A vs. FSC-H, subsequently debris and dead cells were excluded. After gating on $CD11b^+Gr1^+$ cells, CCR5 was gated according to the CCR5 FMO. Quantification of frequency of $CCR5^+CD11b^+Gr1^+$ cells (C., n=8) and MFI of $CCR5^+CD11b^+Gr1^+$ cells (D., n=6) are shown (mean with SD, *p<0.05).

5.1.4 Transwell migration assay

Next, we investigated the functional relevance of the upregulation of CCR5 for the migration of the cells. For this, we compared the migration of IMC and *in vitro* differentiated MDSC (IL-6, GM-CSF) towards the CCR5 ligands in a transwell migration assay. We seeded IMC and MDSC into a transwell system with a pore size of 8 µm and measured the number of

migrated cells after 16 h by flow cytometry (Figure 13A). Importantly, the frequency of spontaneous migrated IMC towards FBS-free control medium without any chemokines was around 9 %, whereas the frequency of migration towards the chemokines CCL3, -4 and 5 was significantly increased to around 18 % (Figure 13B). Interestingly, for the MDSC, there was a frequency of spontaneous migration of around 28 %, which, however, remained the same for the migration towards the CCR5 ligands CCL3, -4 and -5 (Figure 13B).

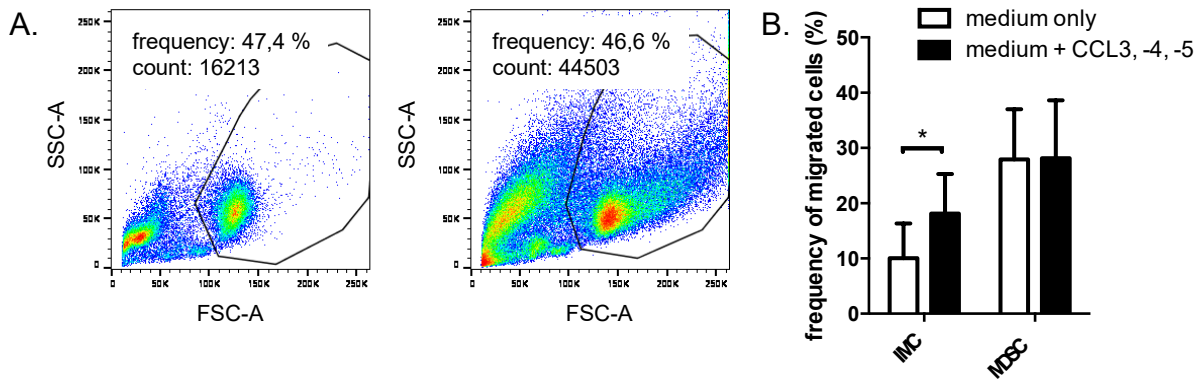

Figure 13. Transwell migration assay of differentiated MDSC and IMC towards CCR5 ligands. $0.75x10^6$ cells were seeded in the upper chamber of a transwell with a pore size of 8 µm and incubated for 16 h with FBS-free medium supplemented or not with 100 ng/ml of the CCR5 ligands CCL3, -4 and -5 in the lower chamber. A.) Representative dot plots with cell frequency and cell count of IMC (left) and MDSC (right) migrated towards the CCR5 ligands. B.) Frequency of migrated cells was calculated by upscaling the count by the flow cytometer to the total volume in the lower well and then calculating the frequency to the number of total seeded cells (IMC: n=9, MDSC: n=6, mean with SD, *p<0.05).

5.1.5 IL-6 accumulation and CCR5$^+$ MDSC in melanoma bearing mice

In the *RET* transgenic melanoma, it was previously shown that CCR5$^+$ MDSC accumulated in skin tumors and metastatic lymph nodes via the CCR5-CCR5 ligand interaction (Blattner *et al.*, 2018). Therefore, we investigated in this model the correlation of IL-6 concentrations and the expression of CCR5 and pSTAT3 in MDSC to validate that the mechanism of IL-6-induced CCR5 upregulation via STAT3 could be also working *in vivo*. We measured IL-6 levels in the tumors from *RET* transgenic mice by ELISA and CCR5 and pSTAT3 expression in tumor-infiltrating MDSC by flow cytometry. The gating strategy for pSTAT3 in tumor-infiltrating MDSC can be found in the appendix (Supplementary Figure 1).

Interestingly, we found a significant positive correlation between the IL-6 level in the tumor and the frequency of CCR5$^+$ tumor-infiltrating MDSC (Figure 14A), suggesting that a higher IL-6 level in the TME could lead to increased expression of CCR5 on MDSC. This result goes in line with our *in vitro* data, showing that IL-6 upregulated CCR5 on myeloid cells.

Furthermore, we could detect an increased frequency of pSTAT3$^+$ cells in CCR5$^+$ MDSC compared to their CCR5$^-$ counterparts (Figure 14B). The average frequency of pSTAT3$^+$ cells was increased by around 20 % in CCR5$^+$ MDSC compared to CCR5$^-$ MDSC infiltrating the tumor of *RET* transgenic mice. In addition, we found an elevation in the MFI of pSTAT3 in pSTAT3$^+$CCR5$^+$ MDSC (Figure 14C), indicating that the pSTAT3$^+$ cells do also show elevated levels of pSTAT3 per cell in the CCR5$^+$ MDSC population. As IL-6 signaling is mediated via STAT3 and since we could show that the blockade of STAT3 can abrogate IL-6-induced CCR5 upregulation *in vitro*, the increase of STAT3 phosphorylation in CCR5$^+$ MDSC suggests a link between STAT3 and CCR5 expression in MDSC in the melanoma microenvironment.

Altogether, the data from the *RET* transgenic mouse tumors showed a positive correlation between IL-6 in the tumor and CCR5 expression on MDSC, as well as a connection between increased STAT3 levels and CCR5 expression in these cells.

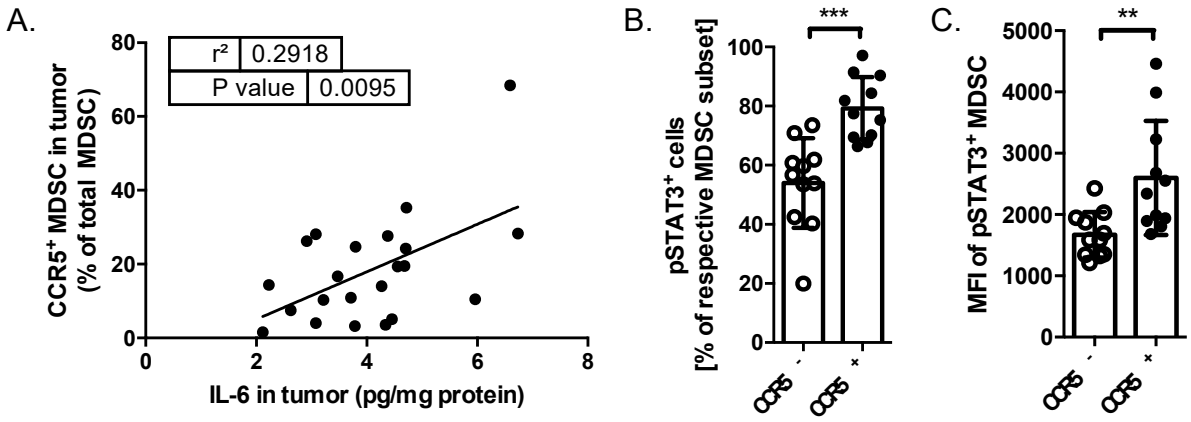

Figure 14. IL-6, pSTAT3 and CCR5$^+$ MDSC in *RET* transgenic mouse tumors *ex vivo*.
IL-6 was measured in tumors of *RET* transgenic mice by ELISA, while CCR5 expression and pSTAT3 in tumor-infiltrating MDSC was measured by flow cytometry. For the detection of pSTAT3 leukocytes were first enriched by a Histopaque gradient centrifugation. The correlation between IL-6 levels and CCR5$^+$ tumor-infiltrating MDSC from the same mice is shown (A., n=21). Frequency (B., n=11) and MFI (C., n=11) of pSTAT3$^+$ tumor-infiltrating CCR5$^+$ MDSC vs. their CCR5$^-$ counterparts is shown (mean with SD, ***p<0.001).

5.1.6 Role of GM-CSF in CCR5 upregulation during MDSC differentiation

To further elucidate the individual roles of IL-6 and GM-CSF in the CCR5 upregulation upon MDSC differentiation, we cultured the bone marrow cells with GM-CSF alone (referred to as MDSC (GM-CSF)) and compared them to the cells differentiated with IL-6 and GM-CSF for four days (referred to as MDSC (IL-6, GM-CSF). Unfortunately, it is not possible to use only IL-6 because the cells do not survive without the growth factor. Interestingly, we found that

GM-CSF alone was also able to significantly upregulate the frequency of CCR5 expression on $CD11b^+Gr1^+$ cells after the four days of differentiation (Figure 15A).

However, the frequency of $CCR5^+CD11b^+Gr1^+$ cells upon differentiation with GM-CSF alone was significantly lower than that of MDSC (IL-6, GM-CSF) (Figure 15A). Therefore, GM-CSF alone can increase the CCR5 expression after four days of incubation, however, IL-6 is needed to exert the full CCR5 upregulation.

As GM-CSF was also able to induce STAT3 signaling (Gu *et al.*, 2007), we aimed at studying the STAT3 dependence of GM-CSF-induced *Ccr5* upregulation. Therefore, we used the STAT3 inhibitor Stattic in parallel to stimulation with GM-CSF to block GM-CSF-induced STAT3 signaling and potentially abrogate CCR5 upregulation. Indeed, Stattic was able to significantly abrogate GM-CSF-induced *Ccr5* upregulation at the mRNA level after 3 h of stimulation indicating that not only IL-6-mediated but also GM-CSF-induced *Ccr5* upregulation was STAT3-dependent (Figure 15B).

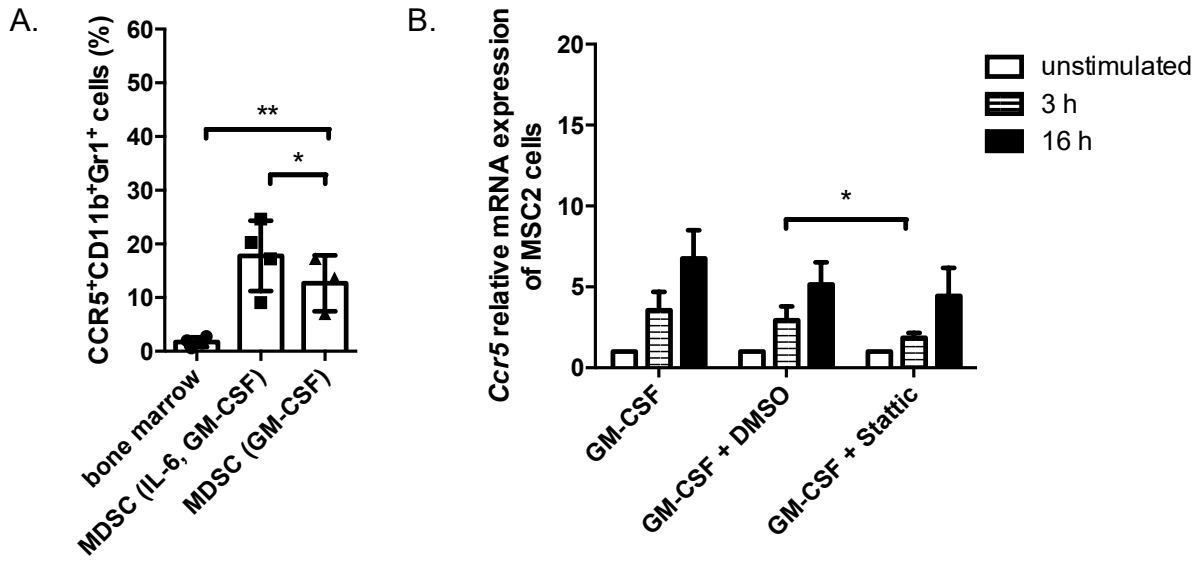

Figure 15. Role of GM-CSF in CCR5 upregulation and its STAT3 dependence.
A.) Murine bone marrow cells were cultured for four days in the presence of IL-6 and GM-CSF or GM-CSF only. CCR5 expression on $CD11b^+Gr1^+$ cells was evaluated by flow cytometry and compared to freshly isolated bone marrow (mean with SD, n=3-4, *p<0.05, **p<0.01). B.) MSC-2 cells were stimulated for 3 h and 16 h with GM-CSF ± DMSO (solvent control) or Stattic and *Ccr5* mRNA expression was measured by qRT-PCR. Relative expression was calculated by the 2^-ΔΔCT method, normalized to the housekeeping gene *Rn18S* and expressed as fold change towards the unstimulated control (mean with SEM, n=3-6, *p<0.05).

5.2 Mechanisms of increased immunosuppression mediated by CCR5$^+$ MDSC

5.2.1 FACS sorting of CCR5$^+$ and CCR5$^-$ tumor-infiltrating MDSC

Previous findings from our lab have demonstrated that CCR5$^+$ tumor-infiltrating MDSC from *RET* transgenic melanoma bearing mice expressed more Arg1 and PD-L1 and produced more ROS and NO compared to their CCR5$^-$ counterparts (Blattner *et al.*, 2018). To evaluate the differences in immunosuppressive capacity between CCR5$^+$ and CCR5$^-$ tumor-infiltrating MDSC, we have established the FACS sorting of these two MDSC populations from the tumors of mice injected s.c. with Ret melanoma cells. Tumors were digested with collagenase and DNAse, TIL were enriched by Histopaque gradient centrifugation and finally the latter cells were FACS sorted for CCR5$^+$ or CCR5$^-$ MDSC, being CD45$^+$CD11b$^+$Gr1$^+$ (Figure 16).

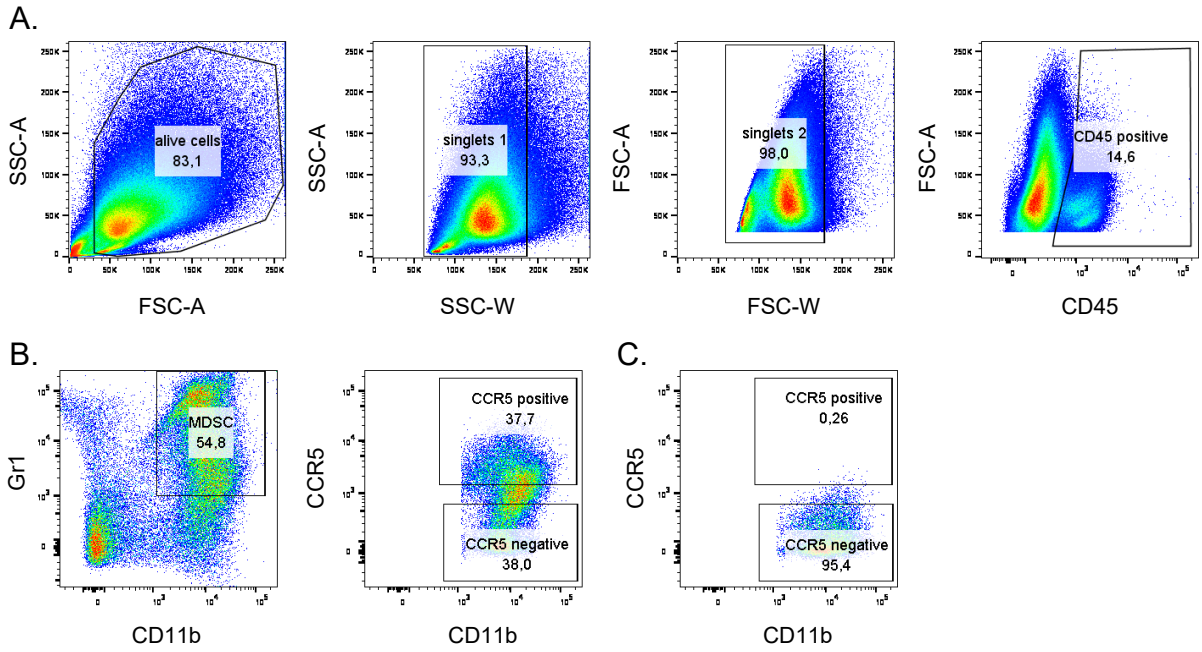

Figure 16. Gating strategy for FACS sorting of CCR5$^+$ and CCR5$^-$ tumor-infiltrating MDSC. Tumor-infiltrating leukocytes (TIL) were isolated from tumors of mice s.c. injected with Ret melanoma cells by a Histopaque gradient centrifugation after collagenase and DNAse digest. Then, the CCR5$^+$ and CCR5$^-$ subpopulations of CD45$^+$CD11b$^+$Gr1$^+$ tumor-infiltrating MDSC were sorted by FACS. A.) Alive cells were gated by the forward and side scatter and duplets were excluded by two different successive strategies. To exclude tumor cells, CD45$^+$ cells were gated. B.) In CD45$^+$ cells, MDSC were defined as CD11b$^+$Gr1$^+$ and CCR5$^+$ or CCR5$^-$ MDSC were gated and sorted. The CCR5 gate was set according to the FMO control (C.).

By sorting into 37 °C warm medium containing high FBS, we were able to sort up to 1x10^6 viable cells for each population, pooling the cells from two tumors with a diameter between 1 and 1.5 cm. These cells could then be used for the suppression of T cell proliferation assay and the isolation of RNA for microarray analysis.

5.2.2 Immunosuppressive capacity of CCR5$^+$ tumor-infiltrating MDSC

We demonstrated that CCR5$^+$ MDSC isolated by FACS sorting from the tumors of mice injected with Ret cells displayed significantly higher capacity to inhibit proliferation of CD8$^+$ T cells than that of CCR5$^-$ MDSC isolated from the same tumors (Figure 17, data were also published in (Blattner *et al.*, 2018)). This result is in agreement with the fact that CCR5$^+$ MDSC show increased expression of Arg1 and ROS. However, the mechanisms of higher immunosuppressive capacity of CCR5$^+$ MDSC remained still elusive.

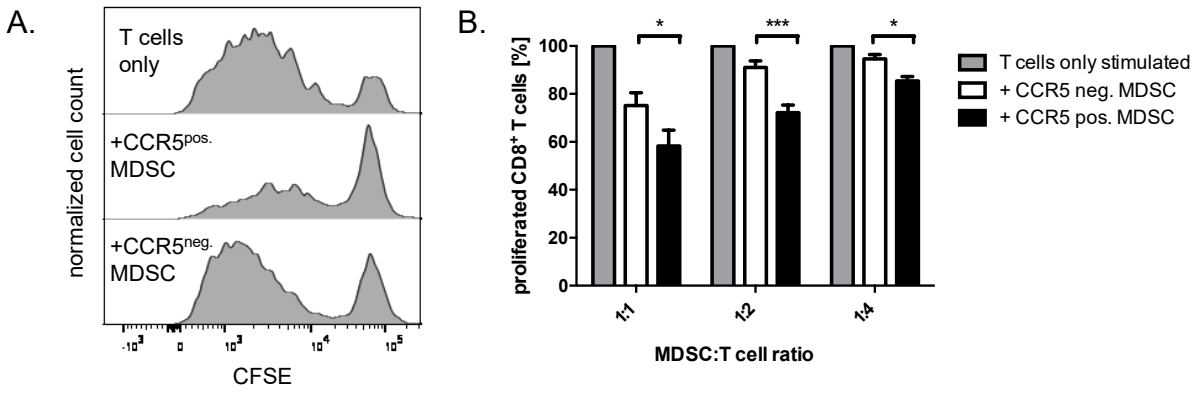

Figure 17. Stronger suppression of CD8$^+$ T cell proliferation by CCR5$^+$ tumor-infiltrating MDSC. Tumor-infiltrating CCR5$^+$ and CCR5$^-$ MDSC populations were isolated by FACS sorting from tumors of mice s.c. injected with Ret cells. For the suppression of T cell proliferation assay, CD8$^+$ T cells were labeled with CFSE, activated with anti-CD3 and anti-CD28 beads and co-cultured with CCR5$^+$ or CCR5$^-$ MDSC at the indicated ratios for 72 h. The dilution of CFSE staining in proliferated CD8$^+$ T cells was assessed by flow cytometry. Representative histograms (A.) and quantification of proliferated T cells (B.) are shown. Data were normalized to the proliferation of T cells only (mean with SD, n=6, 2 independent experiments, *p<0.05, ***p<0.001). Raw data used for this graph were published in a different format by (Blattner *et al.*, 2018).

5.2.3 Microarray analysis of CCR5$^+$ and CCR5$^-$ tumor-infiltrating MDSC

To further asses the differences between the CCR5$^+$ and CCR5$^-$ tumor-infiltrating MDSC populations, we performed a microarray analysis with the RNA isolated from the FACS sorted cell populations.

A first assessment of the data and the quality of the array was done by a correlation heatmap, showing the correlations between the different samples (Figure 18A). When comparing each sample to itself the correlation is 1, which means identity, shown by the diagonal alignment of red squares. In addition, when comparing the replicates of each group (n1, n2, n3 and n4) to each other, there is still a positive correlation as seen in the upper left and lower right corner of the blot (shades of red). This shows the low difference between the repli-

cates of each group. However, when comparing the CCR5$^+$ to the CCR5$^-$ group the correlations are negative as seen in the upper right and lower left corner of the blot (shades of blue). This indicates the differences between the two experimental groups. Therefore, we found that our microarray data showed high differences between the experimental groups and low variances among different replicates.

We next assessed the differentially regulated genes in more detail. The volcano plot showed in blue the genes that are significantly and strongly downregulated in the CCR5$^+$ MDSC compared to their CCR5$^-$ counterparts and in red the genes that are significantly and strongly upregulated (Figure 18B). In total there were 154 genes differentially regulated with an adjusted p-value of below 0.05, among them 51 genes were significantly downregulated and 103 were significantly upregulated in CCR5$^+$ tumor-infiltrating MDSC compared to CCR5$^-$ tumor-infiltrating MDSC. A list of the top 50 upregulated and top 50 downregulated genes can be found in the appendix (Supplementary Table 1).

The strongest downregulated gene in CCR5$^+$ MDSC was found to be the gene for the adhesion G-protein coupled receptor E4 (*Adgre4*) with a fold change of about 0.08. This receptor is expressed on myeloid cells and is thought to play a role in the interaction between myeloid cells and B cells (Stacey *et al.*, 2002). Furthermore, the expression of the gene for the chemokine CCL22 and the genes for the chemokine receptors CCR7 and CCR2 were found to be downregulated in CCR5$^+$ MDSC. In addition, the expression of the *Il1b* gene, the *Stat4* gene and the gene coding for matrix metalloproteinase (MMP)25 were downregulated.

The strongest upregulated gene in CCR5$^+$ MDSC was the *Fabp4* gene coding for the fatty acid binding protein 4 with a fold change of around 10.56. FABP4 is involved in the uptake, transport and metabolism of fatty acids. Importantly, the second strongest upregulated gene in the CCR5$^+$ MDSC was the *Ccl8* gene coding for the chemokine CCL8, a ligand for the CCR5 receptor. Moreover, the genes for other chemokines CCL12, CCL7 and CCL2 as well as the *Mmp27* gene were also upregulated.

Interestingly, we failed to find an upregulation of the genes associated to immunosuppression in CCR5$^+$ tumor-infiltrating MDSC. For example, the *Arg1* gene or genes playing a role in the increase of ROS were not found to be upregulated in CCR5$^+$ MDSC by our microarray analysis.

Altogether, we found many differences in genes playing a role in the migration of immune cells comparing the CCR5$^+$ tumor-infiltrating MDSC to the CCR5$^-$ tumor-infiltrating MDSC and we got new hints for a role of MMP27 and fatty acid metabolism-induced immunosuppression specifically in CCR5$^+$ MDSC. However, we did not find pathways or mechanisms for the induction of Arg1 expression or ROS production in CCR5$^+$ MDSC. Therefore, the mechanisms of induction of immunosuppressive factors in CCR5$^+$ MDSC needed further study.

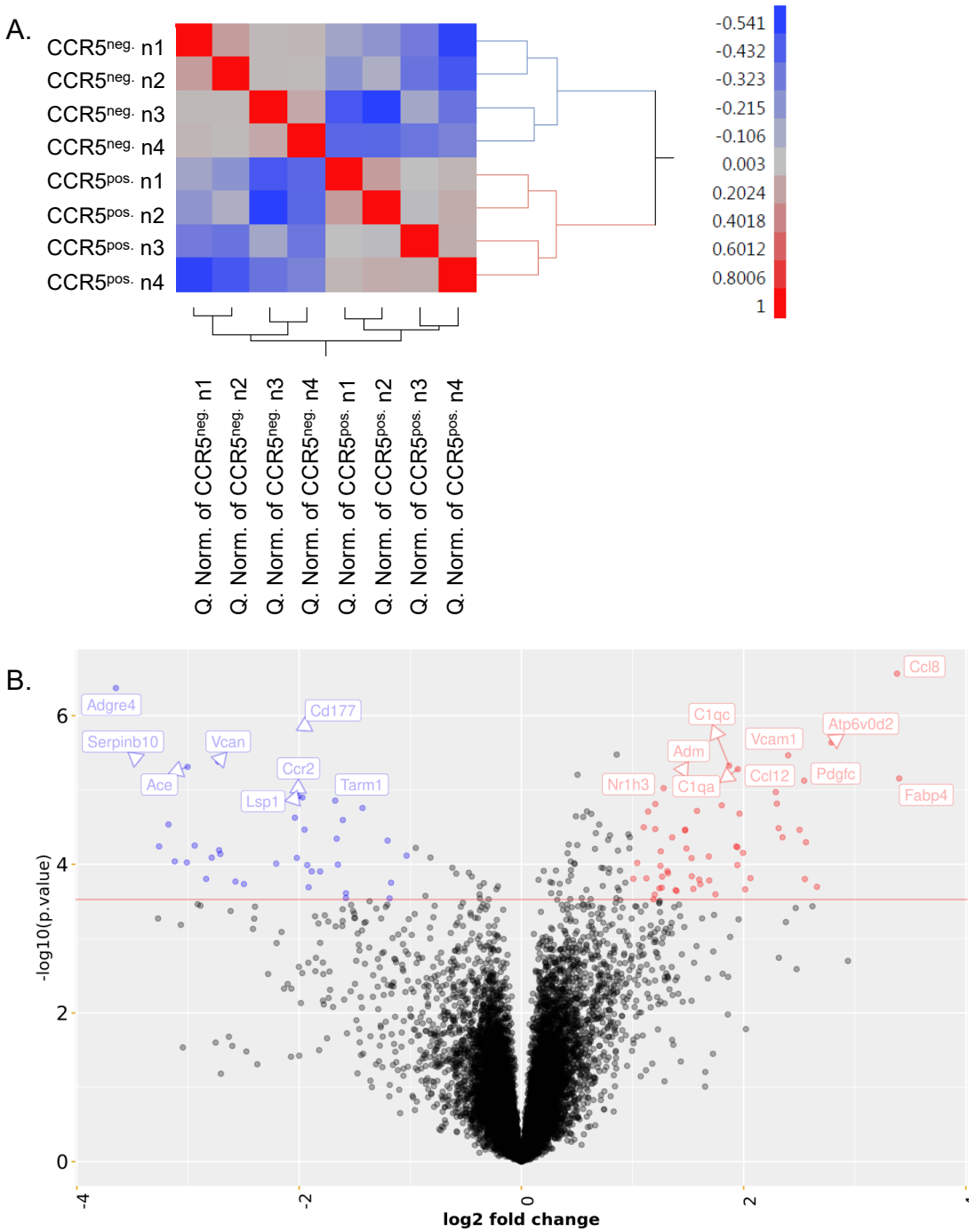

Figure 18. Microarray analysis of CCR5⁺ and CCR5⁻ tumor-infiltrating MDSC.
After FACS sorting of CCR5⁺ and CCR5⁻ tumor-infiltrating MDSC from injected Ret melanoma tumors, a microarray analysis was performed. Correlation heatmap of sample values (A.) and volcano blot of analyzed data (B.) is shown. The red line in the volcano blot shows the adjusted significance cutoff calculated using the number of replicates and the variance upon consideration of the false discovery rate (FDR).

5.2.4 Effect of CCR5 ligands on MDSC immunosuppressive capacity

Next, we investigated if the CCR5 ligands might stimulate the increased expression of immunosuppressive factors in CCR5$^+$ MDSC. To test this hypothesis, we used MSC-2 cells, IMC and *in vitro* differentiated MDSC and stimulated them with the CCR5 ligands CCL3, -4 and -5. Then we analyzed the mRNA expression of various genes that are known to play an important role in MDSC-mediated immunosuppression. Around 15 % of MSC-2 cells are CCR5$^+$, whereas only around 4 % of IMC are CCR5$^+$ (Figure 10). Since the CCR5 ligand-induced signaling will only be active in the cells expressing CCR5, we included the *in vitro* differentiated MDSC, to have a cell population with high CCR5 expression (Figure 12).

However, we were not able to detect an upregulation of the expression of any of the tested genes coding for immunosuppressive factors, including *Pdl1*, *Tgfb*, *Arg1*, *Nos2*, *Ido*, *Cox2*, *Ptges* and *Il10*, on the tested cell types (Figure 19).

These results indicate that the CCR5 downstream signaling induced by the CCR5 ligands is not capable of upregulating the expression of these immunosuppressive factors on mRNA level in myeloid cells.

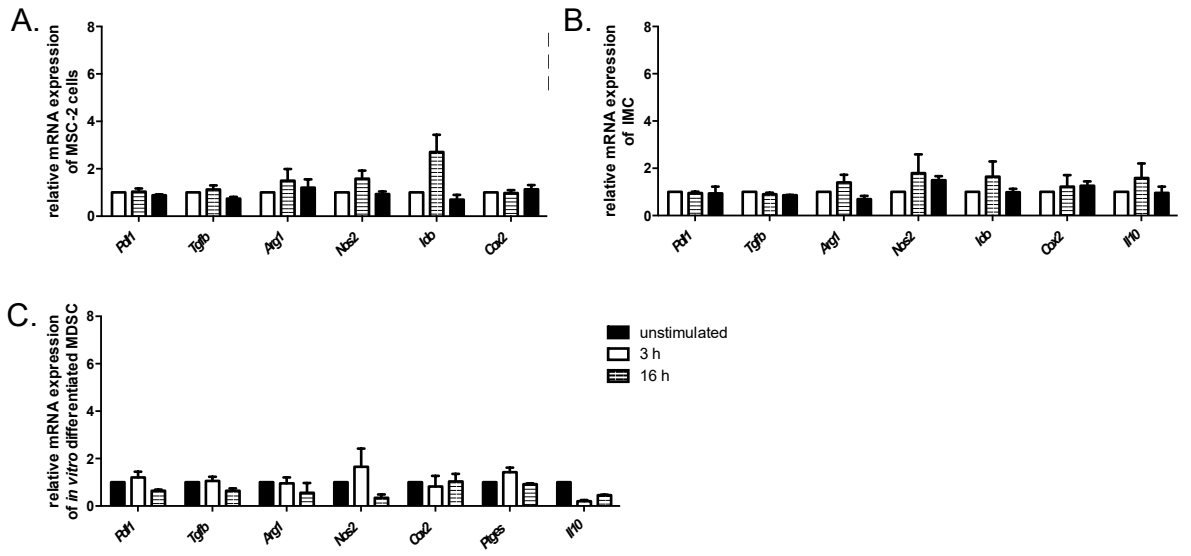

Figure 19. Effect of CCR5 ligands on expression of immunosuppressive factors on mRNA level. MSC-2 cells (A., n=3), IMC (B., n=2) or *in vitro* differentiated MDSC (C., n=3) were stimulated for 3 h and 16 h with 20 ng/ml of the CCR5 ligands CCL3, -4 and -5 and mRNA expression of the immunosuppressive factors indicated on the X-axis was measured by qRT-PCR. Relative expression was calculated by the 2^-ΔΔCT method, normalized to the housekeeping gene *Rn18S* and expressed as fold change towards the unstimulated control (mean with SEM).

To evaluate a direct effect of CCR5 ligands on immunosuppressive functions of CCR5$^+$ cells, we performed suppression of T cell proliferation assays. First, we stimulated IMC overnight with the CCR5 ligands CCL3, -4 and -5, removed the ligands and co-cultured IMC with activated T cells to assess T cell proliferation. As expected from our qRT-PCR data, the

CCL-stimulated IMC failed to suppress CD8⁺ T cell proliferation (Figure 20A). Second, to exclude that the time of chemokine stimulation was too short, we added the CCR5 ligands to the *in vitro* differentiation of MDSC for the entire four days. Importantly, the MDSC differentiated in the presence of the CCR5 ligands were also not capable to suppress T cell proliferation stronger than normally differentiated MDSC (Figure 20B).

In summary, we were not able to show upregulation of any of the tested genes coding for immunosuppressive factors (*Pdl1*, *Tgfb*, *Arg1*, *Nos2*, *Ido*, *Cox2*, *Ptges* and *Il10*) in the three different model cell types for MDSC, which have different expression levels of CCR5. Furthermore, CCR5 ligand stimulation did not make IMC and *in vitro* differentiated MDSC more immunosuppressive in the suppression of T cell proliferation assay than corresponding cells incubated without these chemokines. Therefore, the CCR5-CCR5 ligand interaction does not seem to mediate higher immunosuppressive capacity of CCR5⁺ MDSC in our hands.

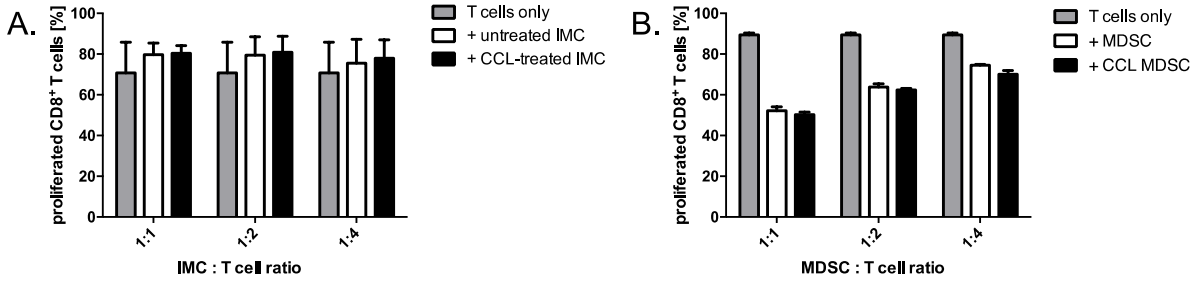

Figure 20. Effect of CCR5 ligands on immunosuppressive capacity of IMC and MDSC.
IMC were stimulated overnight (18 h) with 20 ng/ml of the CCR5 ligands CCL3, -4 and -5. MDSC were *in vitro* differentiated with IL-6 and GM-CSF in the presence of the same CCR5 ligands for four days. For the suppression of T cell proliferation assay, CD8⁺ T cells were labeled with CFSE, activated with anti-CD3 and anti-CD28 beads and co-cultured with untreated or chemokine-treated IMC (A., n=3), or with *in vitro* differentiated MDSC in the presence or absence of CCR5 ligands (B., n=2, representative for two more experiments with the same tendency) at the indicated ratios for 72 h. Dilution of CFSE staining in proliferated CD8⁺ T cells was assessed by flow cytometry. Quantification of proliferated T cells is shown (mean with SD).

5.2.5 Effect of IL-6 on MDSC immunosuppressive capacity

Since the CCR5 ligands were not able to induce immunosuppressive capacity of MDSC, we hypothesized that IL-6 might lead to increased immunosuppression in parallel to upregulation of CCR5 on MDSC. We stimulated IMC and MSC-2 cells with IL-6 and tested the expression of the genes coding for immunosuppressive factors by qRT-PCR. Among the tested genes, we found a significant upregulation of *Arg1* mRNA in MSC-2 cells after IL-6 stimulation for 16 h (Figure 21A). In line with this, a significant upregulation of *Arg1* mRNA could also be seen in primary IMC after 16 h of IL-6 stimulation (Figure 21B). Furthermore, we observed a tendency for upregulation of *Nos2* and *Ido* mRNA after 16 h of IL-6 stimulation in IMC but not in MSC-2 cells (Figure 21).

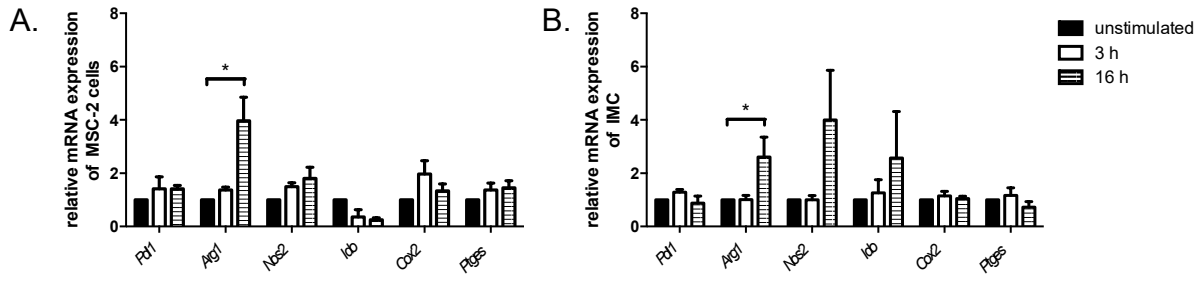

Figure 21. Effect of IL-6 on expression of genes coding for immunosuppressive factors.
MSC-2 cells (A.) and IMC (B.) were stimulated for 3 h and 16 h with 40 ng/ml IL-6. mRNA expression of the immunosuppressive factors indicated on the X-axis was measured by qRT-PCR. Relative expression was calculated by the 2^-ΔΔCT method, normalized to the housekeeping gene *Rn18S* and expressed as fold change towards the unstimulated control (n=3, mean with SEM, *p<0.05).

To test the potential of STAT3 to induce *Arg1* gene expression, we first performed *in silico* analysis of the Arg1 promoter/enhancer for putative STAT3 binding sites. The murine *Arg1* gene sequence was extracted from the NCBI database (Gene-ID: 11846) and the TFbind online tool was used to search for STAT3 binding sites in the *Arg1* promoter/enhancer that is located upstream of the transcription start site (Pauleau *et al.*, 2004). Indeed, we found five putative STAT3 binding sites in the murine *Arg1* promoter/enhancer (Figure 22A), where STAT3 could bind and induce *Arg1* gene expression.

To finally show that *Arg1* mRNA expression induced by IL-6 is STAT3 dependent, we incubated MSC-2 cells with IL-6 in the presence or absence of the STAT3 inhibitor Stattic and studied the *Arg1* mRNA expression by qRT-PCR. Interestingly, *Arg1* was upregulated by IL-6 both after 3 and 16 h, whereas an addition of Stattic significantly decreased *Arg1* expression after 3 h (Figure 22B).

These findings indicated that IL-6 could indeed induce *Arg1* upregulation in a STAT3-dependent manner. It seems that the stimulation of *Arg1* expression by IL-6 is induced via the IL-6/IL-6R/gp130 signaling complex activating JAK family kinases that phosphorylate STAT3. Phosphorylated STAT3 forms homodimers that are translocated to the nucleus and bind to the *Arg1* promoter/enhancer to induce the gene expression of *Arg1*.

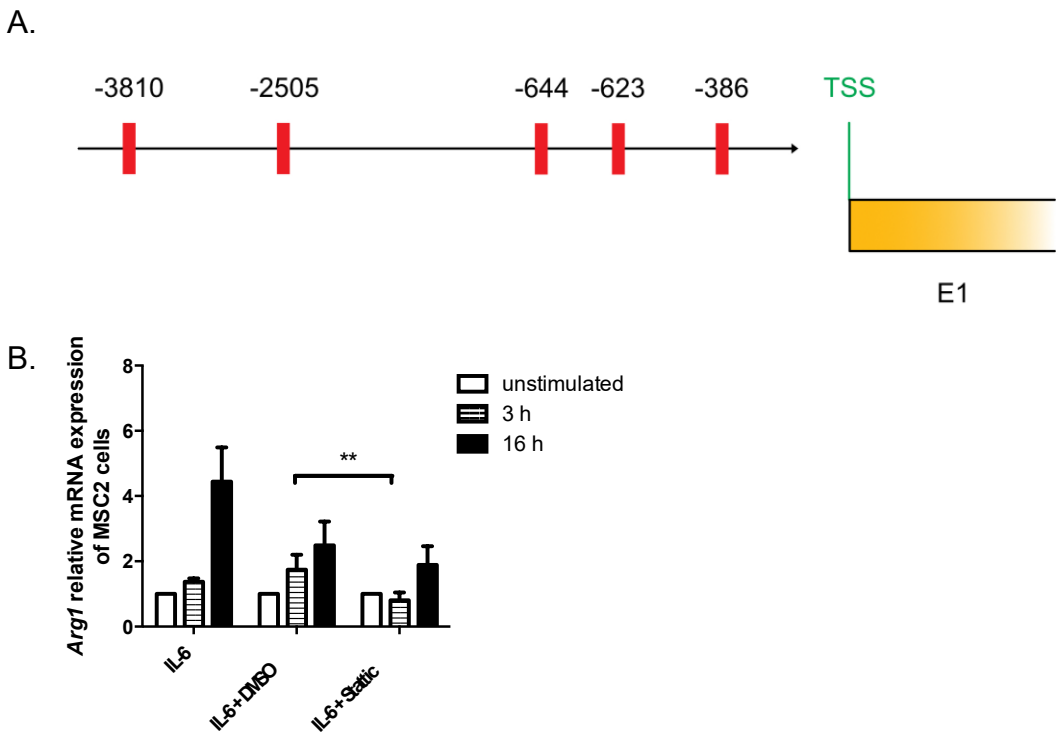

Figure 22. Role of STAT3 in IL-6-induced *Arg1* upregulation.
A.) *In silico* analysis of putative STAT3 binding sites in the murine *Arg1* promoter/enhancer was performed using the TFbind online tool. The predicted binding sites are shown in red with their respective position to the transcription start site (TSS). The black arrow represents the *Arg1* promoter/enhancer, exon (E) is orange. B.) MSC-2 cells were stimulated for 3 h and 16 h with IL-6 ± DMSO (solvent control) or Stattic. *Arg1* mRNA expression was measured by qRT-PCR. Relative expression was calculated by the 2^-ΔΔCT method, normalized to the housekeeping gene *Rn18S* and expressed as fold change towards the unstimulated control (mean with SEM, n=3, *p<0.05).

After having shown the upregulation of *Arg1* mRNA by IL-6 via a STAT3-dependent mechanism, we next investigated the effect of IL-6 on Arg1 at the functional level. We detected a significantly increased enzymatic activity of Arg1 in MSC-2 cells after overnight stimulation with IL-6 (Figure 23A). The upregulation of Arg1 activity could be reproduced after overnight stimulation with IL-6 of primary IMC (Figure 23B). To investigate if this elevation after IL-6 stimulation has an effect on the immunosuppressive capacity of IMC, we performed a suppression of T cell proliferation assay. However, no difference was observed comparing the suppressive capacity of IL-6-stimulated vs. non-stimulated IMC (Figure 23C). Therefore, this increase in Arg1 activity induced by IL-6 stimulation was not sufficient to convert IMC int immunosuppressive MDSC.

To study whether IL-6 could induce immunosuppressive capacity of IMC after longer stimulation, we applied the model of MDSC *in vitro* differentiation by IL-6 and GM-CSF, comparing MDSC differentiated in the presence of both IL-6 and GM-CSF, to the counterparts differentiated only with GM-CSF for four days.

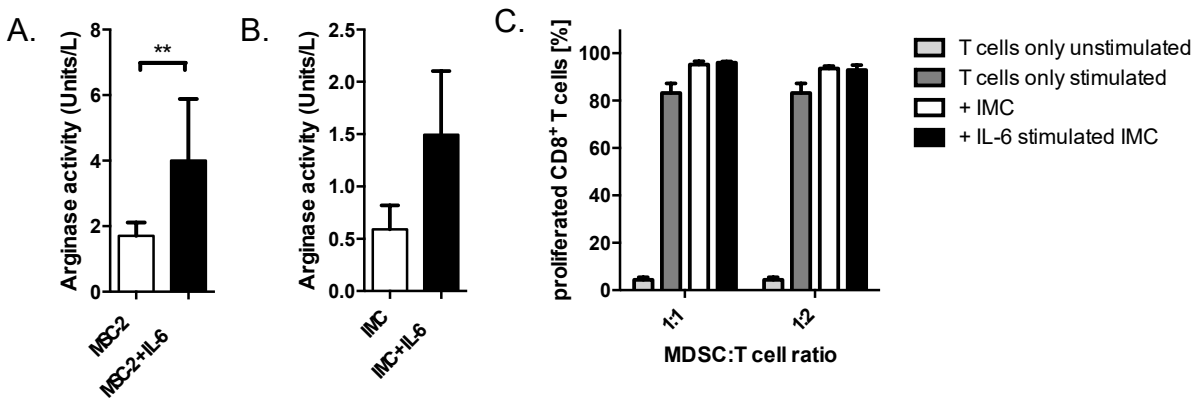

Figure 23. Upregulation of Arg1 activity by IL-6 and effect on immunosuppressive activity of IMC.

MSC-2 cells (A., n=9) or IMC (B., n=3) were stimulated overnight (18 h) with 40 ng/ml IL-6. Arginase activity was measured using the arginase activity assay kit detecting urea by a colorimetric reaction. Arginase activity is shown in Units/L. IMC stimulated overnight with IL-6 were used for a suppression of T cell proliferation assay. Quantification of proliferated T cells is shown (C., n=3, mean with SD, **p<0.01).

Interestingly, we found that after four days of incubation with GM-CSF only, there was still a strong accumulation of around 80 % $CD11b^+Gr1^+$ cells, which is comparable to the accumulation of around 90 % $CD11b^+Gr1^+$ cells with IL-6 and GM-CSF, even though there was a statistically significant difference between the two groups (Figure 24A). Importantly, there was also no difference in the frequency of $PD\text{-}L1^+$ cells within these cell subsets (Figure 24B). In contrast, we were able to detect a significant increase in ROS production by MDSC (IL-6, GM-CSF) as compared to MDSC (GM-CSF) (Figure 24C). Furthermore, we found a significantly higher Arg1 activity in MDSC differentiated with IL-6 and GM-CSF than that in cells differentiated only with GM-CSF (Figure 24D).

Altogether, we found that ROS production and Arg1 activity was significantly increased by using IL-6 in addition to GM-CSF for the differentiation of MDSC.

Finally, we also tested the ability of the both MDSC preparations to suppress $CD8^+$ T cell proliferation. Interestingly, the MDSC differentiated with IL-6 and GM-CSF showed a significantly stronger suppression of T cell proliferation compared to cells differentiated with GM-CSF only (Figure 24E and F). This result confirms that the increase in ROS production and Arg1 activity induced by IL-6 during the differentiation of MDSC could make MDSC (IL-6, GM-CSF) more immunosuppressive than MDSC (GM-CSF).

In conclusion, IL-6 can stimulate an increased suppressive activity of MDSC through upregulation of Arg1 and ROS. However, the MDSC (GM-CSF) are still immunosuppressive and, therefore, could be defined as MDSC.

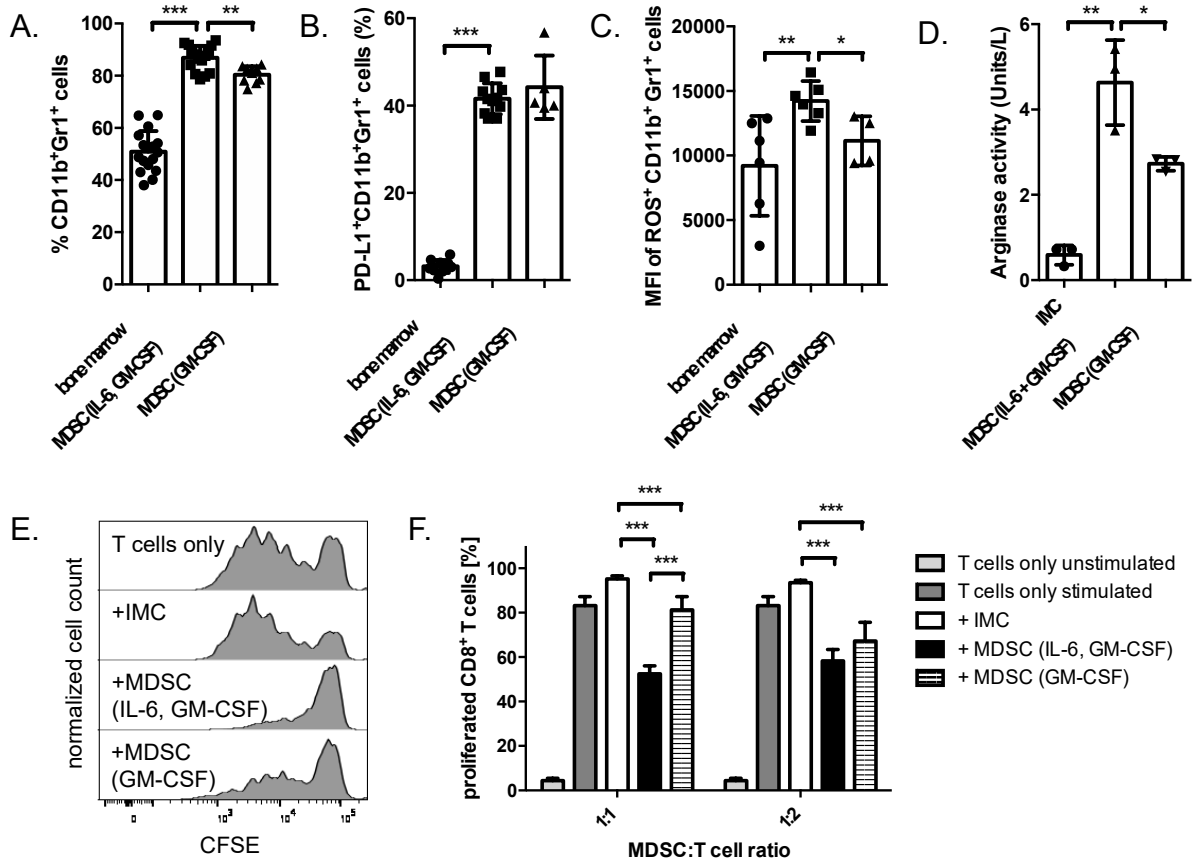

Figure 24. Effect of IL-6 on phenotype and suppressive capacity of *in vitro* differentiated MDSC. Murine bone marrow cells were cultured for four days with IL-6 and GM-CSF or with GM-CSF only for MDSC differentiation and analyzed by flow cytometry for the expression of CD11b and Gr1 (A., n=9-17), PD-L1 (B., n=5-11) and the production of ROS (C., n=4-6). Arginase activity was measured by the arginase activity assay kit detecting urea by a colorimetric reaction (D., n=3). For the suppression of T cell proliferation assay $CD8^+$ T cells were labeled with CFSE, activated with anti-CD3 and anti-CD28 antibodies and co-cultured with respective myeloid cells at the indicated ratios for 72 h. Dilution of CFSE staining in proliferated $CD8^+$ T cells was assessed by flow cytometry. Representative histograms (E.) and quantification of proliferated cells (F., n=6) are shown (mean with SD, *p<0.05, **p<0.01, ***p<0.001).

5.2.6 Microarray analysis of *in vitro* differentiated MDSC

To decipher further the role of IL-6 in MDSC differentiation and activation, we performed a microarray analysis comparing MDSC differentiated with IL-6 and GM-CSF to cells differentiated with GM-CSF only. We first assessed the quality of our data by the correlation heatmap, showing that there is a strong positive correlation between the data of the replicates from the groups, whereas the data comparing two different groups displayed a negative correlation (Figure 25A). This shows that the replicates are comparable in each group, but the differences observed are those between the two experimental groups. The volcano blot shows a strong and significant downregulation of various genes (shown in blue), whereas only some genes displayed a strong and significant upregulation (shown in red) in the MDSC differenti-

ated with IL-6 and GM-CSF as compared to the cells differentiated with GM-CSF only (Figure 25B). In total, there were 1787 genes differentially regulated with an adjusted p-value below 0.05 when comparing both groups. Of the significantly differentially regulated genes, 880 were upregulated and 907 were downregulated. A list of the top 50 upregulated and top 50 downregulated genes with p-values and fold change is presented in the appendix (Supplementary Table 2).

The strongest downregulated gene in the cells differentiated with IL-6 and GM-CSF was the *Cd207* gene with a fold change of about 0.09. This gene encodes for the C-type lectin domain family 4 member K. Furthermore, the *Itgae* gene coding for integrin α E (CD103) as well as the *Cd209a* and *CD209c* genes coding for C-type lectin domain receptors was downregulated. In addition, *Adgre4* and *Egfr* expression was found to be downregulated in the MDSC differentiated with IL-6 and GM-CSF.

The highest upregulated protein-coding gene in the MDSC differentiated with IL-6 and GM-CSF was the *Ccl8* gene, with a fold change of about 23.22 compared to the MDSC differentiated with GM-CSF only. Moreover, the expression of the *Ccl7* gene and the MMP-encoding genes *Mmp13* and *Mmp19* was also upregulated.

In summary, we found that there might be a difference in adhesion of the MDSC differentiated with IL-6 and GM-CSF in comparison to the cells differentiated with GM-CSF only due to a downregulation of several genes implicated in cellular adhesion. Importantly, we failed to find an upregulation of *Arg1*, or any genes implicated in ROS production as observed by functional tests.

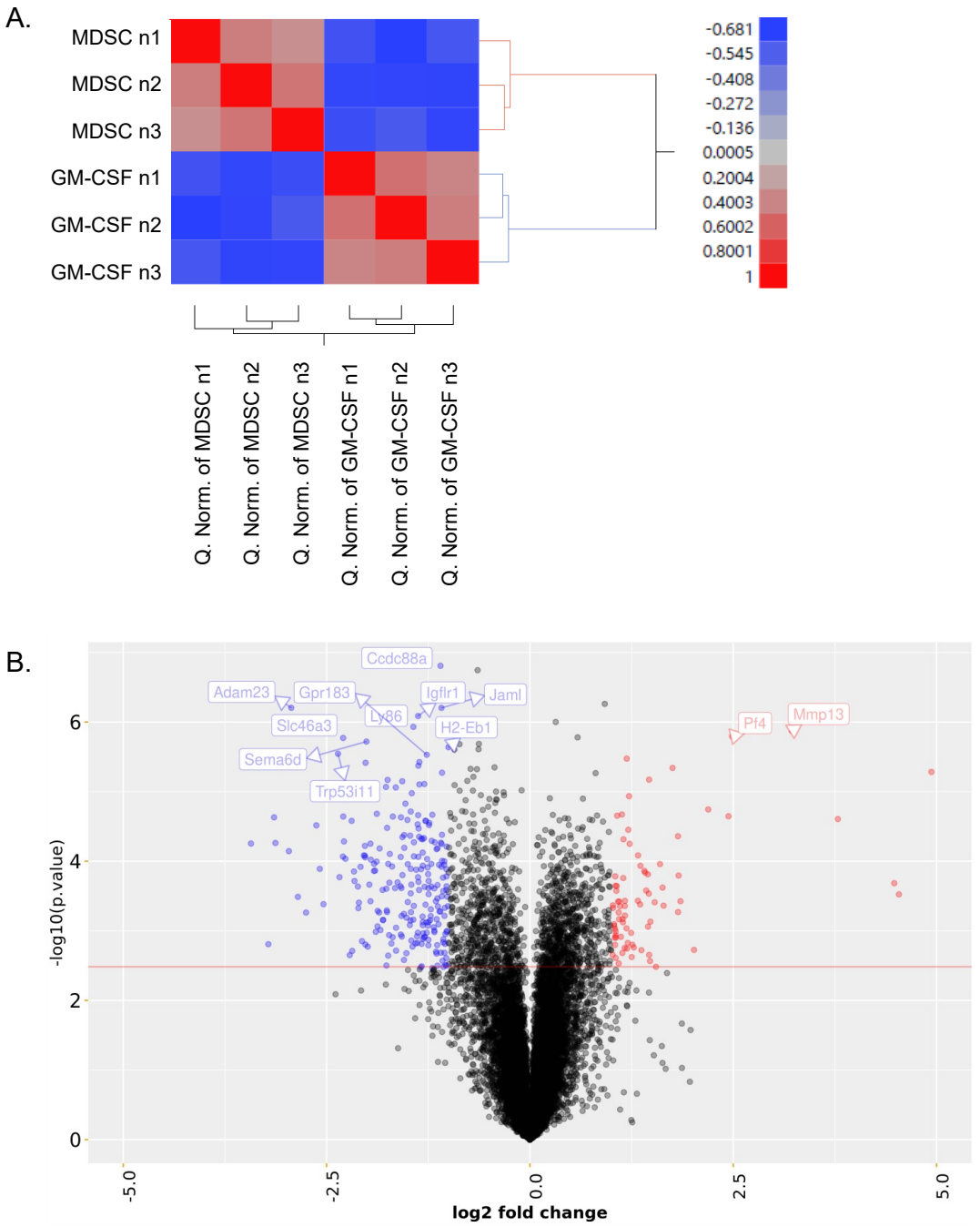

Figure 25. Microarray analysis of *in vitro* differentiated MDSC.
After *in vitro* differentiation of MDSC with IL-6 and GM-CSF or GM-CSF only microarray analysis was performed, and data were assessed by bioinformatics. Correlation heatmap of sample values (A.) and volcano blot of analyzed data (B.) is shown for fold change of MDSC (IL-6, GM-CSF) compared to MDSC (GM-CSF). The red line in the volcano blot shows the adjusted significance cutoff calculated using the number of replicated and the variance upon consideration of the false discovery rate (FDR).

5.3 Investigation of effect of IL-6 OE in melanoma *in vivo*

5.3.1 Generation and validation of IL-6 OE Ret melanoma cells

To investigate the effect of IL-6 on tumor growth, mouse survival and the TME, especially on immune cells like MDSC and T cells, we generated IL-6 OE Ret melanoma cells by lentiviral transduction to inject them s.c. into wild type mice.

After lentiviral transduction we observed a 900-fold upregulation of *Il6* mRNA measured by qRT-PCR in the IL-6 OE Ret cells compared to the empty vector (EV) control Ret cells (Figure 26A). Notably, also the EV control Ret cells showed some basal expression and secretion of IL-6, which was however significantly increased in IL-6 OE Ret cells.

As we aimed to inject the IL-6 OE and EV control Ret cells s.c. into mice to follow up their growth *in vivo*, we first assessed their growth *in vitro* by MTT assay. IL-6 OE Ret cells and EV control Ret cells showed a similar growth behavior until 48 h of culture (Figure 26C). After 72 h, we detected a slight increase in the EV control Ret cells compared to the IL-6 OE Ret cells as a result of the transduction and overexpression of IL-6. However, since the difference was not visible until 48 h and the biological relevance might be minor, we continued with the *in vivo* experiments with these cells.

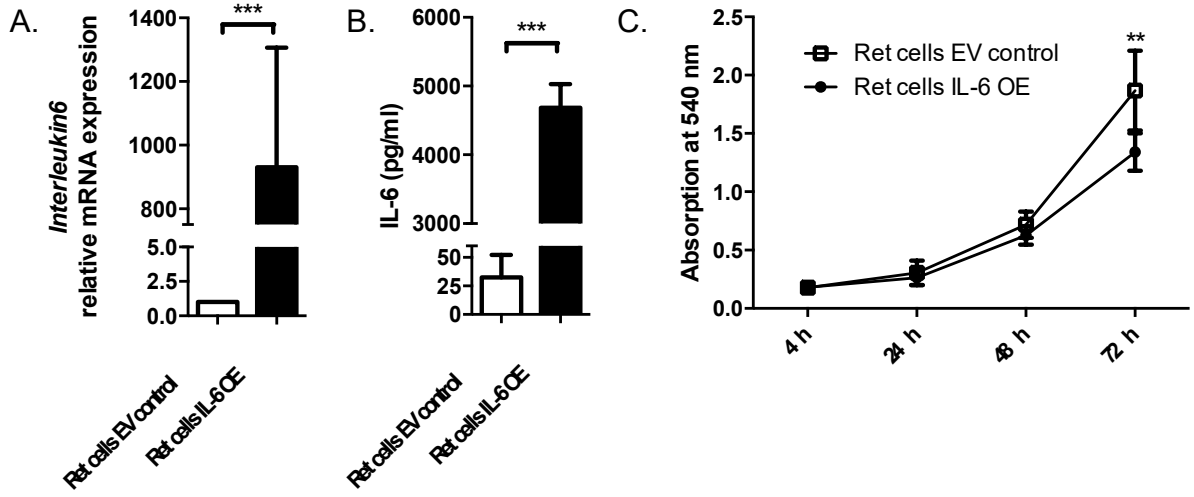

Figure 26. Validation of IL-6 OE in Ret melanoma cells *in vitro*.
The murine Ret melanoma cell line was lentivirally transduced with and IL-6 overexpression (OE) plasmid and the empty vector (EV) as a control. RNA was isolated from EV control and IL-6 OE Ret cells and *Il6* mRNA expression was measured by qRT-PCR. Relative expression calculated by the 2^-ΔΔCT method, normalized to the housekeeping gene *Rn18S* and expressed as fold change towards the unstimulated control is shown (A., n=4). Supernatant of EV control and IL-6 OE Ret cells cultured overnight (18 h) was analyzed for IL-6 by ELISA (B., n=6). *In vitro* growth of EV control and IL-6 OE Ret cells was measured by MTT assay (C., n=6, mean with SD, **p<0.01, ***p<0.001).

5.3.2 Study of IL-6 OE Ret melanoma tumors *in vivo* and *ex vivo*

We used the ectopic melanoma model injecting 5x10^5 Ret melanoma cells s.c. into C57BL/6 wild type mice to analyze the effect of IL-6 overexpression in melanoma. Since we showed *in vitro* that IL-6 can increase CCR5 on MDSC and make MDSC more immunosuppressive through induction of increased Arg1 activity and ROS production, we expected an increased accumulation of MDSC (especially CCR5$^+$ MDSC) and an increased immunosuppression in the TME of IL-6 OE Ret cells and therefore an acceleration in tumor growth and decrease in survival time of mice.

However, we found no difference in the tumor volume in the two experimental mouse groups (Figure 27A). The IL-6 overexpressing tumors and the control tumors grew at the same rate. In addition, there was also no difference in the survival of mice (Figure 27B). We continued to investigate whether there were effects of IL-6 on the immune cells in the TME. Therefore, we studied the accumulation of MDSC, and the expression of immunosuppressive factors like PD-L1, ROS and Arg1 in these cells as well as the tumor-infiltrating T cells (Figure 28).

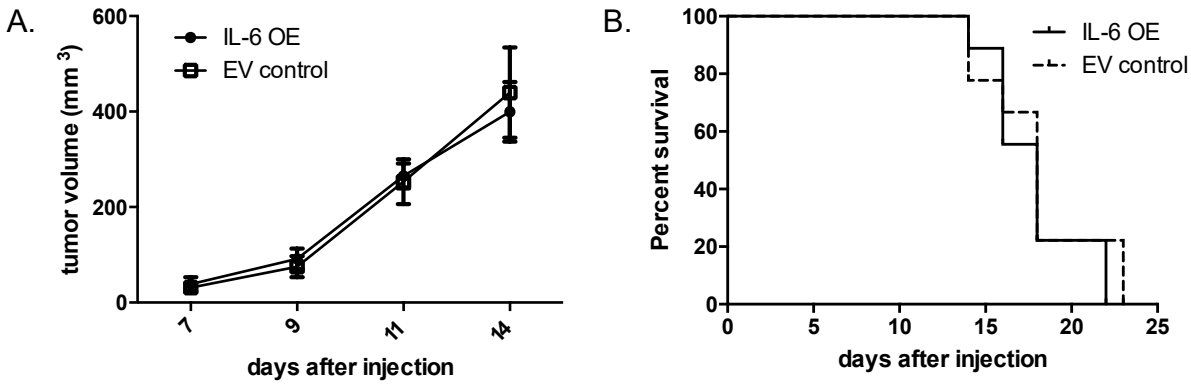

Figure 27. *In vivo* growth of IL-6 OE Ret cells and survival of tumor-bearing mice.
C57BL/6 wild type mice were subcutaneously (s.c.) injected with 5x10^5 Ret melanoma cells (EV control or IL-6 OE) in 100 µl sterile PBS. Mice were monitored three times per week and sacrificed upon reaching one of the termination criteria. Tumor length and width was measured upon progression and the tumor volume was calculated according to the formula: $volume = \frac{width^2 * length}{2}$ (B., n=14, mean with SD). Survival of mice is shown as time point when mouse was sacrificed due to termination criteria (A., n=9).

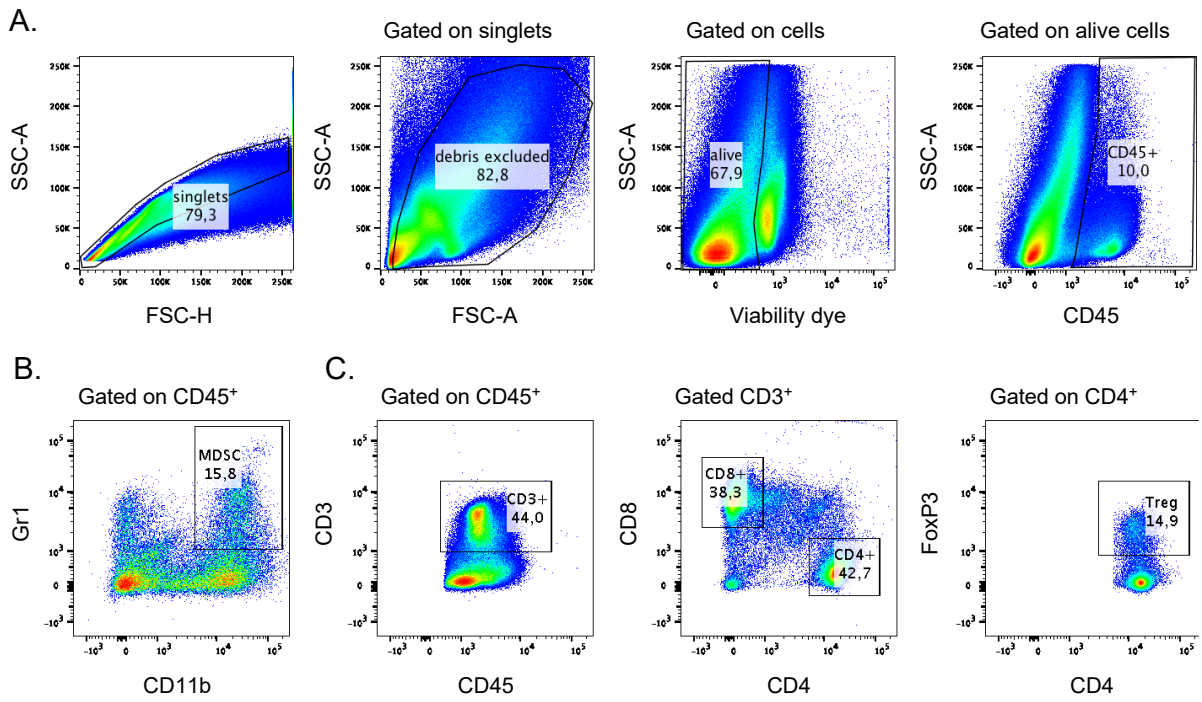

Figure 28. Gating strategy for TIL in murine melanoma tumors.
Single cell suspension from murine tumors was stained with fluorescently labeled antibodies and analyzed at the flow cytometer. We excluded duplets, debris and dead cells followed by the gating on CD45$^+$ leukocytes (A.). For the MDSC panel, CD11b$^+$Gr1$^+$ MDSC were then gated (B.). CCR5-, ROS- and NO-positive gates were set according to the FMO control, whereas Arg1- and PD-L1-positive cells were gated according to the respective isotype control (not shown). T cells were analyzed according to CD3, CD4 and CD8 expression, and Treg were defined as CD4$^+$FoxP3$^+$ cells (C.).

Importantly, we found a more than 10-fold increase in IL-6 production in the tumors derived from IL-6 OE Ret cells, showing that the overexpression is not lost upon *in vivo* tumor progression (Figure 29A). We found no significant changes in the frequency of tumor-infiltrating immune cells in IL-6 OE and control tumors (Figure 29B). However, there was a tendency towards increased frequency of MDSC in the IL-6 OE tumors (Figure 29C). Regarding the frequency of CCR5$^+$ MDSC (Figure 29D) and PD-L1-expressing MDSC (Figure 29E), we were not able to detect an increased accumulation of these cells in IL-6 OE Ret tumors as compared to EV control tumors. Interestingly, we found a slight increase in ROS production in MDSC from IL-6 OE Ret tumors compared to control tumors (Figure 29F). Yet, the frequency of Arg1$^+$ MDSC from IL-6 OE Ret tumors was not changed (Figure 29E).

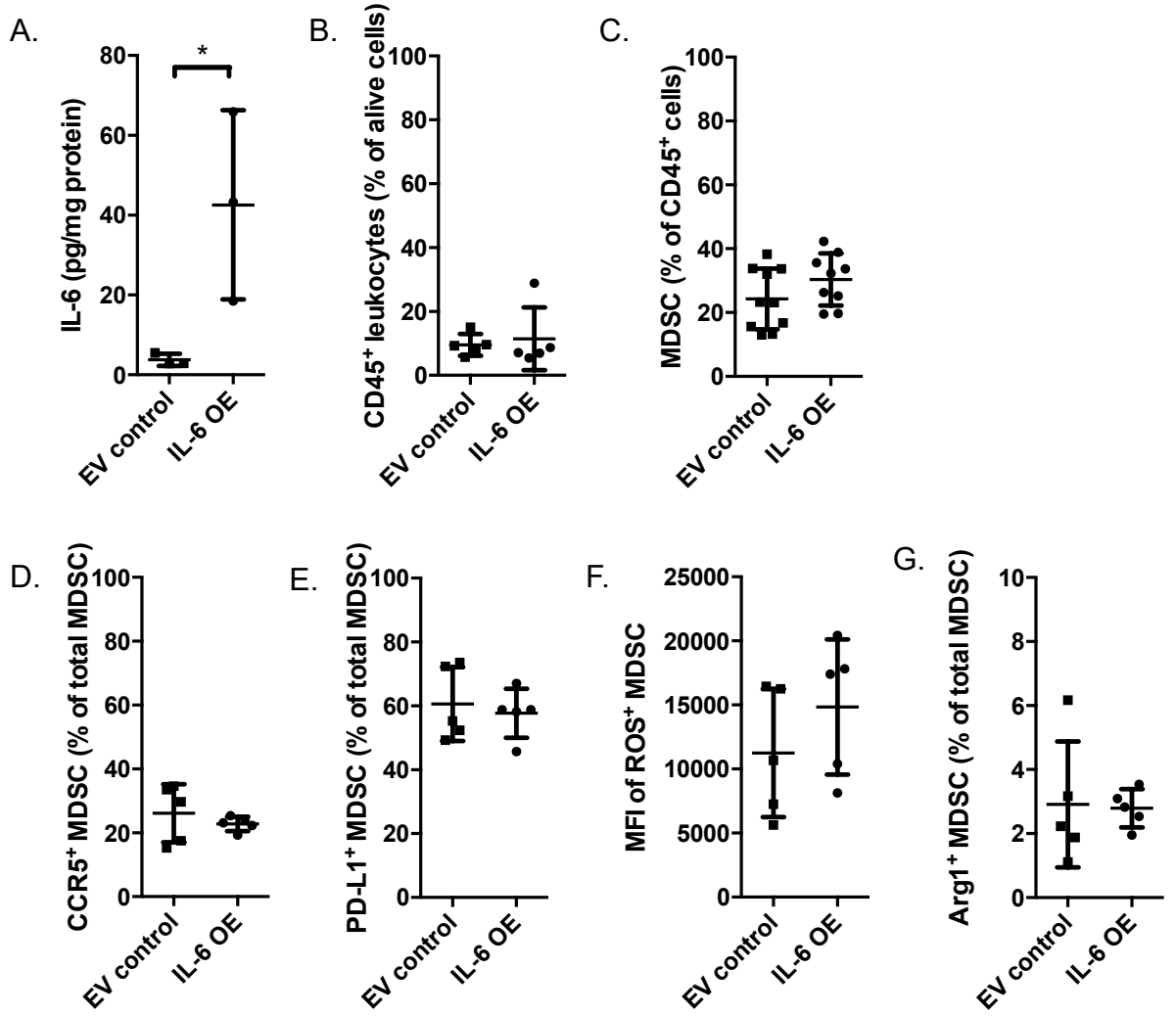

Figure 29. Effect of IL-6 OE in Ret melanoma on tumor-infiltrating MDSC.
14 days after s.c. injection of $5x10^5$ Ret melanoma cells (EV control or IL-6 OE) into C57BL/6 wild type mice tumors were excised, IL-6 was measured by ELISA in tumor lysate (A., n=3) and immune cell populations were measured in single cell suspension from tumor by flow cytometry. Frequencies of $CD45^+$ leukocytes (B.), total MDSC (C.), $CCR5^+$ MDSC (D.), $PD\text{-}L1^+$ MDSC (E.) and $Arg1^+$ MDSC (G.) are shown. The MFI of ROS^+ MDSC (F.) is shown (n=5-10, mean with SD, *$p<0.05$).

Additionally, we analyzed the tumor-infiltrating T cell subpopulations by flow cytometry and found a slight increase in the frequency of $CD3^+$ T cells in the IL-6 OE tumors compared to the EV control tumors (Figure 30A). However, there were no differences in frequencies of $CD8^+$ and $CD4^+$ T cells as well as Treg (Figure 30B-D).

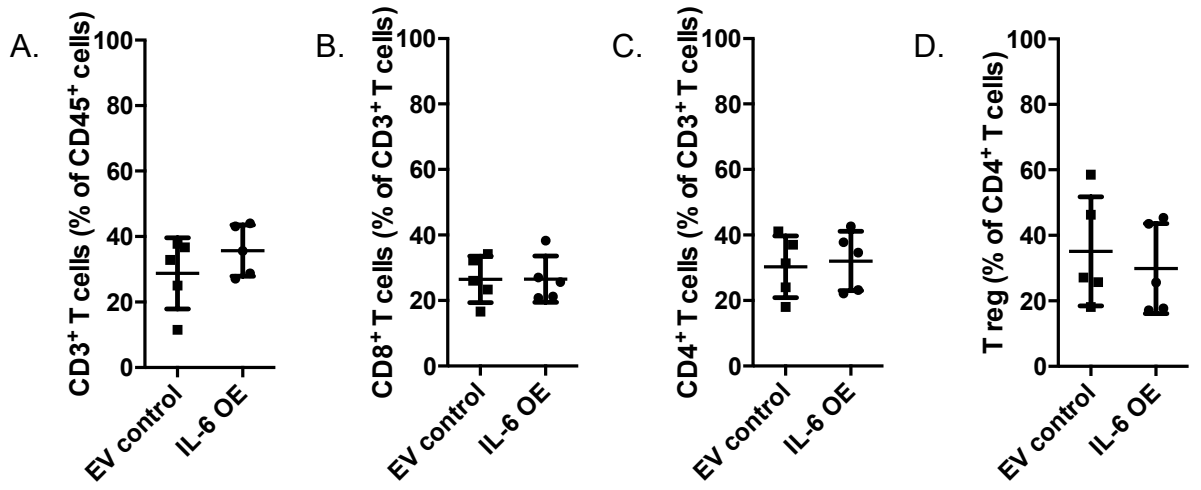

Figure 30. Effect of IL-6 OE in Ret melanoma on tumor-infiltrating T cells.
14 days after s.c. injection of $5x10^5$ Ret melanoma cells (EV control or IL-6 OE) into C57BL/6 wild type mice, tumors were excised and single cell suspension from tumor was analyzed by flow cytometry. Frequencies of total $CD3^+$ T cells (A.), $CD8^+$ T cells (B.), $CD4^+$ T cells (C.) and T reg (D.) are shown (n=5, mean with SD).

5.4 Investigation of the effect of IL-6 blockade in melanoma *in vivo*

In parallel to the experiments with the IL-6 OE melanoma tumors, we were studying the effect of IL-6 blockade on the development of tumors in *RET* transgenic mice. As our *in vitro* experiments have demonstrated that IL-6 can lead to CCR5 upregulation responsible for increased MDSC recruitment and to increased MDSC-mediated immunosuppression, we were aiming to block IL-6 and thereby MDSC recruitment and acquisition of immunosuppressive phenotype. Furthermore, we combined this therapy with PD-1 blockade to study potential synergistic effects.

In contrast to our expectations, we detected a significantly shortened survival of mice receiving the anti-IL-6 therapeutic antibodies compared to the control group (Figure 31A). The combination of anti-IL-6 with anti-PD-1 seemed to rescue this to some extent. However, mice receiving the combination therapy still died earlier compared to the control group. As expected, mice receiving anti-PD-1 therapy did not show a significantly increased survival compared to the control group.

In addition, the anti-IL-6 group showed a tendency to an increased tumor weight in comparison to the control group (Figure 31B). The tumor weights in *RET* transgenic mice are in general highly heterogeneous and resemble the heterogeneous and non-synchronized tumor development in this transgenic mouse model. Still the mice receiving the anti-IL-6 therapy showed the worst survival and the highest tumor weights.

Since the chronic inflammation plays a central role in the melanoma microenvironment and leads to the development and activation of immunosuppressive MDSC, we expected the effect of the IL-6 blockade to have a bigger influence on MDSC-mediated immunosuppression than on the anti-tumor immune response. Therefore, we studied tumor-infiltrating immune cells and their changes upon IL-6 blockade to find reasons for the absence of the expected effect on tumor growth and mouse survival. The different tumor-infiltrating immune cell populations were analyzed according to the gating strategy described earlier (see Figure 28). We found only subtle differences in the frequency of total CD45$^+$ leukocytes. Notably, we saw a slight decrease in CD45$^+$ leukocytes in the anti-IL-6 group compared to the control group (Figure 31C).

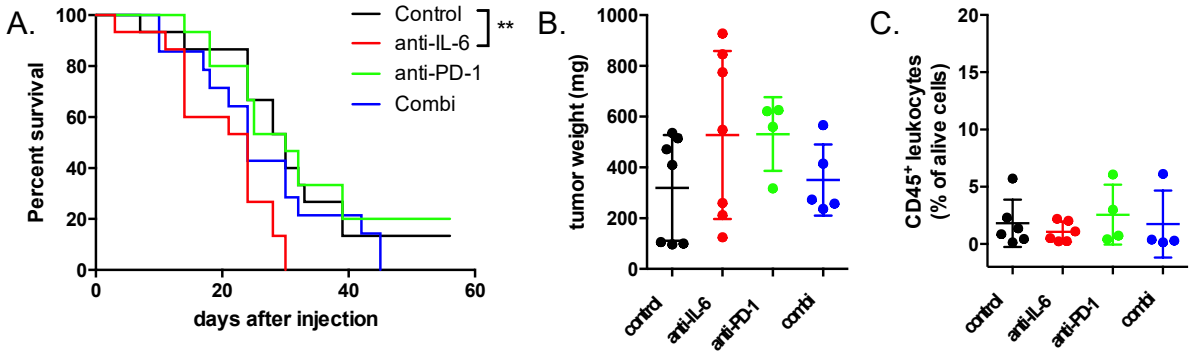

Figure 31. Effect of anti-IL-6 and anti-PD-1 therapy on *RET* mouse survival and tumor weight. *RET* transgenic tumor-bearing mice were treated i.p. with anti-IL-6 or anti-PD-1 antibodies, or the combination of both (combi). Control mice received isotype control antibodies. Therapy was given for four weeks, twice per week. Mice were monitored three times per week and sacrificed upon reaching one of the termination criteria. Survival of mice is shown (B., n=15, **p<0.01). In another experiment, all mice were sacrificed after the four weeks of therapy. Tumor weight after resection of the tumors (C., n=4-7) and frequency of CD45$^+$ leukocytes in the tumor measured by flow cytometry are shown (D., n=4-6, mean with SD).

The changes in the total MDSC frequency were rather minor, with a slight decrease of the tumor-infiltrating MDSC frequency in the anti-PD-1 and combi therapy groups (Figure 32A). We observed an increase in CCR5$^+$ MDSC frequency in the anti-IL-6 therapy group compared to the control group (Figure 32B). In addition, we found no differences in PD-L1$^+$ and Arg1$^+$ MDSC infiltrating tumors from different therapy groups (Figure 32C-D). However, there was a slight increase in NO production by MDSC for all the therapy groups compared to the control non-treated group (Figure 32E). Interestingly, we detected a decrease of ROS production by MDSC in the anti-IL-6 and combi therapy groups compared to the control and anti-PD-1 groups (Figure 32F). In summary, the applied therapies displayed no significant effects on tumor-infiltrating MDSC frequency, or expression of the immunosuppressive factors like PD-L1 and Arg1 and production of NO. Remarkably, we observed a decrease of ROS production by MDSC after anti-IL-6 therapy.

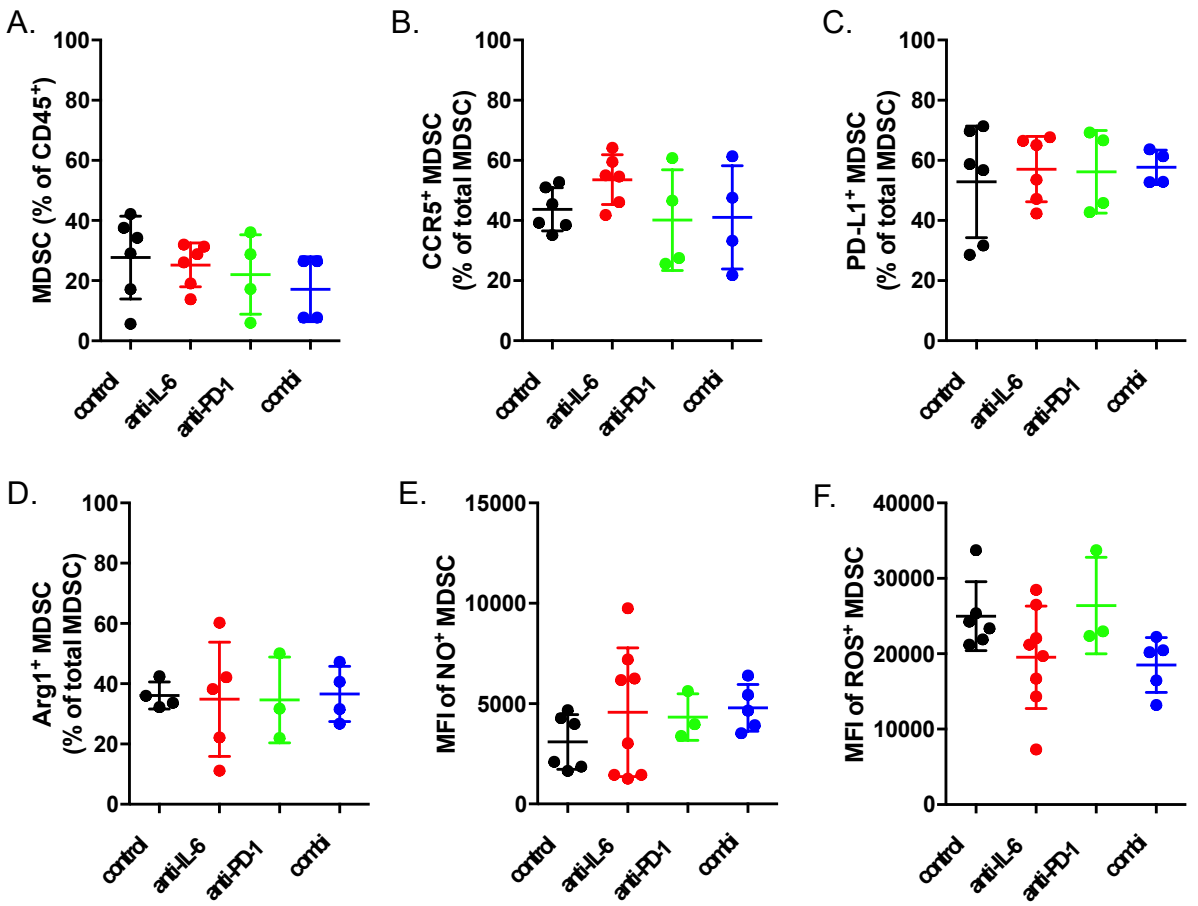

Figure 32. Effect of anti-IL6 and anti-PD-1 therapy on tumor-infiltrating MDSC in *RET* mice. After therapy of *RET* mice for four weeks, all mice were sacrificed, and single tumor cell suspension was analyzed by flow cytometry. Frequency of MDSC (A.), frequency of CCR5$^+$ (B.), PD-L1$^+$ (C.) and Arg1$^+$ (D.) MDSC and production of NO (E.) and ROS (F.) by MDSC are shown (n=4-8, mean with SD).

Analyzing tumor-infiltrating T cells, we demonstrated a tendency of decrease in the frequency of total CD4$^+$ T cells in the anti-IL-6 therapy group but a tendency of increase in the anti-PD-1 and combi-therapy groups (Figure 33A). In contrast, the frequency of CD4$^+$ Treg was unchanged (Figure 33B). Furthermore, there was also a tendency of increase in the frequency of CD8$^+$ T cells in the anti-PD-1 and combi therapy groups (Figure 33C).

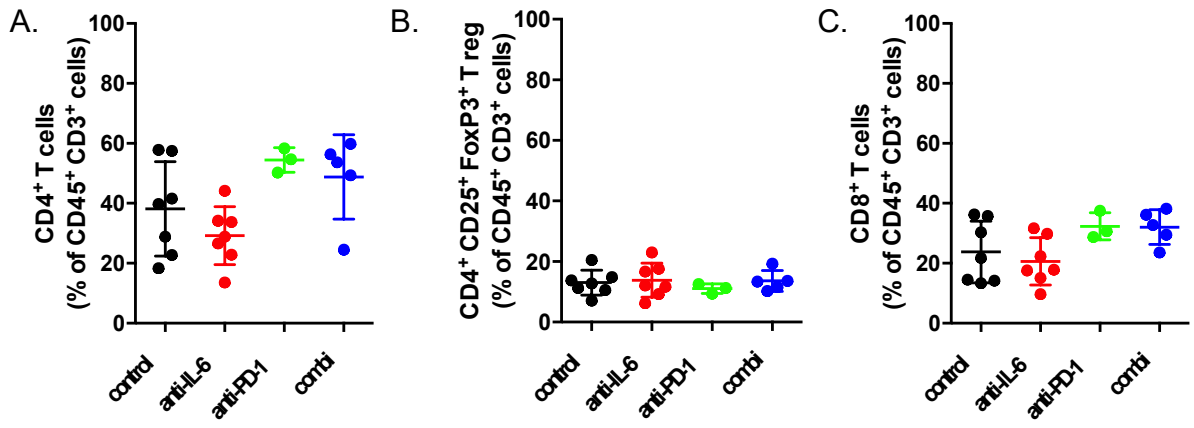

Figure 33. Effect of anti-IL-6 and anti-PD-1 therapy on tumor-infiltrating T cells in *RET* mice. After therapy of *RET* mice for four weeks, all mice were sacrificed, and single tumor cell suspension was analyzed by flow cytometry. Frequency of total $CD4^+$ T cells (A.), Treg (B.) and $CD8^+$ T cells is shown (mean with SD, n=3-7).

6 Discussion

6.1 Upregulation of CCR5 on MDSC

6.1.1 IL-6, GM-CSF and IFN-γ induce *Ccr5* upregulation

The aim of this work was to study the molecular mechanisms of CCR5 upregulation on MDSC in melanoma that lead to increased migration by increasing CCR5 expression on MDSC and could potentially also stimulate immunosuppressive capacity of $CCR5^+$ MDSC. Since it was shown before that $CCR5^+$ MDSC accumulate in the tumors and metastatic lymph nodes of *RET* transgenic melanoma-bearing mice through CCR5-CCR5 ligand dependent migration and that this migration can be inhibited *in vivo* by blocking the CCR5 ligands (Blattner *et al.*, 2018), we investigated the factors responsible for CCR5 upregulation on MDSC. Upon identification of the factors that upregulate CCR5, blockade of these factors could inhibit the upregulation of CCR5 and thereby migration of MDSC to the TME, where they inhibit activity of tumor-infiltrating T cells.

In cancer, MDSC accumulation and activation is orchestrated by factors associated with chronic inflammation like G-CSF, M-CSF, GM-CSF, IL-6, VEGF, IFN-γ, IL-1β and TLR ligands (Condamine and Gabrilovich, 2011). In *RET* transgenic melanoma bearing mice, VEGF levels in the tumors were shown to correlate with the tumor weight and increased levels of VEGF and IL-6 could be detected in the serum of tumor-bearing mice compared to wild type mice (Zhao *et al.*, 2009). Furthermore, IL-1β, IFN-γ and GM-CSF were observed to be increased in fast growing murine melanomas (Meyer *et al.*, 2011). Altogether, these factors can lead to MDSC generation in melanoma. In addition, the endogenous TLR ligand HSP86 was found on melanoma-derived EV, that were able to convert myeloid cells into MDSC (Fleming *et al.*, 2019).

Different studies have shown that CCR5 can be upregulated on long-term activated T cells by IL-2 (Bleul *et al.*, 1997; Wu *et al.*, 1997; Yang *et al.*, 2001). Furthermore, in human mononuclear phagocytes, IFN-γ was able to upregulate CCR5 surface expression and increase migration towards the CCR5 ligands (Hariharan *et al.*, 1999). Moreover, IFN-γ, IL-10, IL-4 and LPS could increase CCR5 expression on mRNA and protein level in murine macrophages (Bosco *et al.*, 2004).

Therefore, we have been testing the effect of a set of the described factors, known to play a role in MDSC development, on the expression of *Ccr5* on MDSC. Interestingly, we found that IFN-γ, GM-CSF and IL-6 can significantly upregulate *Ccr5* mRNA expression on MSC-2 cells *in vitro*. Whereas tumor-derived EV, IL-1β and the TLR ligands LPS, Pam3CSK4 and R848

failed to induce *Ccr5* expression at the mRNA level. We could reproduce IFN-γ-induced *Ccr5* upregulation, as seen by others before (Hariharan *et al.*, 1999; Bosco *et al.*, 2004). Although some publications indicate a potential upregulation of CCR5 on MDSC induced by the CCR5 ligands (Karin and Razon, 2018), we failed to find an upregulation of *Ccr5* upon stimulation of MSC-2 cells with the CCR5 ligands CCL3, -4 and -5. Therefore, no increased *de novo* synthesis of CCR5 could be assumed. The rapid upregulation of CCR5 on PMN-MDSC by its ligands described before (Karin and Razon, 2018) could be due to a transport of the protein to the cell surface without induction of protein synthesis.

6.1.2 CCR5 upregulation via IL-6/STAT3 during MDSC differentiation

Interestingly, we found a strong significant upregulation of *Ccr5* by IL-6 and to a lower extent by GM-CSF. These two factors are very important in MDSC development and are sufficient to differentiate MDSC from murine bone marrow cells *in vitro* (Marigo *et al.*, 2010). Upon the MDSC *in vitro* differentiation with IL-6 and GM-CSF for four days, we were able to show that CCR5 is upregulated at the protein level on the cell surface of $CD11b^{+}Gr1^{+}$ cells. GM-CSF alone induced significant CCR5 upregulation after four days of incubation, yet the addition of IL-6 could significantly increase this upregulation. The frequency of $CCR5^{+}$ MDSC *in vitro* differentiated with IL-6 and GM-CSF were similar to the levels seen for tumor infiltrating MDSC in the *RET* transgenic mice (Blattner *et al.*, 2018).

In addition, we found a positive correlation between the IL-6 level in the tumors of *RET* transgenic mice and the frequency of tumor-infiltrating $CCR5^{+}$ MDSC, suggesting that IL-6-induced CCR5 upregulation on MDSC could play a role in murine melanoma *in vivo*. A significant increase of $CCR5^{+}$ IMC from about 2.5 % to 5 % frequency was already shown for short term IL-6 stimulation for 2 h (Blattner *et al.*, 2018). However, similar to the rapid increase of CCR5 induced by the CCR5 ligands, this might rather be a result of transport of CCR5 to the cell surface than *de novo* synthesis. In our experiments, we could show for the first time, that *Ccr5* mRNA expression is upregulated by IL-6 and GM-CSF and CCR5 on the cell surface is upregulated upon MDSC *in vitro* differentiation with these factors.

Moreover, we determined a molecular mechanism of IL-6-induced CCR5 upregulation on MDSC *in vitro*. IL-6 signaling is mediated by a complex formed between IL-6, the IL-6R and a homodimer of the signal transduction molecule gp130 that leads to the activation of JAK family kinases which phosphorylate STAT3 (Wolf *et al.*, 2014). Phosphorylated STAT3 can form homodimers that translocate to the nucleus and induce target gene expression. Importantly, we showed that the MSC-2 cells are expressing the IL-6R and gp130, and that STAT3 is phosphorylated in these cells upon IL-6 stimulation. Moreover, we found by *in silico* analysis that the murine *Ccr5* promoters have four putative STAT3 binding sites. Finally, we demon-

strated that IL-6-induced *Ccr5* upregulation could be abrogated by the STAT3 inhibitor Stattic.

Altogether, these results show that IL-6 can induce CCR5 upregulation via a STAT3 dependent mechanism. Interestingly, we found an increase in the frequency of pSTAT3^{+}CCR5^{+} tumor-infiltrating MDSC in *RET* transgenic mice, as well as an increase in pSTAT3 intensity, as compared to their CCR5^{-} counterparts from the same tumors. These results indicate that pSTAT3 plays an important role in CCR5 upregulation on MDSC in melanoma *in vivo*.

6.1.3 CCR5 and migratory capacity of *in vitro* differentiated MDSC

Interestingly, an increase in specific migration towards the CCR5 ligands for *in vitro* differentiated MDSC expressing higher levels of CCR5 was not detected. We found a significantly higher migration of IMC towards the CCR5 ligands compared to the spontaneous migration with the control medium, which is an agreement with a previous publication (Blattner *et al.*, 2018). However, in case of the *in vitro* differentiated MDSC, the spontaneous migration was already increased and there were no additional changes under the influence of the CCR5 ligands. This could be due to the fact that STAT3 activity, which is increased in the differentiated MDSC, can promote cellular migration (Teng *et al.*, 2009). Such unspecific effect, which could be induced by IL-6 and GM-CSF, might mask the CCR5 ligand-specific migration.

However, there is already plenty of evidence that CCR5-CCR5 ligand dependent migration of MDSC is active and plays an important role in melanoma (Blattner *et al.*, 2018) and in prostate cancer (Hawila *et al.*, 2017). Thus, Blattner *et al.* (2018) showed that in the *RET* transgenic melanoma model, the CCR5 ligands were enriched in the tumors of mice, and therefore CCR5^{+} MDSC migrated to the tumor. This migration could be inhibited by blocking the CCR5 ligands. Hawila *et al.* (2017) showed that an increase in CCR5 ligands in the peripheral blood of mice induced by CCR5 ligand injection, led to the mobilization of CCR5^{+} MDSC from the bone marrow to the blood. Furthermore, the CCR5-CCR5 ligand axis was also implicated to play a role in NSCLC, where the frequency of CCR5^{+} MDSC was increased in the peripheral blood of patients, and the CCR5 ligands CCL3, -4 and -5 were strongly elevated in tumor tissue compared to the peripheral blood (Yamauchi *et al.*, 2018). In a mouse model of gastric cancer, it has been reported that MDSC could be recruited via the CCR5-CCR5 ligand axis (Yang *et al.*, 2018). Besides, MDSC migration into the peritoneal cavity in endometriosis was shown to be linked to the CCR5-CCR5 ligand axis (Guo *et al.*, 2019).

Our data show that CCR5 was upregulated by IL-6 and GM-CSF through STAT3 during MDSC differentiation *in vitro*, and that IL-6 and STAT3 played an important role in CCR5 upregulation on MDSC in murine melanoma *in vivo*. Subsequently, CCR5^{+} MDSC can be recruited to the tumor by the CCR5 ligands.

There is already some basal expression of CCR5 with a frequency of about 5 % on $CD11b^+Gr1^+$ cells in the bone marrow of wild type mice, which is slightly increased in melanoma bearing mice up to 10 %. IL-6 and GM-CSF could be responsible for this increase of CCR5 on MDSC in the bone marrow and for the mobilization of MDSC from the bone marrow to the peripheral blood as described by Hawila *et al*. (2017). However, in the tumor, the frequency of $CCR5^+$ MDSC was around 30 %, which might be an accumulation of $CCR5^+$ MDSC combined with the induction of CCR5 on MDSC by IL-6 reflected by a positive correlation of the IL-6 level and the frequency of $CCR5^+$ MDSC in the tumor.

Since IFN-γ was described to be elevated in the TME (Meyer *et al.*, 2011) and could upregulate *Ccr5* in our study, an influence of this factor on CCR5 expression in addition to IL-6 and GM-CSF is highly likely but was not further studied in this work.

In conclusion, we could show that IL-6, GM-CSF and IFN-γ upregulated *Ccr5* expression on MDSC. IL-6 and GM-CSF were also found to upregulate CCR5 on the cell surface during MDSC differentiation by a STAT3 dependent mechanism. We have collected evidence that IL-6 and STAT3 play an important role in $CCR5^+$ MDSC in melanoma *in vivo*, highlighting this pathway as a potential new target to block CCR5 upregulation and thereby recruitment of MDSC to the tumor site.

6.2 IL-6 but not the CCR5 ligands induced MDSC immunosuppressive activity

6.2.1 $CCR5^+$ MDSC are more immunosuppressive than $CCR5^-$ MDSC

Melanoma-infiltrating $CCR5^+$ MDSC were shown to express increased levels of the immunosuppressive markers PD-L1 and Arg1 and to produce elevated levels of ROS and NO compared to their $CCR5^-$ counterparts (Blattner *et al.*, 2018). As predicted by these results, we found that $CCR5^+$ MDSC isolated from murine melanoma inhibited the proliferation of $CD8^+$ T cells *in vitro* stronger than their $CCR5^-$ counterparts (results in this thesis and published by Blattner *et al.*, 2018). In line with our findings, it was shown in an ectopic prostate cancer mouse model, that $CCR5^+$ MDSC expressed more Arg1 and stronger suppressed $CD4^+$ T cell proliferation (Hawila *et al.*, 2017). These authors have speculated that the CCR5 ligands can induce Arg1 expression on $CCR5^+$ MDSC and thereby mediate the increased immunosuppressive capacity of these cells. However, their publication does not show any data on Arg1 induction by CCR5 ligands. Furthermore, another publication showed that MDSC from breast cancer-bearing CCL5 knockout mice were less suppressive as compared to MDSC from breast cancer-bearing wild type mice (Zhang *et al.*, 2013). This indicates that CCL5 could be involved in the induction of immunosuppressive capacity of MDSC. This is further

supported by data showing that MDSC from breast cancer-bearing CCL5 knockout mice express less NOS2 and S100A8/9 and have a rather immunostimulatory than immunosuppressive phenotype (Ban *et al.*, 2017). Taken together, there is evidence suggesting that the CCR5-CCR5 ligand axis does not only lead to recruitment of MDSC but also plays a role in MDSC-mediated immunosuppression.

6.2.2 Transcriptional profiling of CCR5$^+$ vs. CCR5$^-$ MDSC from tumors

To get a deeper insight into the mechanisms behind the stronger immunosuppressive phenotype of CCR5$^+$ MDSC, we performed a microarray analysis of the tumor-infiltrating CCR5$^+$ and CCR5$^-$ MDSC subpopulations. Among the top downregulated genes in CCR5$^+$ MDSC (compared to their CCR5$^-$ counterparts) were the chemokine CCL22 and the chemokine receptors CCR7 and CCR2. CCL22 is known to recruit Treg into the TME, and tumor as well as myeloid cells can produce this chemokine (Wiedemann *et al.*, 2016). The downregulation of *Ccl22* expression in CCR5$^+$ MDSC suggests that this MDSC subpopulation might be less responsible for CCL22 dependent Treg recruitment compared to the CCR5$^-$ MDSC.

The strongest upregulated gene in CCR5$^+$ MDSC in our microarray assay was the *Fabp4* gene coding for the fatty acid binding protein 4. FABP4 is involved in the uptake, transport and metabolism of fatty acids (Hotamisligil and Bernlohr, 2015). Interestingly, fatty acid metabolism was described to play a role in MDSC-mediated immunosuppression. The overexpression of FATP2 in PMN-MDSC was shown to lead to an increased uptake of arachidonic acid and, therefore, to the synthesis of PGE2 that had a suppressive effect on T cells (Veglia *et al.*, 2019). FABP4 was also implicated in PGE2 accumulation (Hotamisligil and Bernlohr, 2015). Therefore, the overexpression of FABP4 could be an additional mechanism of increased immunosuppression mediated by CCR5$^+$ MDSC. However, this mechanism of increased immunosuppressive capacity of these cells will need further study.

Importantly, the second strongest upregulated gene in the CCR5$^+$ MDSC in our microarray was the *Ccl8* gene coding for the chemokine CCL8 which is a ligand for the CCR5 receptor (Gong *et al.*, 1998). The increased expression of *Ccl8* by the CCR5$^+$ MDSC suggests a positive feedback loop mediated by CCL8 binding to the CCR5 receptor. In response to CCL8, CCR5$^+$ MDSC could produce more CCL8 to attract more CCR5$^+$ MDSC to the TME.

Moreover, the genes for the chemokines CCL12, CCL7 and CCL2 were among the upregulated genes. CCL12 is a chemotactic factor for eosinophils, monocytes and lymphocytes and plays an important role in the allergic inflammation of the lungs (Jia *et al.*, 1996). In addition, CCL12 was shown to play a role in the recruitment of M-MDSC into the premetastatic lung in a B16-F10 mouse model (Shi *et al.*, 2017). CCL7 and CCL2 are ligands for the CCR2 receptor (Lazennec and Richmond, 2010) and could, therefore, be involved in M-MDSC recruit-

ment. Altogether, CCR5$^+$ MDSC showed increased expression of genes for chemokines that can attract more MDSC but also eosinophils, monocytes and lymphocytes.

MDSC were shown to express MMP, especially MMP9, that promote a lower integrity of the extracellular matrix and the basal membrane and, thereby, enable tumor cells to enter the blood stream and form metastasis (Jacob and Prekeris, 2015; Baniyash, 2016). In our microarray assay, *Mmp27* expression was found to be increased in the CCR5$^+$ MDSC subpopulation. However, the relevance of these data for MDSC function needs further validation.

6.2.3 CCR5 ligands fail to increase immunosuppressive capacity of MDSC

The microarray analysis did not give further directions for the pathways that lead to upregulation of Arg1, PD-L1 or ROS and NO production in CCR5$^+$ MDSC. However, since it was published that the CCR5 ligands might induce increased immunosuppressive capacity of MDSC (Zhang *et al.*, 2013; Ban *et al.*, 2017; Hawila *et al.*, 2017), we tested the effect of the CCR5 ligands on the expression of genes coding for immunosuppressive factors in MDSC and on their capacity to inhibit T cell proliferation. Importantly, we did not find an upregulation of the tested genes like *Pdl1*, *Tgfb*, *Arg1*, *Nos2*, *Ido*, *Cox2*, *Ptges* and *Il10* at the mRNA level upon stimulation of MSC-2 cells, IMC or *in vitro* differentiated MDSC with the CCR5 ligands. We have included these three model cell types with different expression levels of CCR5 to exclude that the effect is too weak because of low basal CCR5 expression. Moreover, we could not find increased ability of MDSC to suppress T cell proliferation when stimulating IMC or *in vitro* differentiated MDSC with the CCR5 ligands. The association of the CCR5 ligands with increased immunosuppressive capacity of MDSC were shown so far only in mice *in vivo* (Zhang *et al.*, 2013; Ban *et al.*, 2017; Hawila *et al.*, 2017), however, as shown by our experiments, it seems not to be a direct upregulation of genes coding for immunosuppressive factors in MDSC upon CCR5 ligand stimulation.

6.2.4 IL-6 can induce increased immunosuppressive capacity of MDSC

Since we were not able to show that the increased immunosuppressive capacity of CCR5$^+$ MDSC could be induced via the CCR5 ligands, we hypothesized that genes coding for immunosuppressive factors could be upregulated by IL-6 in parallel to CCR5 upregulation on MDSC. Therefore, we stimulated MSC-2 cells and IMC with IL-6 and measured the expression of the genes mentioned above. Interestingly, we found a significant increase in the expression of *Arg1* induced by IL-6 in MSC-2 cells and IMC and could also confirm an increased Arg1 activity upon the stimulation of MSC-2 cells with IL-6. Moreover, we demonstrated five putative STAT3 binding sites in the murine *Arg1* promoter/enhancer, and that the

Arg1 upregulation induced by IL-6 was STAT3 dependent since it was blocked by the STAT3 inhibitor Stattic.

Moreover, upon *in vitro* differentiation of MDSC by IL-6 and GM-CSF the Arg1 activity was significantly increased as compared to cells differentiated with GM-CSF only. The Arg1 induction by overnight stimulation of IMC with IL-6 was not sufficient to increase suppressive capacity on T cells exerted by these cells. However, *in vitro* differentiated MDSC (IL-6, GM-CSF) were significantly more suppressive as compared to cells differentiated with GM-CSF only. This increased inhibition of T cell proliferation could be attributed to the increased Arg1 expression induced by IL-6. However, to finally prove that Arg1 is the most important factor induced by IL-6 and responsible for MDSC-mediated immunosuppression, it would be necessary to include an arginase inhibitor in the co-culture of MDSC with T cells. Notably, the MDSC (IL-6, GM-CSF) produce also more ROS compared to the MDSC (GM-CSF).

IL-6 was previously demonstrated to play a role in the accumulation and activation of MDSC and to correlate with increased MDSC frequency in different cancer types, among them hepatocellular carcinoma (Lin *et al.*, 2017; Xu *et al.*, 2017), ovarian cancer (Wu *et al.*, 2017), bladder cancer (Yang *et al.*, 2017), squamous cell carcinoma (Chen *et al.*, 2014) and malignant melanoma (Meyer *et al.*, 2011; Bjoern *et al.*, 2016). It was shown that IL-6 was able to induce Arg1 upregulation in murine $CD11c^+$ DC *in vitro* at the mRNA and protein level and to downregulate expression of MHC class II in fibrosarcoma-bearing mice that correlated with the increased serum IL-6 levels and accelerated tumor progression (Narita *et al.*, 2013). Upon alternative activation of M-CSF differentiated murine macrophages *in vitro* with IL-4 and IL-13, the addition of IL-6 led to an increase in the expression of *Arg1* as well as its activity in these $F4/80^+$ cells (Fernando *et al.*, 2014). In the same publication, it was shown that the IL-6-induced Arg1 upregulation in alternatively activated macrophages was STAT3 dependent, and that the IL-6-treated alternatively activated macrophages suppressed the secretion of INF-γ, IL-4 and IL-2 by activated T cells. The serum IL-6 level in patients with esophageal squamous cell carcinoma was observed to positively correlate with the MDSC frequency in the peripheral blood (Chen *et al.*, 2014). In the same publication, it was reported that the treatment of healthy donor PBMC with IL-6 for six days resulted in an increase of $CD14^+HLA\text{-}DR^-$ cells as well as in an increase in pSTAT3, *ARG1* mRNA expression and ROS production in these cells.

Interestingly, tumor-infiltrating and circulating M-MDSC from head and neck squamous cell carcinoma patients were found to display high pSTAT3 levels, that correlated with Arg1 expression and activity (Vasquez-Dunddel *et al.*, 2013). In the same study, the STAT3 inhibitor Stattic and STAT3-targeted siRNA were able to decrease Arg1 activity and to abrogate MDSC immunosuppressive function. The authors demonstrated by chromatin immunoprecip-

itation that the human *ARG1* promoter had multiple STAT3-binding elements. Recently, it has been reported that immunosuppressive $CD14^+$ M-MDSC from patients with pancreatic ductal adenocarcinoma were characterized as STAT3 and Arg1 expressing cells, whereas non-immunosuppressive $CD14^+$ cells from the same patients were lacking the distinct *STAT3/ARG1* transcriptomic gene signature (Trovato *et al.*, 2019). Moreover, IL-6 produced by hepatocellular carcinoma cells was found to be responsible for the upregulation of *Arg1*, *Cox2* and *Nos2* in MDSC leading to an increase in Arg1 activity, nitrite and ROS production and, thereby, increased immunosuppressive capacity of MDSC (Xu *et al.*, 2017).

In line with these publications, we showed here that IL-6-induced Arg1 upregulation via STAT3 during murine MDSC *in vitro* differentiation, leading to the stimulation of immunosuppressive capacity. Furthermore, IL-6 was also shown to upregulate pSTAT3, *ARG1* expression and ROS production in human monocytic cells (Chen *et al.*, 2014). In addition, a strong correlation between pSTAT3, Arg1 expression in MDSC and immunosuppressive capacity of these cells was observed in cancer patients (Vasquez-Dunddel *et al.*, 2013; Trovato *et al.*, 2019).

We found that IL-6 could induce ROS production in MDSC as it was also reported by others (Chen *et al.*, 2014; Xu *et al.*, 2017). The increased production of ROS by MDSC was reported to be due to the overexpression of the NOX2 enzyme, which is controlled by STAT3 (Corzo *et al.*, 2009). Therefore, the increase in ROS production observed in MDSC upon *in vitro* differentiation with IL-6 could be mediated by a STAT3-dependent upregulation of NOX2. However, this needs to be further studied.

Importantly, using the suppression of T cell proliferation assay, we could show that cells differentiated in the presence of GM-CSF only had suppressive activity on the proliferation of $CD8^+$ T cells that permits defining them as MDSC. Moreover, GM-CSF stimulated the upregulation of PD-L1 during *in vitro* differentiation of MDSC that was confirmed by another publication (Wang *et al.*, 2017). Even though IL-6 was also shown to induce PD-L1 by a STAT3-dependent mechanism in human tolerogenic APC generated by TLR ligand stimulation from $CD14^+$ monocytes (Wölfle *et al.*, 2011), we were not able to detect increased PD-L1 expression by the addition of IL-6 to the MDSC differentiation. This might be due to the fact that there was already a strong upregulation of PD-L1 induced by GM-CSF alone and IL-6 failed to further increase this upregulation. Moreover, we did not observe an increase in *Pdl1* mRNA expression in MSC-2 cells or IMC stimulated with IL-6, indicating that the IL-6-induced PD-L1 upregulation in the murine system might not be as strong as in the human settings used by Wölfle *et al*. (2011).

Interestingly, GM-CSF was shown to play a crucial role in inducing PMN-MDSC immunosuppressive capacity by upregulating fatty acid transport protein 2 (FATP2) (Veglia *et al.*, 2019).

FATP2 is involved in the uptake of arachidonic acid and the synthesis of PGE2. Therefore, GM-CSF led to increased expression of FATP2, which resulted in accumulation of PGE2 that suppresses T cell activity (Veglia *et al.*, 2019).

The GM-CSF-induced upregulation of PD-L1 and accumulation of PGE2 are two major mechanisms explaining why the cells differentiated only with GM-CSF are immunosuppressive as well. However, IL-6 induces in addition the Arg1 upregulation and the increased expression of ROS.

6.2.5 Transcriptional profiling of *in vitro* differentiated MDSC

To further study the specific role of IL-6 during MDSC differentiation we performed a microarray analysis of MDSC differentiated with IL-6 and GM-CSF in comparison to GM-CSF only. The strongest downregulated gene in the cells differentiated with IL-6 and GM-CSF was the *Cd207* gene coding for the C-type lectin domain family 4 member K. Furthermore, the *Itgae* gene coding for integrin α E (CD103), as well as the *Cd209a* and *CD209c* genes coding for C-type lectin domain receptors were downregulated. The C-type lectin receptors are carbohydrate-binding proteins that are involved in cellular adhesion and migration as well as in sensing and uptake of pathogens (Cambi and Figdor, 2003). Here, the selectins are more implicated in adhesion and migration, whereas the mannose receptor subfamily is specialized on pathogen binding. However, CD209 for example has both functions (Cambi and Figdor, 2003). Integrins are cell adhesion receptors that bind to the extracellular matrix (Takada *et al.*, 2007). The downregulation of these genes involved in cellular adhesion suggests that MDSC differentiated by IL-6 and GM-CSF were less adhesive and might show a worse pathogen recognition via C-type lectin receptors compared to cells differentiated with GM-CSF only.

The highest upregulated protein-coding gene in the MDSC differentiated with IL-6 and GM-CSF was the *Ccl8* gene. Moreover, the *Ccl7* gene expression was also upregulated. CCL8 is a ligand for CCR5 and CCR2, while CCL7 is a ligand for CCR2, -3 and -4 (Lazennec and Richmond, 2010). Therefore, the MDSC differentiated with IL-6 and GM-CSF could recruit more MDSC expressing CCR2 and CCR5 to the TME. However, also other immune cells expressing these receptors could be recruited via CCL7 and -8.

Furthermore, the MMP-encoding genes *Mmp13* and *Mmp19* were upregulated. As described above, MDSC were shown to express MMP, in particular MMP9, that promote a lower integrity of the extracellular matrix and the basal membrane and thereby enable tumor cells to enter the blood stream and form metastasis (Jacob and Prekeris, 2015; Baniyash, 2016). MMP13 has been also found in circulating MDSC from patients with hepatocellular carcinoma (Shen *et al.*, 2014).

Altogether, we found that the addition of IL-6 to the MDSC *in vitro* differentiation could lead to decreased expression of C-type lectins and integrins involved in cellular adhesion, to an increased expression of chemokines, stimulating further MDSC recruitment, and to an increase in MMP expression that might play a role in the pro-metastatic function of MDSC. However, there was no increase of *Arg1* expression in the MDSC differentiated with IL-6 and GM-CSF compared to the cells differentiated with GM-CSF only. We found an increase in *Arg1* expression after overnight IL-6 stimulation and an increase in Arg1 activity in the MDSC differentiated with IL-6 and GM-CSF compared to the cells differentiated with GM-CSF only. The expression kinetics of *Arg1* mRNA might therefore be quite fast, and after the four days of differentiation, Arg1 is expressed at the protein level and shows increased enzymatic activity but the mRNA expression is decreased to the basal level.

6.3 Effect of IL-6 on melanoma growth *in vivo*

6.3.1 IL-6 OE fails to affect *in vivo* growth of Ret melanoma cells

Since we observed that IL-6 can upregulate CCR5 on MDSC and in addition led to increased immunosuppressive capacity of MDSC via Arg1 and ROS upregulation *in vitro*, we investigated the role of IL-6 *in vivo*. We had provided evidence that IL-6 concentration correlated with pSTAT3 and CCR5 expression in MDSC in tumors and serum from *RET* transgenic melanoma bearing mice, and that $CCR5^+$ MDSC isolated from murine melanomas were more immunosuppressive compared to $CCR5^-$ MDSC. To study directly an effect of IL-6 on melanoma tumor growth, mouse survival, MDSC and T cells, we lentivirally transduced the Ret melanoma cell line to stably overexpress IL-6 and injected the IL-6 OE cells and EV control Ret cells s.c. into wild type mice.

Even though the IL-6 OE Ret cells expressed more IL-6 on the mRNA and secreted protein level *in vitro* and the IL-6 increase was still significantly detectable in tumors isolated from mice injected with IL-6 OE Ret cells compared to EV control Ret cells, there was no significant differences in mouse survival and tumor growth. We found also no changes in the frequency of total $CD45^+$ tumor-infiltrating leukocytes and only a very slight increase in MDSC frequency in the IL-6 OE tumors. In addition, frequency of $CCR5^+$, $PD\text{-}L1^+$ and $Arg1^+$ MDSC remained unchanged. However, we detected a tendency towards elevated ROS production by MDSC in the IL-6 OE tumors. In addition, there was also a small increase in $CD3^+$ T cells in the IL-6 OE tumors. Moreover, the Treg frequency showed a tendency to be decreased in the IL-6 OE tumors.

The explanation for the lack of upregulation of immunosuppressive mediators in MDSC infiltrating IL-6 OE tumors might be the very fast tumor growth upon Ret cell injection. Longer

time and a slower, more physiologic, tumor growth might be necessary to see the differences between the IL-6 OE tumors and the EV control tumors in terms of tumor growth, survival and the composition of immune cells. In addition, the potentially increased immunosuppressive effect mediated by the slight upregulation of MDSC in IL-6 OE tumors could have been counteracted by the stimulation of T cells that can be mediated by the IL-6 OE.

Importantly, IL-6 is known to have pro- as well as anti-inflammatory properties in cancer (Kumari *et al.*, 2016). IL-6 signaling led to the expression of chemokines attracting T cells (such as CCL4, CCL5, CCL17 and CXCL10), thereby promoting T cell infiltration and inflammation at the site of IL-6 production (McLoughlin *et al.*, 2005). Furthermore, by the STAT3-dependent upregulation of anti-apoptotic factors (such as Bcl-2 and Bcl-xL) and the modulation of the surface expression of Fas receptor, IL-6 can prevent the apoptosis of T cells (Atreya *et al.*, 2000; Curnow *et al.*, 2004). These pro-inflammatory effects of IL-6 on T cells could explain a slight increase in $CD3^+$ T cell frequency found in the IL-6 OE tumors.

Usually, when it comes to the switch between pro- and anti-inflammatory properties, the IL-6 signaling is generating negative feedback loops to control inflammation and prevent too strong immune reaction, inducing also the accumulation and activation of MDSC. However, the limited time, that the fast tumor growth of injected Ret melanomas provides, might be insufficient for the switch towards the tolerogenic and immunosuppressive effects of IL-6. Therefore, more experiments are needed, including the injection of lower numbers of Ret melanoma cells or a slowly growing melanoma model, to elucidate the effect of increased IL-6 levels in murine melanoma *in vivo*.

6.3.2 Potential of IL-6 blockade as immunotherapy in melanoma

Next, we applied the blocking of IL-6 with antibodies in the *RET* transgenic melanoma-bearing mice to inhibit IL-6 mediated MDSC accumulation and immunosuppression in the TME. To observe potential sensitizing or synergistic effects of the therapy, we included the combination of anti-IL-6 with anti-PD-1 blocking antibodies. It was previously found that the anti-PD-1 therapy alone exerted only very limited effects in the *RET* transgenic mouse model (Grees *et al.*, 2018), resembling non-responding melanoma patients.

Unexpectedly, mice treated with anti-IL-6 antibodies developed tumors faster and died significantly earlier as compared to the control group. This effect was partly rescued when mice were treated with anti-PD-1 in addition to the anti-IL-6, suggesting that anti-IL-6 had a negative effect on T cells that was reversed by the T cell activating properties of anti-PD-1. Although the mice from the combination therapy group survived longer than the mice treated with ani-IL-6 alone, they still died earlier than the mice from the control group. In line with the

significantly decreased survival of the anti-IL-6-treated mice, these mice showed the highest tumor weight among all groups after four weeks of therapy.

Analyzing tumor-infiltrating immune cells, we did not observe any significant differences between the groups. There were no significant effects on tumor-infiltrating MDSC frequency, or expression of the immunosuppressive factors like PD-L1, Arg1 and production of NO. However, there was an unexpected increase in $CCR5^+$ MDSC frequency and a decrease in ROS production by MDSC in the anti-IL-6 therapy group. The decrease of ROS production in the anti-IL-6 therapy group is in agreement with our *in vitro* experiments showing that IL-6 induces an increase of ROS production in MDSC. Why IL-6 blockade leads to an increase in $CCR5^+$ MDSC requires further investigation. There might be other factors that upregulate CCR5 on MDSC that are still present upon IL-6 blockade, for example GM-CSF and IFN-γ. Moreover, the accumulation of $CCR5^+$ MDSC could be mediated by the CCR5 ligands that are not affected by the IL-6 blockade.

Interestingly, we found that the frequency of $CD4^+$ T cells was decreased in the anti-IL-6 therapy group but increased in groups with anti-PD-1 alone and combination therapy groups with nearly unchanged $CD4^+$ Treg frequency. This observation confirms the data generated in the IL-6 OE Ret melanoma model, that IL-6 plays an important role in T cell accumulation in the tumors. In the IL-6 OE melanomas we saw an increase in $CD3^+$ T cells whereas upon IL-6 blockade we saw a decrease in $CD4^+$ helper T cells. This decrease in T cells upon anti-IL-6 therapy could explain the accelerated tumor growth and decreased survival time of the mice. Furthermore, there was also an increase in $CD8^+$ T cells observed in the anti-PD-1 and combination therapy groups. Altogether, the IL-6 blocking therapy failed to improve the survival and tumor growth of *RET* transgenic melanoma-bearing mice. In contrast, it accelerated tumor growth associated with a decreased number of tumor-infiltrating T cells.

However, several preclinical studies investigating the effect of IL-6 blockade on relieving immunosuppression were successful. Limited efficacy of immune checkpoint inhibitors in hepatocellular carcinoma and pancreatic cancer led to further investigation of combination therapies with IL-6 blockade. High IL-6 expression by cancer-associated fibroblasts was shown to increase immunosuppression in a mouse model for hepatocellular carcinoma by increasing MDSC infiltration (H. Liu *et al.*, 2017). In addition, high IL-6 expression impaired tumor infiltrating T-cell function via upregulation of inhibitory immune checkpoints in the same study. Therefore, using IL-6 blockade could reverse anti-PD-L1 therapy resistance and prolong mouse survival (H. Liu *et al.*, 2017). Additionally, in ectopic, orthotopic and transgenic mouse models of pancreatic cancer the combination of IL-6 and PD-L1 blockade elicited efficacy, which was accompanied by increased infiltration of effector T lymphocytes (Mace *et al.*, 2018). Colorectal cancer patients with high IL-6 expression tended to have a shorter survival

as compared to patients with low IL-6 expression; in colorectal cancer mouse models, tumors with IL-6 OE tended to grow faster than tumors with IL-6 knockout (J. Li *et al.*, 2018). In the same study, it was demonstrated that $CD8^+$ and $CD4^+$ T cells were decreased in IL-6 OE tumors whereas MDSC and Treg were increased. Importantly, IL-6 blockade reversed the anti-PD-L1 resistance and prolonged tumor-bearing mouse survival (J. Li *et al.*, 2018). As described above, serum IL-6 levels in patients with esophageal squamous cell carcinoma were observed to positively correlate with the MDSC frequency in the peripheral blood (Chen *et al.*, 2014). In the same study, blockade of IL-6 prevented induction of MDSC and the incidence of chemically-induced invasive esophageal tumors in mice. In a carcinoma mouse model of intradermal (i.d.) CMC-1 cell injection, the administration of anti-IL-6R antibodies was able to downregulate the accumulation of MDSC, and the elimination of MDSC caused subsequent enhancement of antitumor T cell responses (Sumida *et al.*, 2012). Here, the therapeutic effect of anti-IL-6R antibodies was further enhanced by combination with gemcitabine.

Moreover, the IL-6 blockade influences not only the immune system but also exerts direct effects on the tumor cell proliferation and metastasis, since aberrant IL-6 production plays an important role in the growth of malignant cells (Kumari *et al.*, 2016).

Maraviroc (CCR5 inhibitor) and tocilizumab (anti-IL-6R antibodies) were used to block the proliferation and migration of triple negative breast cancer cells in an athymic nude mouse model, achieving reduced tumor growth and reduced thoracic metastasis (Jin *et al.*, 2018). In ovarian cancer cell lines, the treatment with siltuximab (anti-IL-6 antibodies) significantly decreased the levels of anti-apoptotic proteins expressed downstream of STAT3 (Guo *et al.*, 2010). Furthermore, siltuximab increased the cytotoxic effects of paclitaxel in a paclitaxel resistant ovarian cancer cell line (Guo *et al.*, 2010). Tocilizumab as a single agent was able to inhibit the growth of human oral squamous cell carcinoma xenografts in mice by blockade of IL-6/STAT3 signaling and angiogenesis (Shinriki *et al.*, 2009).

Altogether, these preclinical studies highlighted IL-6 blockade as a promising approach for the therapy of cancer. However, we were not able to show similar effects in the *RET* transgenic mouse model of malignant melanoma. To date, there are several clinical trials completed and running that involved IL-6 or IL-6R blockade, mainly in phase I/II (Kampan *et al.*, 2018). However, in various cancer entities, large randomized trials did not show significant activity of anti-IL-6 or anti-IL-6R as monotherapies. Yet, in combination with chemotherapy or other therapeutic agents IL-6 blockade enhanced efficacy of the treatment (Kampan *et al.*, 2018).

As described above, IL-6 signaling leads to the expression of T cell-attracting chemokines (such as CCL4, CCL5, CCL17 and CXCL10) thereby promoting inflammation (McLoughlin *et*

al., 2005). Furthermore, by the STAT3-dependent upregulation of anti-apoptotic factors (such as Bcl-2 and Bcl-xL) and the modulation of the surface expression of Fas receptor, IL-6 can prevent the apoptosis of T cells (Atreya *et al.*, 2000; Curnow *et al.*, 2004). The inhibition of IL-6 signaling has even been described to be a strategy to induce immune tolerance, for example in autoimmune diseases or transplant rejection (Zhang *et al.*, 2014). It has been recently described that IL-6R deficiency in patients could cause severe effects, like immunodeficiency and aberrant inflammatory responses, (Spencer *et al.*, 2019).

Since, IL-6 has pleiotropic effects in inflammation and cancer, it could be an interesting target to relief chronic inflammation and immunosuppression in the TME; however, it might be hard to compensate the loss of the immune stimulatory effects of IL-6.

6.4 Conclusion

MDSC play a major role in the immunosuppressive TME created by various cancer types, among them malignant melanoma (Umansky *et al.*, 2014). This heterogeneous population of immunosuppressive myeloid cells can suppress the activity of anti-tumor immune cells, especially T cells, by depletion of metabolites, production of reactive oxygen and nitrogen species, expression of immune-checkpoint molecules and secretion of anti-inflammatory cytokines (Groth *et al.*, 2019). The recruitment of MDSC to the TME was shown to be mediated by the interaction between chemokine receptor CCR5 expressed on MDSC and the accumulation of the CCR5 ligands in the TME (Blattner *et al.*, 2018).

We could show that IL-6, GM-CSF and IFN-γ upregulated *Ccr5* expression of MDSC and that IL-6 and GM-CSF led to increased CCR5 surface expression during MDSC differentiation. CCR5 upregulation induced by IL-6 and GM-CSF was STAT3 dependent, and in *RET* transgenic mice, IL-6 levels positively correlated with the frequency of $CCR5^+$ tumor-infiltrating MDSC, that showed increased pSTAT3 levels. Moreover, IL-6 increased immunosuppressive capacity of MDSC by upregulating Arg1 via a STAT3-dependent mechanism and increasing ROS production *in vitro*. We conclude that IL-6 can upregulate CCR5 and immunosuppressive capacity of MDSC in parallel, explaining the increased expression of immunosuppressive factors Arg1 and ROS on $CCR5^+$ MDSC and their strong ability to suppress $CD8^+$ T cell proliferation. In addition, we showed that GM-CSF can also upregulate CCR5 and modulate immunosuppressive capacity of MDSC, potentially by upregulating FATP2 and PGE2 production (Veglia *et al.*, 2019).

Although the IL-6 blockade for the treatment of *RET* transgenic melanoma bearing mice seemed promising based on the data obtained *in vitro*, we failed to observe a beneficial effect on tumor progression *in vivo*. Here the anti-IL-6 therapy resulted in accelerated tumor

progression and earlier death of mice, which was most likely due to the negative effect of anti-IL-6 on T cell activation.

Further research could help to understand the challenges of IL-6 blocking immunotherapy and might identify particular combination therapies, cancer entities or patient subsets that benefit from anti-IL-6 or anti-IL-6R therapies.

7 References

Abschuetz, O. *et al.* (2012) 'T-Cell Mediated Immune Responses Induced in ret Transgenic Mouse Model of Malignant Melanoma', *Cancers (Basel)*, 4(2), pp. 490–503. doi: 10.3390/cancers4020490.

Aldinucci, D. and Colombatti, A. (2014) 'The inflammatory chemokine CCL5 and cancer progression.', *Mediators Inflamm*, 2014, p. 292376. doi: 10.1155/2014/292376.

Alfaro, C. *et al.* (2016) 'Tumor-Produced Interleukin-8 Attracts Human Myeloid-Derived Suppressor Cells and Elicits Extrusion of Neutrophil Extracellular Traps (NETs).', *Clin Cancer Res*, 22(15), pp. 3924–36. doi: 10.1158/1078-0432.CCR-15-2463.

Andtbacka, R. H. I. *et al.* (2015) 'Talimogene Laherparepvec Improves Durable Response Rate in Patients With Advanced Melanoma.', *J Clin Oncol*, 33(25), pp. 2780–8. doi: 10.1200/JCO.2014.58.3377.

Apolloni, E. *et al.* (2000) 'Immortalized Myeloid Suppressor Cells Trigger Apoptosis in Antigen-Activated T Lymphocytes', *J Immunol*, 165(12), pp. 6723–6730. doi: 10.4049/jimmunol.165.12.6723.

Atreya, R. *et al.* (2000) 'Blockade of interleukin 6 trans signaling suppresses T-cell resistance against apoptosis in chronic intestinal inflammation: evidence in crohn disease and experimental colitis in vivo.', *Nat Med*, 6(5), pp. 583–8. doi: 10.1038/75068.

Balistreri, C. R. *et al.* (2009) 'CCR5 Proinflammatory Allele in Prostate Cancer Risk', *Ann N Y Acad Sci*, 1155(1), pp. 289–292. doi: 10.1111/j.1749-6632.2008.03691.x.

Ban, Y. *et al.* (2017) 'Targeting Autocrine CCL5–CCR5 Axis Reprograms Immunosuppressive Myeloid Cells and Reinvigorates Antitumor Immunity', *Cancer Res*, 77(11), pp. 2857–2868. doi: 10.1158/0008-5472.CAN-16-2913.

Baniyash, M. (2016) 'Myeloid-derived suppressor cells as intruders and targets: clinical implications in cancer therapy.', *Cancer Immunol Immunother*, 65(7), pp. 857–67. doi: 10.1007/s00262-016-1849-y.

Bardhan, K., Anagnostou, T. and Boussiotis, V. A. (2016) 'The PD1:PD-L1/2 Pathway from Discovery to Clinical Implementation.', *Front Immunol*, 7, p. 550. doi: 10.3389/fimmu.2016.00550.

Barmania, F. and Pepper, M. S. (2013) 'C-C chemokine receptor type five (CCR5): An emerging target for the control of HIV infection', *Appl Transl Genomics*, 2, pp. 3–16. doi: 10.1016/j.atg.2013.05.004.

Bennett, J. A., Rao, V. S. and Mitchell, M. S. (1978) 'Systemic bacillus Calmette-Guérin (BCG) activates natural suppressor cells.', *Proc Natl Acad Sci U S A*, 75(10), pp. 5142–4. doi: 10.1073/pnas.75.10.5142.

Beury, D. W. *et al.* (2014) 'Cross-talk among myeloid-derived suppressor cells, macrophages, and tumor cells impacts the inflammatory milieu of solid tumors.', *J Leukoc Biol*, 96(6), pp. 1109–18. doi: 10.1189/jlb.3A0414-210R.

Bjoern, J. *et al.* (2016) 'Immunological correlates of treatment and response in stage IV malignant melanoma patients treated with Ipilimumab.', *Oncoimmunology*, 5(4), p. e1100788. doi: 10.1080/2162402X.2015.1100788.

Blair, A. B. *et al.* (2019) 'IDO1 inhibition potentiates vaccine-induced immunity against pancreatic adenocarcinoma.', *J Clin Invest*. doi: 10.1172/JCI124077.

Blanpain, C. *et al.* (1999) ‘Multiple charged and aromatic residues in CCR5 amino-terminal domain are involved in high affinity binding of both chemokines and HIV-1 Env protein.’, *J Biol Chem*, 274(49), pp. 34719–27. doi: 10.1074/jbc.274.49.34719.

Blattner, C. *et al.* (2018) ‘CCR5 + Myeloid-Derived Suppressor Cells Are Enriched and Activated in Melanoma Lesions’, *Cancer Res*, 78(1), pp. 157–167. doi: 10.1158/0008-5472.CAN-17-0348.

Bleul, C. C. *et al.* (1997) ‘The HIV coreceptors CXCR4 and CCR5 are differentially expressed and regulated on human T lymphocytes.’, *Proc Natl Acad Sci U S A*, 94(5), pp. 1925–30. doi: 10.1073/pnas.94.5.1925.

Bode, J. G. *et al.* (1999) ‘LPS and TNFalpha induce SOCS3 mRNA and inhibit IL-6-induced activation of STAT3 in macrophages.’, *FEBS Lett*, 463(3), pp. 365–70. doi: 10.1016/s0014-5793(99)01662-2.

Bosco, M. C. *et al.* (2004) ‘Hypoxia inhibits the expression of the CCR5 chemokine receptor in macrophages.’, *Cell Immunol*, 228(1), pp. 1–7. doi: 10.1016/j.cellimm.2004.03.006.

Brimnes, M. K. *et al.* (2010) ‘Increased Level of both CD4+FOXP3+ Regulatory T Cells and CD14+HLA-DR−/low Myeloid-Derived Suppressor Cells and Decreased Level of Dendritic Cells in Patients with Multiple Myeloma’, *Scand J Immunol*, 72(6), pp. 540–547. doi: 10.1111/j.1365-3083.2010.02463.x.

Bronte, V. *et al.* (2016) ‘Recommendations for myeloid-derived suppressor cell nomenclature and characterization standards’, *Nat Commun*, 7, p. 12150. doi: 10.1038/ncomms12150.

Buessow, S. C., Paul, R. D. and Lopez, D. M. (1984) ‘Influence of mammary tumor progression on phenotype and function of spleen and in situ lymphocytes in mice.’, *J Natl Cancer Inst*, 73(1), pp. 249–55. Available at: http://www.ncbi.nlm.nih.gov/pubmed/6610791.

Burnet, M. F. (1970) ‘The concept of immunological surveillance.’, *Prog Exp Tumor Res*, 13, pp. 1–27. doi: 10.1159/000386035.

Califano, J. A. *et al.* (2015) ‘Tadalafil augments tumor specific immunity in patients with head and neck squamous cell carcinoma.’, *Clin Cancer Res*, 21(1), pp. 30–8. doi: 10.1158/1078-0432.CCR-14-1716.

Cambi, A. and Figdor, C. G. (2003) ‘Dual function of C-type lectin-like receptors in the immune system.’, *Curr Opin Cell Biol*, 15(5), pp. 539–46. doi: 10.1016/j.ceb.2003.08.004.

Campoli, M. and Ferrone, S. (2008) ‘HLA antigen changes in malignant cells: epigenetic mechanisms and biologic significance.’, *Oncogene*, 27(45), pp. 5869–85. doi: 10.1038/onc.2008.273.

Carey, T. E. *et al.* (1976) ‘Cell surface antigens of human malignant melanoma: mixed hemadsorption assays for humoral immunity to cultured autologous melanoma cells.’, *Proc Natl Acad Sci U S A*, 73(9), pp. 3278–82. doi: 10.1073/pnas.73.9.3278.

Catlett-Falcone, R. *et al.* (1999) ‘Constitutive activation of Stat3 signaling confers resistance to apoptosis in human U266 myeloma cells.’, *Immunity*, 10(1), pp. 105–15. doi: 10.1016/s1074-7613(00)80011-4.

Chang, A. L. *et al.* (2016) ‘CCL2 Produced by the Glioma Microenvironment Is Essential for the Recruitment of Regulatory T Cells and Myeloid-Derived Suppressor Cells.’, *Cancer Res*, 76(19), pp. 5671–5682. doi: 10.1158/0008-5472.CAN-16-0144.

Chang, L.-Y. *et al.* (2012) 'The indispensable role of CCR5 for in vivo suppressor function of tumor-derived CD103+ effector/memory regulatory T cells.', *J Immunol*, 189(2), pp. 567–74. doi: 10.4049/jimmunol.1200266.

Chen, M.-F. *et al.* (2014) 'IL-6-stimulated CD11b+ CD14+ HLA-DR- myeloid-derived suppressor cells, are associated with progression and poor prognosis in squamous cell carcinoma of the esophagus.', *Oncotarget*, 5(18), pp. 8716–28. doi: 10.18632/oncotarget.2368.

Chiu, D. K.-C. *et al.* (2016) 'Hypoxia induces myeloid-derived suppressor cell recruitment to hepatocellular carcinoma through chemokine (C-C motif) ligand 26.', *Hepatology*, 64(3), pp. 797–813. doi: 10.1002/hep.28655.

Chun, E. *et al.* (2015) 'CCL2 Promotes Colorectal Carcinogenesis by Enhancing Polymorphonuclear Myeloid-Derived Suppressor Cell Population and Function.', *Cell Rep*, 12(2), pp. 244–57. doi: 10.1016/j.celrep.2015.06.024.

Clark, W. H. *et al.* (1989) 'Model predicting survival in stage I melanoma based on tumor progression.', *J Natl Cancer Inst*, 81(24), pp. 1893–904. doi: 10.1093/jnci/81.24.1893.

Clemente, C. G. *et al.* (1996) 'Prognostic value of tumor infiltrating lymphocytes in the vertical growth phase of primary cutaneous melanoma.', *Cancer*, 77(7), pp. 1303–10. doi: 10.1002/(SICI)1097-0142(19960401)77:7<1303::AID-CNCR12>3.0.CO;2-5.

Combadiere, C. *et al.* (1996) 'Cloning and functional expression of CC CKR5, a human monocyte CC chemokine receptor selective for MIP-1(alpha), MIP-1(beta), and RANTES.', *J Leukoc Biol*, 60(1), pp. 147–52. doi: 10.1002/jlb.60.1.147.

Condamine, T. *et al.* (2016) 'Lectin-type oxidized LDL receptor-1 distinguishes population of human polymorphonuclear myeloid-derived suppressor cells in cancer patients.', *Sci Immunol*, 1(2). doi: 10.1126/sciimmunol.aaf8943.

Condamine, T. and Gabrilovich, D. I. (2011) 'Molecular mechanisms regulating myeloid-derived suppressor cell differentiation and function', *Trends Immunol*, 32(1), pp. 19–25. doi: 10.1016/j.it.2010.10.002.

Corzo, C. A. *et al.* (2009) 'Mechanism regulating reactive oxygen species in tumor-induced myeloid-derived suppressor cells.', *J Immunol*, 182(9), pp. 5693–701. doi: 10.4049/jimmunol.0900092.

van Cruijsen, H. *et al.* (2008) 'Sunitinib-Induced Myeloid Lineage Redistribution in Renal Cell Cancer Patients: CD1c+ Dendritic Cell Frequency Predicts Progression-Free Survival', *Clin Cancer Res*, 14(18), pp. 5884–5892. doi: 10.1158/1078-0432.CCR-08-0656.

Curnow, S. J. *et al.* (2004) 'Inhibition of T cell apoptosis in the aqueous humor of patients with uveitis by IL-6/soluble IL-6 receptor trans-signaling.', *J Immunol*, 173(8), pp. 5290–7. doi: 10.4049/jimmunol.173.8.5290.

Cust, A. E., Mishra, K. and Berwick, M. (2018) 'Melanoma - role of the environment and genetics.', *Photochem Photobiol Sci*, 17(12), pp. 1853–1860. doi: 10.1039/c7pp00411g.

Dai, M. *et al.* (2005) 'Evolving gene/transcript definitions significantly alter the interpretation of GeneChip data.', *Nucleic Acids Res*, 33(20), p. e175. doi: 10.1093/nar/gni179.

Danilin, S. *et al.* (2012) 'Myeloid-derived suppressor cells expand during breast cancer progression and promote tumor-induced bone destruction.', *Oncoimmunology*, 1(9), pp. 1484–1494. doi: 10.4161/onci.21990.

Dantonio, P. M. *et al.* (2018) ‘Exploring major signaling cascades in melanomagenesis: a rationale route for targetted skin cancer therapy.’, *Biosci Rep*, 38(5). doi: 10.1042/BSR20180511.

Deng, H. *et al.* (1996) ‘Identification of a major co-receptor for primary isolates of HIV-1.’, *Nature*, 381(6584), pp. 661–6. doi: 10.1038/381661a0.

van Deventer, H. W. *et al.* (2005) ‘C-C chemokine receptor 5 on stromal cells promotes pulmonary metastasis’, *Cancer Res*, 65(8), pp. 3374–3379. doi: 10.1158/0008-5472.CAN-04-2616.

Dighe, A. S. *et al.* (1994) ‘Enhanced in vivo growth and resistance to rejection of tumor cells expressing dominant negative IFN gamma receptors.’, *Immunity*, 1(6), pp. 447–56. doi: 10.1016/1074-7613(94)90087-6.

Dighe, A. S., Farrar, M. A. and Schreiber, R. D. (1993) ‘Inhibition of cellular responsiveness to interferon-gamma (IFN gamma) induced by overexpression of inactive forms of the IFN gamma receptor.’, *J Biol Chem*, 268(14), pp. 10645–53. Available at: http://www.ncbi.nlm.nih.gov/pubmed/8387525.

Domingues, B. *et al.* (2018) ‘Melanoma treatment in review.’, *ImmunoTargets Ther*, 7, pp. 35–49. doi: 10.2147/ITT.S134842.

Dragic, T. *et al.* (1996) ‘HIV-1 entry into CD4+ cells is mediated by the chemokine receptor CC-CKR-5.’, *Nature*, 381(6584), pp. 667–73. doi: 10.1038/381667a0.

Dunn, G. P. *et al.* (2002) ‘Cancer immunoediting: from immunosurveillance to tumor escape.’, *Nat Immunol*, 3(11), pp. 991–8. doi: 10.1038/ni1102-991.

Dunn, G. P., Old, L. J. and Schreiber, R. D. (2004) ‘The three Es of cancer immunoediting.’, *Annu Rev Immunol*, 22, pp. 329–60. doi: 10.1146/annurev.immunol.22.012703.104803.

Eggermont, A. M. M., Spatz, A. and Robert, C. (2014) ‘Cutaneous melanoma.’, *Lancet (London, England)*, 383(9919), pp. 816–27. doi: 10.1016/S0140-6736(13)60802-8.

Ehrlich, P. (1909) ‘Über den jetzigen Stand der Karzinomforschung.’, *Ned Tijdschr Geneeskd*, 5, pp. 273–290.

Engel, A. M. *et al.* (1997) ‘MCA sarcomas induced in scid mice are more immunogenic than MCA sarcomas induced in congenic, immunocompetent mice.’, *Scand J Immunol*, 45(5), pp. 463–70. doi: 10.1046/j.1365-3083.1997.d01-419.x.

Eriksson, E. *et al.* (2016) ‘Gemcitabine reduces MDSCs, tregs and TGFβ-1 while restoring the teff/treg ratio in patients with pancreatic cancer’, *J Transl Med*, 14(1), p. 282. doi: 10.1186/s12967-016-1037-z.

Fallarino, F. and Gajewski, T. F. (1999) ‘Cutting edge: differentiation of antitumor CTL in vivo requires host expression of Stat1.’, *J Immunol*, 163(8), pp. 4109–13. Available at: http://www.ncbi.nlm.nih.gov/pubmed/10510345.

Farkona, S., Diamandis, E. P. and Blasutig, I. M. (2016) ‘Cancer immunotherapy: the beginning of the end of cancer?’, *BMC Med*, 14(1), p. 73. doi: 10.1186/s12916-016-0623-5.

Faustino-Rocha, A. *et al.* (2013) ‘Estimation of rat mammary tumor volume using caliper and ultrasonography measurements.’, *Lab Anim (NY)*, 42(6), pp. 217–24. doi: 10.1038/laban.254.

Fernando, M. R. *et al.* (2014) ‘The pro-inflammatory cytokine, interleukin-6, enhances the polarization of alternatively activated macrophages.’, *PLoS One*, 9(4), p. e94188. doi: 10.1371/journal.pone.0094188.

Fleming, V. *et al.* (2018) 'Targeting Myeloid-Derived Suppressor Cells to Bypass Tumor-Induced Immunosuppression.', *Front Immunol*, 9, p. 398. doi: 10.3389/fimmu.2018.00398.

Fleming, V. *et al.* (2019) 'Melanoma Extracellular Vesicles Generate Immunosuppressive Myeloid Cells by Upregulating PD-L1 via TLR4 Signaling.', *Cancer Res*, 79(18), pp. 4715–4728. doi: 10.1158/0008-5472.CAN-19-0053.

Gabrilovich, D. I. and Nagaraj, S. (2009) 'Myeloid-derived suppressor cells as regulators of the immune system', *Nat Rev Immunol*, 9(3), pp. 162–174. doi: 10.1038/nri2506.

Gabrilovich, D. I., Ostrand-Rosenberg, S. and Bronte, V. (2012) 'Coordinated regulation of myeloid cells by tumours.', *Nat Rev Immunol*, 12(4), pp. 253–68. doi: 10.1038/nri3175.

Garbe, C. *et al.* (2016) 'Diagnosis and treatment of melanoma. European consensus-based interdisciplinary guideline - Update 2016.', *Eur J Cancer*, 63, pp. 201–17. doi: 10.1016/j.ejca.2016.05.005.

Garrido, F. (2019) 'MHC/HLA Class I Loss in Cancer Cells.', *Adv Exp Med Biol*, 1151, pp. 15–78. doi: 10.1007/978-3-030-17864-2_2.

Girardi, M. *et al.* (2001) 'Regulation of cutaneous malignancy by gammadelta T cells.', *Science*, 294(5542), pp. 605–9. doi: 10.1126/science.1063916.

Gong, W. *et al.* (1998) 'Monocyte chemotactic protein-2 activates CCR5 and blocks CD4/CCR5-mediated HIV-1 entry/replication.', *J Biol Chem*, 273(8), pp. 4289–92. doi: 10.1074/jbc.273.8.4289.

Gray-Schopfer, V., Wellbrock, C. and Marais, R. (2007) 'Melanoma biology and new targeted therapy.', *Nature*, 445(7130), pp. 851–7. doi: 10.1038/nature05661.

Green, H. N. (1954) 'An immunological concept of cancer: a preliminary report.', *Br Med J*, 2(4901), pp. 1374–80. doi: 10.1136/bmj.2.4901.1374.

Grees, M. *et al.* (2018) 'Optimized dendritic cell vaccination induces potent CD8 T cell responses and anti-tumor effects in transgenic mouse melanoma models.', *Oncoimmunology*, 7(7), p. e1445457. doi: 10.1080/2162402X.2018.1445457.

Groh, V. *et al.* (2002) 'Tumour-derived soluble MIC ligands impair expression of NKG2D and T-cell activation.', *Nature*, 419(6908), pp. 734–8. doi: 10.1038/nature01112.

Groth, C. *et al.* (2019) 'Immunosuppression mediated by myeloid-derived suppressor cells (MDSCs) during tumour progression.', *Br J Cancer*, 120(1), pp. 16–25. doi: 10.1038/s41416-018-0333-1.

Gruys, E. *et al.* (2005) 'Acute phase reaction and acute phase proteins.', *J Zhejiang Univ Sci B*, 6(11), pp. 1045–56. doi: 10.1631/jzus.2005.B1045.

Gu, L. *et al.* (2007) 'Contribution of STAT3 to the activation of survivin by GM-CSF in CD34+ cell lines.', *Exp Hematol*, 35(6), pp. 957–66. doi: 10.1016/j.exphem.2007.03.007.

Guo, P. *et al.* (2019) 'CCR5/CCR5 ligand-induced myeloid-derived suppressor cells are related to the progression of endometriosis.', *Reprod Biomed Online*. doi: 10.1016/j.rbmo.2019.05.014.

Guo, Y. *et al.* (2010) 'Effects of siltuximab on the IL-6-induced signaling pathway in ovarian cancer.', *Clin Cancer Res*, 16(23), pp. 5759–69. doi: 10.1158/1078-0432.CCR-10-1095.

Halama, N. *et al.* (2016) 'Tumoral Immune Cell Exploitation in Colorectal Cancer Metastases Can Be Targeted Effectively by Anti-CCR5 Therapy in Cancer Patients.', *Cancer Cell*, 29(4), pp. 587–601. doi: 10.1016/j.ccell.2016.03.005.

Halvorsen, E. C. *et al.* (2016) ‘Maraviroc decreases CCL8-mediated migration of CCR5(+) regulatory T cells and reduces metastatic tumor growth in the lungs.’, *Oncoimmunology*, 5(6), p. e1150398. doi: 10.1080/2162402X.2016.1150398.

Hanahan, D. and Weinberg, R. A. (2011) ‘Hallmarks of cancer: the next generation.’, *Cell*, 144(5), pp. 646–74. doi: 10.1016/j.cell.2011.02.013.

Hariharan, D. *et al.* (1999) ‘Interferon-gamma upregulates CCR5 expression in cord and adult blood mononuclear phagocytes.’, *Blood*, 93(4), pp. 1137–44. doi: 10.1182/blood.V93.4.1137.

Hassel, J. C. *et al.* (2017) ‘Tadalafil has biologic activity in human melanoma. Results of a pilot trial with Tadalafil in patients with metastatic Melanoma (TaMe)’, *Oncoimmunology*, 6(9), p. e1326440. doi: 10.1080/2162402X.2017.1326440.

Hawila, E. *et al.* (2017) ‘CCR5 Directs the Mobilization of CD11b+Gr1+Ly6ClowPolymorphonuclear Myeloid Cells from the Bone Marrow to the Blood to Support Tumor Development.’, *Cell Rep*, 21(8), pp. 2212–2222. doi: 10.1016/j.celrep.2017.10.104.

Heink, S. *et al.* (2017) ‘Trans-presentation of IL-6 by dendritic cells is required for the priming of pathogenic TH17 cells.’, *Nat Immunol*, 18(1), pp. 74–85. doi: 10.1038/ni.3632.

Hillmer, E. J. *et al.* (2016) ‘STAT3 signaling in immunity.’, *Cytokine Growth Factor Rev*, 31, pp. 1–15. doi: 10.1016/j.cytogfr.2016.05.001.

Hirano, T. *et al.* (1985) ‘Purification to homogeneity and characterization of human B-cell differentiation factor (BCDF or BSFp-2).’, *Proc Natl Acad Sci U S A*, 82(16), pp. 5490–4. doi: 10.1073/pnas.82.16.5490.

Hodi, F. S. *et al.* (2010) ‘Improved survival with ipilimumab in patients with metastatic melanoma.’, *N Engl J Med*, 363(8), pp. 711–23. doi: 10.1056/NEJMoa1003466.

Hoechst, B. *et al.* (2008) ‘A New Population of Myeloid-Derived Suppressor Cells in Hepatocellular Carcinoma Patients Induces CD4+CD25+Foxp3+ T Cells’, *Gastroenterology*, 135(1), pp. 234–243. doi: 10.1053/j.gastro.2008.03.020.

Hoejberg, L., Bastholt, L. and Schmidt, H. (2012) ‘Interleukin-6 and melanoma.’, *Melanoma Res*, 22(5), pp. 327–33. doi: 10.1097/CMR.0b013e3283543d72.

Hoskin, D. W. *et al.* (2008) ‘Inhibition of T cell and natural killer cell function by adenosine and its contribution to immune evasion by tumor cells (Review).’, *Int J Oncol*, 32(3), pp. 527–35. Available at: http://www.ncbi.nlm.nih.gov/pubmed/18292929.

Hotamisligil, G. S. and Bernlohr, D. A. (2015) ‘Metabolic functions of FABPs--mechanisms and therapeutic implications.’, *Nat Rev Endocrinol*, 11(10), pp. 592–605. doi: 10.1038/nrendo.2015.122.

Huang, B. *et al.* (2006) ‘Gr-1+CD115+ immature myeloid suppressor cells mediate the development of tumor-induced T regulatory cells and T-cell anergy in tumor-bearing host.’, *Cancer Res*, 66(2), pp. 1123–31. doi: 10.1158/0008-5472.CAN-05-1299.

Huber, V. *et al.* (2018) ‘Tumor-derived microRNAs induce myeloid suppressor cells and predict immunotherapy resistance in melanoma.’, *J Clin Invest*, 128(12), pp. 5505–5516. doi: 10.1172/JCI98060.

Huttenrauch, F. *et al.* (2002) ‘Beta-arrestin binding to CC chemokine receptor 5 requires multiple C-terminal receptor phosphorylation sites and involves a conserved Asp-Arg-Tyr sequence motif.’, *J Biol Chem*, 277(34), pp. 30769–77. doi: 10.1074/jbc.M204033200.

Iclozan, C. *et al.* (2013) ‘Therapeutic regulation of myeloid-derived suppressor cells and immune response to cancer vaccine in patients with extensive stage small cell lung cancer’, *Cancer Immunol Immunother*, 62(5), pp. 909–918. doi: 10.1007/s00262-013-1396-8.

Jacob, A. and Prekeris, R. (2015) ‘The regulation of MMP targeting to invadopodia during cancer metastasis.’, *Front cell Dev Biol*, 3, p. 4. doi: 10.3389/fcell.2015.00004.

Jia, G. Q. *et al.* (1996) ‘Distinct expression and function of the novel mouse chemokine monocyte chemotactic protein-5 in lung allergic inflammation.’, *J Exp Med*, 184(5), pp. 1939–51. doi: 10.1084/jem.184.5.1939.

Jiang, H. *et al.* (2015) ‘Elevated chronic inflammatory factors and myeloid-derived suppressor cells indicate poor prognosis in advanced melanoma patients.’, *Int J cancer*, 136(10), pp. 2352–60. doi: 10.1002/ijc.29297.

Jin, K., Pandey, N. B. and Popel, A. S. (2018) ‘Simultaneous blockade of IL-6 and CCL5 signaling for synergistic inhibition of triple-negative breast cancer growth and metastasis.’, *Breast Cancer Res*, 20(1), p. 54. doi: 10.1186/s13058-018-0981-3.

Johnson, D. B. and Puzanov, I. (2015) ‘Treatment of NRAS-mutant melanoma.’, *Curr Treat Options Oncol*, 16(4), p. 15. doi: 10.1007/s11864-015-0330-z.

Jordan, K. R. *et al.* (2013) ‘Myeloid-derived suppressor cells are associated with disease progression and decreased overall survival in advanced-stage melanoma patients.’, *Cancer Immunol Immunother*, 62(11), pp. 1711–22. doi: 10.1007/s00262-013-1475-x.

Juffermans, N. P. *et al.* (2001) ‘Patients with active tuberculosis have increased expression of HIV coreceptors CXCR4 and CCR5 on CD4(+) T cells.’, *Clin Infect Dis*, 32(4), pp. 650–2. doi: 10.1086/318701.

Kampan, N. C. *et al.* (2018) ‘Immunotherapeutic Interleukin-6 or Interleukin-6 Receptor Blockade in Cancer: Challenges and Opportunities.’, *Curr Med Chem*, 25(36), pp. 4785–4806. doi: 10.2174/0929867324666170712160621.

Kaplan, D. H. *et al.* (1998) ‘Demonstration of an interferon gamma-dependent tumor surveillance system in immunocompetent mice.’, *Proc Natl Acad Sci U S A*, 95(13), pp. 7556–61. doi: 10.1073/pnas.95.13.7556.

Karin, N. and Razon, H. (2018) ‘The role of CCR5 in directing the mobilization and biological function of CD11b+Gr1+Ly6Clow polymorphonuclear myeloid cells in cancer.’, *Cancer Immunol Immunother*, 67(12), pp. 1949–1953. doi: 10.1007/s00262-018-2245-6.

Kato, M. *et al.* (1998) ‘Transgenic mouse model for skin malignant melanoma’, *Oncogene*, 17(14), pp. 1885–1888. doi: 10.1038/sj.onc.1202077.

Kimpfler, S. *et al.* (2009) ‘Skin melanoma development in ret transgenic mice despite the depletion of CD25+Foxp3+ regulatory T cells in lymphoid organs.’, *J Immunol*, 183(10), pp. 6330–7. doi: 10.4049/jimmunol.0900609.

Knuth, A. *et al.* (1984) ‘T-cell-mediated cytotoxicity against autologous malignant melanoma: analysis with interleukin 2-dependent T-cell cultures.’, *Proc Natl Acad Sci U S A*, 81(11), pp. 3511–5. doi: 10.1073/pnas.81.11.3511.

Kraft, K. *et al.* (2001) ‘Characterization of sequence determinants within the carboxyl-terminal domain of chemokine receptor CCR5 that regulate signaling and receptor internalization.’, *J Biol Chem*, 276(37), pp. 34408–18. doi: 10.1074/jbc.M102782200.

Krishnamoorthy, N. *et al.* (2007) 'A critical role for IL-6 secretion by dendritic cells promoting Th2 and limiting Th1 response.', *J Immunol*, 178(1), p. S181. Available at: https://www.jimmunol.org/content/178/1_Supplement/S181.4.

Ku, A. W. *et al.* (2016) 'Tumor-induced MDSC act via remote control to inhibit L-selectin-dependent adaptive immunity in lymph nodes.', *Elife*, 5. doi: 10.7554/eLife.17375.

Kumari, N. *et al.* (2016) 'Role of interleukin-6 in cancer progression and therapeutic resistance.', *Tumour Biol*, 37(9), pp. 11553–11572. doi: 10.1007/s13277-016-5098-7.

Lazennec, G. and Richmond, A. (2010) 'Chemokines and chemokine receptors: new insights into cancer-related inflammation.', *Trends Mol Med*, 16(3), pp. 133–44. doi: 10.1016/j.molmed.2010.01.003.

Lee, M. Y. and Rosse, C. (1982) 'Depletion of lymphocyte subpopulations in primary and secondary lymphoid organs of mice by a transplanted granulocytosis-inducing mammary carcinoma.', *Cancer Res*, 42(4), pp. 1255–60. Available at: http://www.ncbi.nlm.nih.gov/pubmed/7060002.

Lesokhin, A. M. *et al.* (2012) 'Monocytic CCR2(+) myeloid-derived suppressor cells promote immune escape by limiting activated CD8 T-cell infiltration into the tumor microenvironment.', *Cancer Res*, 72(4), pp. 876–86. doi: 10.1158/0008-5472.CAN-11-1792.

Li, J. *et al.* (2017) 'CD39/CD73 upregulation on myeloid-derived suppressor cells via TGF-β-mTOR-HIF-1 signaling in patients with non-small cell lung cancer.', *Oncoimmunology*, 6(6), p. e1320011. doi: 10.1080/2162402X.2017.1320011.

Li, J. *et al.* (2018) 'Targeting Interleukin-6 (IL-6) Sensitizes Anti-PD-L1 Treatment in a Colorectal Cancer Preclinical Model.', *Med Sci Monit*, 24, pp. 5501–5508. doi: 10.12659/MSM.907439.

Li, L. *et al.* (2018) 'Metformin-Induced Reduction of CD39 and CD73 Blocks Myeloid-Derived Suppressor Cell Activity in Patients with Ovarian Cancer.', *Cancer Res*, 78(7), pp. 1779–1791. doi: 10.1158/0008-5472.CAN-17-2460.

Lin, Y. *et al.* (2017) 'Chemerin has a protective role in hepatocellular carcinoma by inhibiting the expression of IL-6 and GM-CSF and MDSC accumulation.', *Oncogene*, 36(25), pp. 3599–3608. doi: 10.1038/onc.2016.516.

Lindau, D. *et al.* (2013) 'The immunosuppressive tumour network: myeloid-derived suppressor cells, regulatory T cells and natural killer T cells.', *Immunology*, 138(2), pp. 105–15. doi: 10.1111/imm.12036.

Linnemann, C. *et al.* (2009) 'Adenosine regulates CD8 T-cell priming by inhibition of membrane-proximal T-cell receptor signalling.', *Immunology*, 128(1 Suppl), pp. e728-37. doi: 10.1111/j.1365-2567.2009.03075.x.

Liu, C.-Y. *et al.* (2010) 'Population alterations of l-arginase- and inducible nitric oxide synthase-expressed CD11b+/CD14−/CD15+/CD33+ myeloid-derived suppressor cells and CD8+ T lymphocytes in patients with advanced-stage non-small cell lung cancer', *J Cancer Res Clin Oncol*, 136(1), pp. 35–45. doi: 10.1007/s00432-009-0634-0.

Liu, H., Shen, J. and Lu, K. (2017) 'IL-6 and PD-L1 blockade combination inhibits hepatocellular carcinoma cancer development in mouse model.', *Biochem Biophys Res Commun*, 486(2), pp. 239–244. doi: 10.1016/j.bbrc.2017.02.128.

Liu, Q. *et al.* (2017) 'Targeting interlukin-6 to relieve immunosuppression in tumor microenvironment.', *Tumour Biol*, 39(6), p. 1010428317712445. doi: 10.1177/1010428317712445.

Liu, R. *et al.* (1998) 'Functional analysis of the proximal CCR5 promoter.', *AIDS Res Hum Retroviruses*, 14(17), pp. 1509–19. doi: 10.1089/aid.1998.14.1509.

Liu, Y. *et al.* (2019) 'Lactoferrin-induced myeloid-derived suppressor cell therapy attenuates pathologic inflammatory conditions in newborn mice.', *J Clin Invest*, 129(10), pp. 4261–4275. doi: 10.1172/JCI128164.

Loeb, L. A., Loeb, K. R. and Anderson, J. P. (2003) 'Multiple mutations and cancer.', *Proc Natl Acad Sci U S A*, 100(3), pp. 776–81. doi: 10.1073/pnas.0334858100.

Ma, H. and Xia, C.-Q. (2018) 'Phenotypic and Functional Diversities of Myeloid-Derived Suppressor Cells in Autoimmune Diseases.', *Mediators Inflamm*, 2018, p. 4316584. doi: 10.1155/2018/4316584.

Mace, T. A. *et al.* (2018) 'IL-6 and PD-L1 antibody blockade combination therapy reduces tumour progression in murine models of pancreatic cancer.', *Gut*, 67(2), pp. 320–332. doi: 10.1136/gutjnl-2016-311585.

Marigo, I. *et al.* (2010) 'Tumor-Induced Tolerance and Immune Suppression Depend on the C/EBPβ Transcription Factor', *Immunity*, 32(6), pp. 790–802. doi: 10.1016/j.immuni.2010.05.010.

Marik, P. E. and Flemmer, M. (2012) 'The immune response to surgery and trauma: Implications for treatment.', *J Trauma Acute Care Surg*, 73(4), pp. 801–8. doi: 10.1097/TA.0b013e318265cf87.

Marincola, F. M. *et al.* (2000) 'Escape of human solid tumors from T-cell recognition: molecular mechanisms and functional significance.', *Adv Immunol*, 74, pp. 181–273. doi: 10.1016/S0065-2776(08)60911-6.

Martens, A. *et al.* (2016) 'Baseline Peripheral Blood Biomarkers Associated with Clinical Outcome of Advanced Melanoma Patients Treated with Ipilimumab.', *Clin Cancer Res*, 22(12), pp. 2908–18. doi: 10.1158/1078-0432.CCR-15-2412.

McLoughlin, R. M. *et al.* (2005) 'IL-6 trans-signaling via STAT3 directs T cell infiltration in acute inflammation.', *Proc Natl Acad Sci U S A*, 102(27), pp. 9589–94. doi: 10.1073/pnas.0501794102.

Medina, E. and Hartl, D. (2018) 'Myeloid-Derived Suppressor Cells in Infection: A General Overview.', *J Innate Immun*, 10(5–6), pp. 407–413. doi: 10.1159/000489830.

Meyer, C. *et al.* (2011) 'Chronic inflammation promotes myeloid-derived suppressor cell activation blocking antitumor immunity in transgenic mouse melanoma model', *Proc Natl Acad Sci*, 108(41), pp. 17111–17116. doi: 10.1073/pnas.1108121108.

Mihm, M. C., Clemente, C. G. and Cascinelli, N. (1996) 'Tumor infiltrating lymphocytes in lymph node melanoma metastases: a histopathologic prognostic indicator and an expression of local immune response.', *Lab Invest*, 74(1), pp. 43–7. Available at: http://www.ncbi.nlm.nih.gov/pubmed/8569196.

Mira, J. C. *et al.* (2017) 'Persistent Inflammation, Immunosuppression and Catabolism Syndrome.', *Crit Care Clin*, 33(2), pp. 245–258. doi: 10.1016/j.ccc.2016.12.001.

Mirza, N. *et al.* (2006) 'All-trans-retinoic acid improves differentiation of myeloid cells and immune response in cancer patients.', *Cancer Res*, 66(18), pp. 9299–307. doi: 10.1158/0008-5472.CAN-06-1690.

Di Mitri, D. *et al.* (2014) 'Tumour-infiltrating Gr-1+ myeloid cells antagonize senescence in cancer.', *Nature*, 515(7525), pp. 134–7. doi: 10.1038/nature13638.

Moriuchi, M., Moriuchi, H. and Fauci, A. S. (1999) 'GATA-1 transcription factor transactivates the promoter for CCR5, a coreceptor for human immunodeficiency virus type 1 entry.', *Blood*, 93(4), pp. 1433–5. doi: 10.1182/blood.V93.4.1433.

Mummidi, S. *et al.* (1997) 'The human CC chemokine receptor 5 (CCR5) gene. Multiple transcripts with 5'-end heterogeneity, dual promoter usage, and evidence for polymorphisms within the regulatory regions and noncoding exons.', *J Biol Chem*, 272(49), pp. 30662–71. doi: 10.1074/jbc.272.49.30662.

Munn, D. H. *et al.* (2005) 'GCN2 kinase in T cells mediates proliferative arrest and anergy induction in response to indoleamine 2,3-dioxygenase.', *Immunity*, 22(5), pp. 633–42. doi: 10.1016/j.immuni.2005.03.013.

Nagaraj, S. *et al.* (2007) 'Altered recognition of antigen is a mechanism of CD8+ T cell tolerance in cancer', *Nat Med*, 13(7), pp. 828–835. doi: 10.1038/nm1609.

Nakamura, T. and Ushigome, H. (2018) 'Myeloid-Derived Suppressor Cells as a Regulator of Immunity in Organ Transplantation.', *Int J Mol Sci*, 19(8). doi: 10.3390/ijms19082357.

Narita, Y. *et al.* (2013) 'The key role of IL-6-arginase cascade for inducing dendritic cell-dependent CD4(+) T cell dysfunction in tumor-bearing mice.', *J Immunol*, 190(2), pp. 812–20. doi: 10.4049/jimmunol.1103797.

Nefedova, Y. *et al.* (2007) 'Mechanism of all-trans retinoic acid effect on tumor-associated myeloid-derived suppressor cells.', *Cancer Res*, 67(22), pp. 11021–8. doi: 10.1158/0008-5472.CAN-07-2593.

New, D. C. and Wong, Y. H. (2003) 'CC chemokine receptor-coupled signalling pathways.', *Sheng Wu Hua Xue Yu Sheng Wu Wu Li Xue Bao (Shanghai)*, 35(9), pp. 779–88. Available at: http://www.ncbi.nlm.nih.gov/pubmed/12958648.

Ng-Cashin, J. *et al.* (2003) 'Host Absence of CCR5 Potentiates Dendritic Cell Vaccination', *J Immunol*, 170(8), pp. 4201–4208. doi: 10.4049/jimmunol.170.8.4201.

Nirschl, C. J. and Drake, C. G. (2013) 'Molecular Pathways: Coexpression of Immune Checkpoint Molecules: Signaling Pathways and Implications for Cancer Immunotherapy', *Clin Cancer Res*, 19(18), pp. 4917–4924. doi: 10.1158/1078-0432.CCR-12-1972.

Noman, M. Z. *et al.* (2014) 'PD-L1 is a novel direct target of HIF-1α, and its blockade under hypoxia enhanced MDSC-mediated T cell activation', *J Exp Med*, 211(5), pp. 781–790. doi: 10.1084/jem.20131916.

Noy, R. and Pollard, J. W. (2014) 'Tumor-associated macrophages: from mechanisms to therapy.', *Immunity*, 41(1), pp. 49–61. doi: 10.1016/j.immuni.2014.06.010.

Obermajer, N. *et al.* (2011) 'PGE(2)-induced CXCL12 production and CXCR4 expression controls the accumulation of human MDSCs in ovarian cancer environment.', *Cancer Res*, 71(24), pp. 7463–70. doi: 10.1158/0008-5472.CAN-11-2449.

Oppermann, M. *et al.* (1999) 'Differential effects of CC chemokines on CC chemokine receptor 5 (CCR5) phosphorylation and identification of phosphorylation sites on the CCR5 carboxyl terminus.', *J Biol Chem*, 274(13), pp. 8875–85. doi: 10.1074/jbc.274.13.8875.

Oppermann, M. (2004) 'Chemokine receptor CCR5: insights into structure, function, and regulation.', *Cell Signal*, 16(11), pp. 1201–10. doi: 10.1016/j.cellsig.2004.04.007.

Ouyang, Z. *et al.* (2016) 'Regulatory T cells in the immunotherapy of melanoma.', *Tumour Biol*, 37(1), pp. 77–85. doi: 10.1007/s13277-015-4315-0.

Pan, P.-Y. *et al.* (2010) 'Immune stimulatory receptor CD40 is required for T-cell suppression and T regulatory cell activation mediated by myeloid-derived suppressor cells in cancer.', *Cancer Res*, 70(1), pp. 99–108. doi: 10.1158/0008-5472.CAN-09-1882.

Patterson, B. K. *et al.* (1999) 'Regulation of CCR5 and CXCR4 expression by type 1 and type 2 cytokines: CCR5 expression is downregulated by IL-10 in CD4-positive lymphocytes.', *Clin Immunol*, 91(3), pp. 254–62. doi: 10.1006/clim.1999.4713.

Pauleau, A.-L. *et al.* (2004) 'Enhancer-mediated control of macrophage-specific arginase I expression.', *J Immunol*, 172(12), pp. 7565–73. doi: 10.4049/jimmunol.172.12.7565.

Penn, I. (1996) 'Malignant melanoma in organ allograft recipients.', *Transplantation*, 61(2), pp. 274–8. doi: 10.1097/00007890-199601270-00019.

Pérez-Guijarro, E. *et al.* (2017) 'Genetically engineered mouse models of melanoma.', *Cancer*, 123(S11), pp. 2089–2103. doi: 10.1002/cncr.30684.

Pervaiz, A. *et al.* (2019) 'CCR5 blockage by maraviroc: a potential therapeutic option for metastatic breast cancer.', *Cell Oncol (Dordr)*, 42(1), pp. 93–106. doi: 10.1007/s13402-018-0415-3.

Pol, J., Kroemer, G. and Galluzzi, L. (2015) 'First oncolytic virus approved for melanoma immunotherapy.', *Oncoimmunology*, 5(1), p. e1115641. doi: 10.1080/2162402X.2015.1115641.

Pollok-Kopp, B. *et al.* (2003) 'Analysis of ligand-stimulated CC chemokine receptor 5 (CCR5) phosphorylation in intact cells using phosphosite-specific antibodies.', *J Biol Chem*, 278(4), pp. 2190–8. doi: 10.1074/jbc.M209844200.

Poschke, I. *et al.* (2010) 'Immature Immunosuppressive CD14+HLA-DR-/low Cells in Melanoma Patients Are Stat3hi and Overexpress CD80, CD83, and DC-Sign', *Cancer Res*, 70(11), pp. 4335–4345. doi: 10.1158/0008-5472.CAN-09-3767.

Raber, P. L. *et al.* (2014) 'Subpopulations of myeloid-derived suppressor cells impair T cell responses through independent nitric oxide-related pathways.', *Int J cancer*, 134(12), pp. 2853–64. doi: 10.1002/ijc.28622.

Raedler, L. A. (2015) 'Opdivo (Nivolumab): Second PD-1 Inhibitor Receives FDA Approval for Unresectable or Metastatic Melanoma.', *Am Heal drug benefits*, 8(Spec Feature), pp. 180–3. Available at: http://www.ncbi.nlm.nih.gov/pubmed/26629287.

Raport, C. J. *et al.* (1996) 'Molecular cloning and functional characterization of a novel human CC chemokine receptor (CCR5) for RANTES, MIP-1beta, and MIP-1alpha.', *J Biol Chem*, 271(29), pp. 17161–6. doi: 10.1074/jbc.271.29.17161.

Robert, C. *et al.* (2015) 'Nivolumab in Previously Untreated Melanoma without BRAF Mutation', *N Engl J Med*, 372(4), pp. 320–330. doi: 10.1056/NEJMoa1412082.

Robinson, S. C. *et al.* (2003) 'A chemokine receptor antagonist inhibits experimental breast tumor growth.', *Cancer Res*, 63(23), pp. 8360–5. Available at: http://www.ncbi.nlm.nih.gov/pubmed/14678997.

Rodriguez, P. C. *et al.* (2004) 'Arginase I production in the tumor microenvironment by mature myeloid cells inhibits T-cell receptor expression and antigen-specific T-cell responses.', *Cancer Res*, 64(16), pp. 5839–49. doi: 10.1158/0008-5472.CAN-04-0465.

Rodriguez, P. C., Quiceno, D. G. and Ochoa, A. C. (2007) 'L-arginine availability regulates T-lymphocyte cell-cycle progression.', *Blood*, 109(4), pp. 1568–73. doi: 10.1182/blood-2006-06-031856.

Rosati, M. *et al.* (2001) 'CCAAT-enhancer-binding protein beta (C/EBP beta) activates CCR5 promoter: increased C/EBP beta and CCR5 in T lymphocytes from HIV-1-infected individuals.', *J Immunol*, 167(3), pp. 1654–62. doi: 10.4049/jimmunol.167.3.1654.

Rottman, J. B. *et al.* (1997) 'Cellular localization of the chemokine receptor CCR5. Correlation to cellular targets of HIV-1 infection.', *Am J Pathol*, 151(5), pp. 1341–51. Available at: http://www.ncbi.nlm.nih.gov/pubmed/9358760.

Russell, J. H. and Ley, T. J. (2002) 'Lymphocyte-mediated cytotoxicity.', *Annu Rev Immunol*, 20, pp. 323–70. doi: 10.1146/annurev.immunol.20.100201.131730.

Saleh, J. (2018) 'Murine models of melanoma.', *Pathol Res Pract*, 214(9), pp. 1235–1238. doi: 10.1016/j.prp.2018.07.008.

Samson, M. *et al.* (1996) 'Molecular cloning and functional expression of a new human CC-chemokine receptor gene.', *Biochemistry*, 35(11), pp. 3362–7. doi: 10.1021/bi952950g.

Sceneay, J. *et al.* (2012) 'Primary tumor hypoxia recruits CD11b+/Ly6Cmed/Ly6G+ immune suppressor cells and compromises NK cell cytotoxicity in the premetastatic niche.', *Cancer Res*, 72(16), pp. 3906–11. doi: 10.1158/0008-5472.CAN-11-3873.

Schachter, J. *et al.* (2017) 'Pembrolizumab versus ipilimumab for advanced melanoma: final overall survival results of a multicentre, randomised, open-label phase 3 study (KEYNOTE-006).', *Lancet (London, England)*, 390(10105), pp. 1853–1862. doi: 10.1016/S0140-6736(17)31601-X.

Schlecker, E. *et al.* (2012) 'Tumor-infiltrating monocytic myeloid-derived suppressor cells mediate CCR5-dependent recruitment of regulatory T cells favoring tumor growth.', *J Immunol*, 189(12), pp. 5602–11. doi: 10.4049/jimmunol.1201018.

Schreiber, R. D., Old, L. J. and Smyth, M. J. (2011) 'Cancer immunoediting: integrating immunity's roles in cancer suppression and promotion.', *Science*, 331(6024), pp. 1565–70. doi: 10.1126/science.1203486.

Schust, J. *et al.* (2006) 'Stattic: a small-molecule inhibitor of STAT3 activation and dimerization.', *Chem Biol*, 13(11), pp. 1235–42. doi: 10.1016/j.chembiol.2006.09.018.

Seidl, H. *et al.* (2007) 'Profiles of chemokine receptors in melanocytic lesions: de novo expression of CXCR6 in melanoma.', *Hum Pathol*, 38(5), pp. 768–80. doi: 10.1016/j.humpath.2006.11.013.

Seliger, B. and Ferrone, S. (2020) 'HLA Class I Antigen Processing Machinery Defects in Cancer Cells-Frequency, Functional Significance, and Clinical Relevance with Special Emphasis on Their Role in T Cell-Based Immunotherapy of Malignant Disease.', *Methods Mol Biol*, 2055, pp. 325–350. doi: 10.1007/978-1-4939-9773-2_15.

Serafini, P. *et al.* (2006) 'Phosphodiesterase-5 inhibition augments endogenous antitumor immunity by reducing myeloid-derived suppressor cell function.', *J Exp Med*, 203(12), pp. 2691–702. doi: 10.1084/jem.20061104.

Sevko, A. *et al.* (2013) 'Antitumor effect of paclitaxel is mediated by inhibition of myeloid-derived suppressor cells and chronic inflammation in the spontaneous melanoma model.', *J Immunol*, 190(5), pp. 2464–71. doi: 10.4049/jimmunol.1202781.

Shankaran, V. *et al.* (2001) 'IFNgamma and lymphocytes prevent primary tumour development and shape tumour immunogenicity.', *Nature*, 410(6832), pp. 1107–11. doi: 10.1038/35074122.

Sheil, A. G. (1986) ‘Cancer after transplantation.’, *World J Surg*, 10(3), pp. 389–96. doi: 10.1007/bf01655298.

Shen, P. *et al.* (2014) ‘Increased circulating Lin(-/low) CD33(+) HLA-DR(-) myeloid-derived suppressor cells in hepatocellular carcinoma patients.’, *Hepatol Res*, 44(6), pp. 639–50. doi: 10.1111/hepr.12167.

Shi, H. *et al.* (2017) ‘Recruited monocytic myeloid-derived suppressor cells promote the arrest of tumor cells in the premetastatic niche through an IL-1β-mediated increase in E-selectin expression.’, *Int J cancer*, 140(6), pp. 1370–1383. doi: 10.1002/ijc.30538.

Shinkai, Y. *et al.* (1992) ‘RAG-2-deficient mice lack mature lymphocytes owing to inability to initiate V(D)J rearrangement.’, *Cell*, 68(5), pp. 855–67. doi: 10.1016/0092-8674(92)90029-c.

Shinriki, S. *et al.* (2009) ‘Humanized anti-interleukin-6 receptor antibody suppresses tumor angiogenesis and in vivo growth of human oral squamous cell carcinoma.’, *Clin Cancer Res*, 15(17), pp. 5426–34. doi: 10.1158/1078-0432.CCR-09-0287.

Shtivelman, E. *et al.* (2014) ‘Pathways and therapeutic targets in melanoma.’, *Oncotarget*, 5(7), pp. 1701–52. doi: 10.18632/oncotarget.1892.

Signoret, N. *et al.* (2000) ‘Endocytosis and recycling of the HIV coreceptor CCR5.’, *J Cell Biol*, 151(6), pp. 1281–94. doi: 10.1083/jcb.151.6.1281.

Smyth, M. J., Crowe, N. Y. and Godfrey, D. I. (2001) ‘NK cells and NKT cells collaborate in host protection from methylcholanthrene-induced fibrosarcoma.’, *Int Immunol*, 13(4), pp. 459–63. doi: 10.1093/intimm/13.4.459.

Solito, S. *et al.* (2014) ‘Myeloid-derived suppressor cell heterogeneity in human cancers’, *Ann N Y Acad Sci*, 1319(1), pp. 47–65. doi: 10.1111/nyas.12469.

Song, J. K. *et al.* (2012) ‘Deficiency of C-C chemokine receptor 5 suppresses tumor development via inactivation of NF-κB and upregulation of IL-1Ra in melanoma model.’, *PLoS One*. Edited by J. Li, 7(5), p. e33747. doi: 10.1371/journal.pone.0033747.

Soriano, C. *et al.* (2012) ‘Increased proteinase inhibitor-9 (PI-9) and reduced granzyme B in lung cancer: mechanism for immune evasion?’, *Lung Cancer*, 77(1), pp. 38–45. doi: 10.1016/j.lungcan.2012.01.017.

Sozzani, S. *et al.* (1998) ‘Interleukin 10 increases CCR5 expression and HIV infection in human monocytes.’, *J Exp Med*, 187(3), pp. 439–44. doi: 10.1084/jem.187.3.439.

Spencer, S. *et al.* (2019) ‘Loss of the interleukin-6 receptor causes immunodeficiency, atopy, and abnormal inflammatory responses.’, *J Exp Med*, 216(9), pp. 1986–1998. doi: 10.1084/jem.20190344.

Stacey, M. *et al.* (2002) ‘EMR4, a novel epidermal growth factor (EGF)-TM7 molecule up-regulated in activated mouse macrophages, binds to a putative cellular ligand on B lymphoma cell line A20.’, *J Biol Chem*, 277(32), pp. 29283–93. doi: 10.1074/jbc.M204306200.

Stiff, A. *et al.* (2018) ‘Nitric Oxide Production by Myeloid-Derived Suppressor Cells Plays a Role in Impairing Fc Receptor-Mediated Natural Killer Cell Function.’, *Clin Cancer Res*. doi: 10.1158/1078-0432.CCR-17-0691.

Stone, M. J. *et al.* (2017) ‘Mechanisms of Regulation of the Chemokine-Receptor Network.’, *Int J Mol Sci*, 18(2). doi: 10.3390/ijms18020342.

Street, S. E. A. *et al.* (2002) ‘Suppression of lymphoma and epithelial malignancies effected by interferon gamma.’, *J Exp Med*, 196(1), pp. 129–34. doi: 10.1084/jem.20020063.

Street, S. E., Cretney, E. and Smyth, M. J. (2001) ‘Perforin and interferon-gamma activities independently control tumor initiation, growth, and metastasis.’, *Blood*, 97(1), pp. 192–7. doi: 10.1182/blood.v97.1.192.

Subramanian, A. *et al.* (2005) ‘Gene set enrichment analysis: a knowledge-based approach for interpreting genome-wide expression profiles.’, *Proc Natl Acad Sci U S A*, 102(43), pp. 15545–50. doi: 10.1073/pnas.0506580102.

Sumida, K. *et al.* (2012) ‘Anti-IL-6 receptor mAb eliminates myeloid-derived suppressor cells and inhibits tumor growth by enhancing T-cell responses.’, *Eur J Immunol*, 42(8), pp. 2060–72. doi: 10.1002/eji.201142335.

Svane, I. M. *et al.* (1996) ‘Chemically induced sarcomas from nude mice are more immunogenic than similar sarcomas from congenic normal mice.’, *Eur J Immunol*, 26(8), pp. 1844–50. doi: 10.1002/eji.1830260827.

Takada, Y., Ye, X. and Simon, S. (2007) ‘The integrins.’, *Genome Biol*, 8(5), p. 215. doi: 10.1186/gb-2007-8-5-215.

Takeda, K. *et al.* (2002) ‘Critical role for tumor necrosis factor-related apoptosis-inducing ligand in immune surveillance against tumor development.’, *J Exp Med*, 195(2), pp. 161–9. doi: 10.1084/jem.20011171.

Talmadge, J. E. and Gabrilovich, D. I. (2013) ‘History of myeloid-derived suppressor cells.’, *Nat Rev Cancer*, 13(10), pp. 739–52. doi: 10.1038/nrc3581.

Tan, M. C. B. *et al.* (2009) ‘Disruption of CCR5-dependent homing of regulatory T cells inhibits tumor growth in a murine model of pancreatic cancer.’, *J Immunol*, 182(3), pp. 1746–55. doi: 10.4049/jimmunol.182.3.1746.

Tas, F. (2012) ‘Metastatic behavior in melanoma: timing, pattern, survival, and influencing factors.’, *J Oncol*, 2012, p. 647684. doi: 10.1155/2012/647684.

Taube, J. M. *et al.* (2012) ‘Colocalization of inflammatory response with B7-h1 expression in human melanocytic lesions supports an adaptive resistance mechanism of immune escape.’, *Sci Transl Med*, 4(127), p. 127ra37. doi: 10.1126/scitranslmed.3003689.

Teng, T. S. *et al.* (2009) ‘Stat3 promotes directional cell migration by regulating Rac1 activity via its activator betaPIX.’, *J Cell Sci*, 122(Pt 22), pp. 4150–9. doi: 10.1242/jcs.057109.

Thelen, M. and Stein, J. V (2008) ‘How chemokines invite leukocytes to dance.’, *Nat Immunol*, 9(9), pp. 953–9. doi: 10.1038/ni.f.207.

Tobin, R. P. *et al.* (2017) ‘The clinical evidence for targeting human myeloid-derived suppressor cells in cancer patients.’, *J Leukoc Biol*, 102(2), pp. 381–391. doi: 10.1189/jlb.5VMR1016-449R.

Trovato, R. *et al.* (2019) ‘Immunosuppression by monocytic myeloid-derived suppressor cells in patients with pancreatic ductal carcinoma is orchestrated by STAT3.’, *J Immunother cancer*, 7(1), p. 255. doi: 10.1186/s40425-019-0734-6.

Tsunoda, T. and Takagi, T. (1999) ‘Estimating transcription factor bindability on DNA.’, *Bioinformatics*, 15(7–8), pp. 622–30. doi: 10.1093/bioinformatics/15.7.622.

Ueda, R. *et al.* (1979) ‘Cell surface antigens of human renal cancer defined by autologous typing.’, *J Exp Med*, 150(3), pp. 564–79. doi: 10.1084/jem.150.3.564.

Umansky, V. *et al.* (2008) 'Melanoma-specific memory T cells are functionally active in Ret transgenic mice without macroscopic tumors.', *Cancer Res*, 68(22), pp. 9451–8. doi: 10.1158/0008-5472.CAN-08-1464.

Umansky, V. *et al.* (2014) 'Myeloid-derived suppressor cells in malignant melanoma.', *J Dtsch Dermatol Ges*, 12(11), pp. 1021–7. doi: 10.1111/ddg.12411.

Valenti, R. *et al.* (2006) 'Human tumor-released microvesicles promote the differentiation of myeloid cells with transforming growth factor-beta-mediated suppressive activity on T lymphocytes.', *Cancer Res*, 66(18), pp. 9290–8. doi: 10.1158/0008-5472.CAN-06-1819.

Vasquez-Dunddel, D. *et al.* (2013) 'STAT3 regulates arginase-I in myeloid-derived suppressor cells from cancer patients.', *J Clin Invest*, 123(4), pp. 1580–9. doi: 10.1172/JCI60083.

Veglia, F. *et al.* (2019) 'Fatty acid transport protein 2 reprograms neutrophils in cancer.', *Nature*, 569(7754), pp. 73–78. doi: 10.1038/s41586-019-1118-2.

Veglia, F., Perego, M. and Gabrilovich, D. (2018) 'Myeloid-derived suppressor cells coming of age', *Nat Immunol*, 19(2), pp. 108–119. doi: 10.1038/s41590-017-0022-x.

Velasco-Velázquez, M. *et al.* (2012) 'CCR5 antagonist blocks metastasis of basal breast cancer cells.', *Cancer Res*, 72(15), pp. 3839–50. doi: 10.1158/0008-5472.CAN-11-3917.

Vuk-Pavlović, S. *et al.* (2010) 'Immunosuppressive CD14 + HLA-DR low/− monocytes in prostate cancer', *Prostate*, 70(4), pp. 443–455. doi: 10.1002/pros.21078.

Wang, R. F. and Rosenberg, S. A. (1999) 'Human tumor antigens for cancer vaccine development.', *Immunol Rev*, 170, pp. 85–100. doi: 10.1111/j.1600-065x.1999.tb01331.x.

Wang, T.-T. *et al.* (2017) 'Tumour-activated neutrophils in gastric cancer foster immune suppression and disease progression through GM-CSF-PD-L1 pathway.', *Gut*, 66(11), pp. 1900–1911. doi: 10.1136/gutjnl-2016-313075.

Ward, S. T. *et al.* (2015) 'The effects of CCR5 inhibition on regulatory T-cell recruitment to colorectal cancer', *Br J Cancer*, 112(2), pp. 319–328. doi: 10.1038/bjc.2014.572.

Weber, R. *et al.* (2018) 'Myeloid-Derived Suppressor Cells Hinder the Anti-Cancer Activity of Immune Checkpoint Inhibitors.', *Front Immunol*, 9, p. 1310. doi: 10.3389/fimmu.2018.01310.

Weed, D. T. *et al.* (2015) 'Tadalafil reduces myeloid-derived suppressor cells and regulatory T cells and promotes tumor immunity in patients with head and neck squamous cell carcinoma.', *Clin Cancer Res*, 21(1), pp. 39–48. doi: 10.1158/1078-0432.CCR-14-1711.

Weide, B. *et al.* (2014) 'Myeloid-derived suppressor cells predict survival of patients with advanced melanoma: comparison with regulatory T cells and NY-ESO-1- or melan-A-specific T cells.', *Clin Cancer Res*, 20(6), pp. 1601–9. doi: 10.1158/1078-0432.CCR-13-2508.

Whiteman, D. C., Green, A. C. and Olsen, C. M. (2016) 'The Growing Burden of Invasive Melanoma: Projections of Incidence Rates and Numbers of New Cases in Six Susceptible Populations through 2031.', *J Invest Dermatol*, 136(6), pp. 1161–1171. doi: 10.1016/j.jid.2016.01.035.

Wiedemann, G. M. *et al.* (2016) 'Cancer cell-derived IL-1α induces CCL22 and the recruitment of regulatory T cells.', *Oncoimmunology*, 5(9), p. e1175794. doi: 10.1080/2162402X.2016.1175794.

Wierda, R. J. and van den Elsen, P. J. (2012) 'Genetic and Epigenetic Regulation of CCR5 Transcription.', *Biology (Basel)*, 1(3), pp. 869–79. doi: 10.3390/biology1030869.

Wolf, J., Rose-John, S. and Garbers, C. (2014) 'Interleukin-6 and its receptors: a highly regulated and dynamic system.', *Cytokine*, 70(1), pp. 11–20. doi: 10.1016/j.cyto.2014.05.024.

Wölfle, S. J. *et al.* (2011) 'PD-L1 expression on tolerogenic APCs is controlled by STAT-3.', *Eur J Immunol*, 41(2), pp. 413–24. doi: 10.1002/eji.201040979.

Wong, D. J. L. and Ribas, A. (2016) 'Targeted Therapy for Melanoma.', *Cancer Treat Res*, 167, pp. 251–62. doi: 10.1007/978-3-319-22539-5_10.

Wu, L. *et al.* (1997) 'CCR5 levels and expression pattern correlate with infectability by macrophage-tropic HIV-1, in vitro.', *J Exp Med*, 185(9), pp. 1681–91. doi: 10.1084/jem.185.9.1681.

Wu, L. *et al.* (2017) 'Ascites-derived IL-6 and IL-10 synergistically expand CD14+HLA-DR-/low myeloid-derived suppressor cells in ovarian cancer patients.', *Oncotarget*, 8(44), pp. 76843–76856. doi: 10.18632/oncotarget.20164.

Xu, M. *et al.* (2017) 'Interactions between interleukin-6 and myeloid-derived suppressor cells drive the chemoresistant phenotype of hepatocellular cancer.', *Exp Cell Res*, 351(2), pp. 142–149. doi: 10.1016/j.yexcr.2017.01.008.

Yamauchi, Y. *et al.* (2018) 'Circulating and Tumor Myeloid-derived Suppressor Cells in Resectable Non-Small Cell Lung Cancer.', *Am J Respir Crit Care Med*, 198(6), pp. 777–787. doi: 10.1164/rccm.201708-1707OC.

Yang, G. *et al.* (2017) 'Accumulation of myeloid-derived suppressor cells (MDSCs) induced by low levels of IL-6 correlates with poor prognosis in bladder cancer.', *Oncotarget*, 8(24), pp. 38378–38388. doi: 10.18632/oncotarget.16386.

Yang, L. *et al.* (2018) 'Blockade of CCR5-mediated myeloid derived suppressor cell accumulation enhances anti-PD1 efficacy in gastric cancer', *Immunopharmacol Immunotoxicol*, 40(1), pp. 91–97. doi: 10.1080/08923973.2017.1417997.

Yang, Y.-F. F. *et al.* (2001) 'IL-12 as well as IL-2 upregulates CCR5 expression on T cell receptor-triggered human CD4+ and CD8+ T cells.', *J Clin Immunol*, 21(2), pp. 116–25. doi: 10.1023/A:1011059906777.

Young, K., Minchom, A. and Larkin, J. (2012) 'BRIM-1, -2 and -3 trials: improved survival with vemurafenib in metastatic melanoma patients with a BRAF(V600E) mutation.', *Future Oncol*, 8(5), pp. 499–507. doi: 10.2217/fon.12.43.

Young, M. R., Newby, M. and Wepsic, H. T. (1987) 'Hematopoiesis and suppressor bone marrow cells in mice bearing large metastatic Lewis lung carcinoma tumors.', *Cancer Res*, 47(1), pp. 100–5. Available at: http://www.ncbi.nlm.nih.gov/pubmed/2947676.

Yu, J. *et al.* (2013) 'Myeloid-derived suppressor cells suppress antitumor immune responses through IDO expression and correlate with lymph node metastasis in patients with breast cancer.', *J Immunol*, 190(7), pp. 3783–97. doi: 10.4049/jimmunol.1201449.

Zamarron, B. F. and Chen, W. (2011) 'Dual roles of immune cells and their factors in cancer development and progression.', *Int J Biol Sci*, 7(5), pp. 651–8. doi: 10.7150/ijbs.7.651.

Zhang, C., Zhang, X. and Chen, X.-H. (2014) 'Inhibition of the interleukin-6 signaling pathway: a strategy to induce immune tolerance.', *Clin Rev Allergy Immunol*, 47(2), pp. 163–73. doi: 10.1007/s12016-014-8413-3.

Zhang, Y. *et al.* (2013) 'A novel role of hematopoietic CCL5 in promoting triple-negative mammary tumor progression by regulating generation of myeloid-derived suppressor cells.', *Cell Res*, 23(3), pp. 394–408. doi: 10.1038/cr.2012.178.

Zhao, A.-M. *et al.* (2016) ‘New insights into myeloid-derived suppressor cells and their roles in feto-maternal immune cross-talk.’, *J Reprod Immunol*, 113, pp. 35–41. doi: 10.1016/j.jri.2015.11.001.

Zhao, F. *et al.* (2009) ‘Activation of p38 mitogen-activated protein kinase drives dendritic cells to become tolerogenic in ret transgenic mice spontaneously developing melanoma.’, *Clin Cancer Res*, 15(13), pp. 4382–90. doi: 10.1158/1078-0432.CCR-09-0399.

Danksagung

Ich möchte allen danken, die diese Doktorarbeit ermöglicht und unterstützt haben. Die beschriebene Arbeit begann im Februar 2017 und wurde im November 2019 abgeschlossen. Sie wurde unter der Betreuung von Prof. Dr. Viktor Umansky in der Klinischen Kooperationseinheit Dermato-Onkologie des DKFZ Heidelberg und der Klinik für Dermatologie des Universitätsklinikums Mannheim durchgeführt.

Mein herzlicher Dank gilt zuallererst Prof. Dr. Viktor Umansky für die Betreuung meiner Arbeit, für seine Ideen, die Diskussionen und die Unterstützung zu jeder Zeit, für das Korrigieren der Arbeit und für die Übernahme der Aufgabe des Erstgutachters. Lieber Viktor, du warst ein fürsorglicher, respektvoller, wissenschaftlich erfahrener und begeisterter Doktorvater, ich kann mir keinen Besseren vorstellen, vielen lieben Dank.

Danke an die weiteren Mitglieder des Prüfungsausschusses dieser Doktorarbeit, Prof. Dr. Adelheid Cerwenka, Prof. Dr. Stefan Wiemann und Prof. Dr. Thomas Wieland. Ein besonderes Dankeschön an Prof. Dr. Adelheid Cerwenka für die Übernahme des Zweitgutachtens und an Prof. Dr. Thomas Wieland für den Prüfungsvorsitz bei der Verteidigung.

Vielen Dank an die Mitglieder meines thesis advisory committee (TAC), Prof. Dr. Viktor Umansky, Prof. Dr. Adelheid Cerwenka, Prof. Dr. Alexander Dalpke und Prof. Dr. Jochen Utikal. Danke, dass Sie sich die Zeit genommen haben, das Projekt immer wieder zu diskutieren und aufzuarbeiten. Die TAC-Treffen haben nochmal neue Wege aufgezeigt und einen hilfreichen Beitrag zum Gelingen der Arbeit geleistet.

Ohne die Finanzierung durch die Deutsche Forschungsgemeinschaft (DFG) wäre diese Arbeit nicht möglich gewesen. Ich möchte mich bei allen Mitgliedern des Graduiertenkollegs 2099 „Hallmarks of Skin Cancer“ für die gemeinsame Zeit bedanken, für die Vorlesungen und Kurse, für die Konferenzen und Summer Schools und für den Austausch, der immer auf höchstem Niveau stattgefunden hat; insbesondere herzlichen Dank an Prof. Dr. Sergij Goerdt, Martina Nolte-Bohres und Dr. Lisa Jakobi. Durch die DFG wurde auch mein Aufenthalt in Paris ermöglicht, bei dem ich viel Neues lernen konnte. Herzlichen Dank an Prof. Dr. Fathia Mami-Chouaib und ihre Gruppe für die tolle und interessante Zeit.

Ein großes Dankeschön geht an alle aktuellen und ehemaligen Mitglieder der AG Umansky, Alina Siebenmorgen, Bea Goméz, Dr. Carolin Blattner, Céline Weller, Christopher Groth, Daniel Thomas, Elisabeth Fury, Elizabeth Cordell, Germann Lysak, Ihor Arkhypov, Isabel Steimbach, Joel Altmann, Dr. Mareike Grees, Prof. Dr. Peter Altevogt, Sonja Simon, Sophie Kopetschke, Dr. Vasyl Nagibin, Vera Petrova, Dr. Viktor Fleming, Dr. Xiaoying Hu und Zeno Riester für die tolle Zeit im Labor und darüber hinaus, für die vielen interessanten Besprechungen und Diskussionen, die gegenseitige Hilfe und das Verständnis für alle klei-

nen und großen Probleme und Fehler und natürlich für die Abende im Eichbaum und im Irish Pub und die gemeinsamen Ausflüge und Konferenzbesuche.

Danke auch an Prof. Dr. Jochen Utikal für das Führen der KKE Dermato-Onkologie, an die gesamte AG Utikal im DKFZ für die Antworten auf Fragen und die gemeinsamen Lab Meetings und an Jennifer Dworacek, Sayran Arif-Said und Yvonne Nowak für die technische Unterstützung und die Bestellungen.

Besonders bedanken möchte ich mich bei Alina Siebenmorgen, Elizabeth Cordell, Germann Lysak und Zeno Riester für ihren Einsatz für das „CCR5 Projekt“ und dafür, dass ich mit ihnen erfahren durfte, wie man Studenten betreut und im Teamwork ein nicht immer einfaches Projekt umsetzt. Lieber Zeno, ein ganz besonderer Dank an dich, dafür dass du zur richtigen Zeit am richtigen Ort warst und mich mit dem Projekt unterstützt hast, auch wenn damals bei Weitem nicht alles geklappt hat. Du hast das Projekt vorangebracht und hast einen großen Beitrag zur Ermöglichung der Doktorarbeit geleistet. Danke, dass ich dich als ersten Studenten betreuen durfte. Wir waren ein super Team.

Danke an Dr. Viktor Fleming für die Unterstützung in der Anfangszeit im Labor, das Vermitteln von Methoden und die herausfordernden Fragen.

Dr. Laura Hüser, Dr. Aniello Federico und Dr. Daniel Nowak, vielen Dank für eure Unterstützung mit der Transduktion der Ret Zellen.

Dr. Loreen Kloss (AG Schmieder) und Céline Weller (AG Géraud) möchte ich für die Hilfe mit Reagenzien und den Austausch von Methoden danken. Wir haben fachlich und persönlich immer bestens harmoniert.

Danke an alle Kolleginnen und Kollegen im Uniklinikum Mannheim, Haus 42, für den Austausch von Methoden und Reagenzien, wenn mal was gefehlt hat, und besonders für die gemeinsame Nutzung des FACSLyric™.

Vielen Dank an Stefanie Uhlig von FlowCore Mannheim für die schier endlosen Sorting Termine und die Verbesserungen, solange bis die CCR5$^+$ Zellen endlich lebendig gesorted waren.

Danke an die Microarray Core Facility des DKFZ Heidelberg für die Durchführung der Microarrays, an Dr. Carolina DeLaTorre für die Hilfe mit dem Bioanalyzer und an Dr. Carsten Sticht (beide vom ZMF Mannheim) für die Hilfe mit der Auswertung.

Den Tierpflegern des DKFZ Heidelberg und des ZMF Mannheim möchte ich danken, dass Sie die Tierversuche überhaupt erst ermöglichen. Besten Dank für das Züchten und die gewissenhafte Pflege unserer Mäuse.

Meinen Eltern, meiner Familie und Mirko möchte ich danke sagen für die nie endende Unterstützung und Fürsorge. Danke, dass ihr diesen Weg mit mir gegangen seid und immer für mich da wart.

Appendix

GeneSymbol	GeneName	Fold change	Adjusted p-value
Adgre4	adhesion G protein-coupled receptor E4	0,079683971	0,00540123
Serpinb10	serine (or cysteine) peptidase inhibitor, clade B (ovalbumin), member 10	0,090871898	0,0117595
Ccl22	chemokine (C-C motif) ligand 22	0,104365413	0,025414462
Ccr7	chemokine (C-C motif) receptor 7	0,110651635	0,021196436
I830127L07Rik	RIKEN cDNA I830127L07 gene	0,115043312	0,030605857
Gm9733	predicted gene 9733	0,124041227	0,030988196
Ace	angiotensin I converting enzyme (peptidyl-dipeptidase A) 1	0,124638276	0,0117595
Hp	haptoglobin	0,130277682	0,025414462
Sell	selectin, lymphocyte	0,139951066	0,036766063
Stat4	signal transducer and activator of transcription 4	0,144857624	0,028343303
Vcan	versican	0,15086199	0,0117595
Napsa	napsin A aspartic peptidase	0,151726082	0,026009819
Gpr141	G protein-coupled receptor 141	0,152860038	0,027138212
Serpinb6b	serine (or cysteine) peptidase inhibitor, clade B, member 6b	0,167997733	0,038062925
Itgal	integrin alpha L	0,177169767	0,038574242
Il1b	interleukin 1 beta	0,216607013	0,030988196
Fscn1	fascin actin-bundling protein 1	0,243404169	0,018760672
Dpp4	dipeptidylpeptidase 4	0,246476619	0,028343303
Ccr2	chemokine (C-C motif) receptor 2	0,24826094	0,016872873
Lsp1	lymphocyte specific 1	0,255063906	0,016872873
Fgr	FGR proto-oncogene, Src family tyrosine kinase	0,258529511	0,021249034
Cd177	CD177 antigen	0,258748353	0,0117595
Clec7a	C-type lectin domain family 7, member a	0,262941714	0,030988196
F10	coagulation factor X	0,265209632	0,040618105
Mmp25	matrix metallopeptidase 25	0,270307023	0,033050761
Ntng2	netrin G2	0,284962261	0,033050761
Tarm1	T cell-interacting, activating receptor on myeloid cells 1	0,313042919	0,017639116
Sema7a	sema domain, immunoglobulin domain (Ig), and GPI membrane anchor, (semaphorin) 7A	0,315983503	0,023439734
Gm14548	predicted gene 14548	0,318345071	0,030988196
Rhof	ras homolog family member F (in filopodia)	0,32834748	0,019535229
Cacnb3	calcium channel, voltage-dependent, beta 3 subunit	0,334697332	0,048979135
Cd244	CD244 natural killer cell receptor 2B4	0,334753976	0,044527265
Igkc	immunoglobulin kappa constant	0,371187735	0,018343656
Tnfsf4	tumor necrosis factor (ligand) superfamily, member 4	0,433979883	0,023898309

Itgax	integrin alpha X	0,439518367	0,048979135
Gcnt2	glucosaminyl (N-acetyl) transferase 2, I-branching enzyme	0,44351564	0,038225306
Il12b	interleukin 12b	0,488706777	0,028169154
Fn1	fibronectin 1	0,517474812	0,025414462
Nr4a1	nuclear receptor subfamily 4, group A, member 1	0,549491639	0,046927945
Stk10	serine/threonine kinase 10	0,567074468	0,028343303
Net1	neuroepithelial cell transforming gene 1	0,650054054	0,032456535
Spag4	sperm associated antigen 4	0,666047184	0,033887565
Npr1	natriuretic peptide receptor 1	0,720194626	0,033695221
Gm14064	predicted gene 14064	0,733873916	0,03582816
Klhl2	kelch-like 2, Mayven	0,770062194	0,045471667
Tmem176a	transmembrane protein 176A	0,771366438	0,040301076
Stk4	serine/threonine kinase 4	0,771758142	0,048979135
Add3	adducin 3 (gamma)	0,790929546	0,038225306
Brd4	bromodomain containing 4	0,815185444	0,049323589
Pitpnm2	phosphatidylinositol transfer protein, membrane-associated 2	0,855681903	0,041492929
Hk3	hexokinase 3	2,297173174	0,045551396
Snx24	sorting nexing 24	2,304863633	0,021249034
Lgmn	legumain	2,306180399	0,017775424
Rnf144b	ring finger protein 144B	2,365869677	0,04117822
Rapgef5	Rap guanine nucleotide exchange factor (GEF) 5	2,380830385	0,03135116
Pla2g15	phospholipase A2, group XV	2,38567006	0,026123477
Rab7b	RAB7B, member RAS oncogene family	2,400451295	0,040618105
Scarf1	scavenger receptor class F, member 1	2,405483501	0,03582816
Nr1h3	nuclear receptor subfamily 1, group H, member 3	2,427874087	0,015032466
Adgre1	adhesion G protein-coupled receptor E1	2,486028393	0,033050761
Bcar3	breast cancer anti-estrogen resistance 3	2,495828915	0,033887565
Cd22	CD22 antigen	2,561185102	0,022975643
Cd93	CD93 antigen	2,616548127	0,041719809
Ccl2	chemokine (C-C motif) ligand 2	2,633149713	0,042436496
Adm	adrenomedullin	2,724831451	0,0117595
Ctsl	cathepsin L	2,774854469	0,021249034
C1qb	complement component 1, q subcompo-nent, beta polypeptide	2,779319027	0,021249034
Frmd4b	FERM domain containing 4B	2,7990841	0,025414462
Slc27a1	solute carrier family 27 (fatty acid trans-porter), member 1	2,890422755	0,028343303
Flrt2	fibronectin leucine rich transmembrane protein 2	2,893573264	0,03582816
Anpep	alanyl (membrane) aminopeptidase	2,922206448	0,041492929
Plau	plasminogen activator, urokinase	2,990745962	0,018343656
Rab3il1	RAB3A interacting protein (rabin3)-like 1	3,031510083	0,03706519

Cd200r4	CD200 receptor 4	3,053197775	0,038574242
Dhrs3	dehydrogenase/reductase (SDR family) member 3	3,219618273	0,028343303
Ccl7	chemokine (C-C motif) ligand 7	3,227801271	0,03743139
Lpl	lipoprotein lipase	3,35491649	0,045471667
Cd36	CD36 molecule	3,489841758	0,017775424
C1qc	complement component 1, q subcomponent, C chain	3,653149069	0,0117595
Ms4a7	membrane-spanning 4-domains, subfamily A, member 7	3,820055901	0,025414462
Blnk	B cell linker	3,846896643	0,030988196
Stab1	stabilin 1	3,848443061	0,025414462
C1qa	complement component 1, q subcomponent, alpha polypeptide	3,858550753	0,0117595
Siglec1	sialic acid binding Ig-like lectin 1, sialoadhesin	3,898093119	0,018352399
Abca1	ATP-binding cassette, sub-family A (ABC1), member 1	3,98665351	0,026903907
Trem2	triggering receptor expressed on myeloid cells 2	4,037232575	0,041492929
Rnase4	ribonuclease, RNase A family 4	4,173385707	0,036766063
Ccl12	chemokine (C-C motif) ligand 12	4,887384132	0,015952644
Peak1os	pseudopodium-enriched atypical kinase 1, opposite strand	4,920162807	0,017775424
Pf4	platelet factor 4	4,975528765	0,021249034
Ms4a14	membrane-spanning 4-domains, subfamily A, member 14	5,098264078	0,022975643
Vcam1	vascular cell adhesion molecule 1	5,27946092	0,0117595
Ctla2b	cytotoxic T lymphocyte-associated protein 2 beta	5,669912283	0,021249034
Pdgfc	platelet-derived growth factor, C polypeptide	5,833173581	0,012702383
Mmp27	matrix metallopeptidase 27	5,860134746	0,036766063
Ang	angiogenin, ribonuclease, RNase A family, 5	5,900685508	0,024630541
Folr2	folate receptor 2 (fetal)	6,319678097	0,040555524
Atp6v0d2	ATPase, H+ transporting, lysosomal V0 subunit D2	6,919704592	0,0117595
Ccl8	chemokine (C-C motif) ligand 8	10,41671774	0,00540123
Fabp4	fatty acid binding protein 4, adipocyte	10,55557205	0,012670317

Supplementary Table 1. Differentially regulated genes between CCR5$^+$ and CCR5$^-$ MDSC.
The table shows the top 50 significantly down- and significantly upregulated genes (by fold change) in CCR5$^+$ tumor-infiltrating MDSC compared to CCR5$^-$ tumor-infiltrating MDSC by microarray analysis.

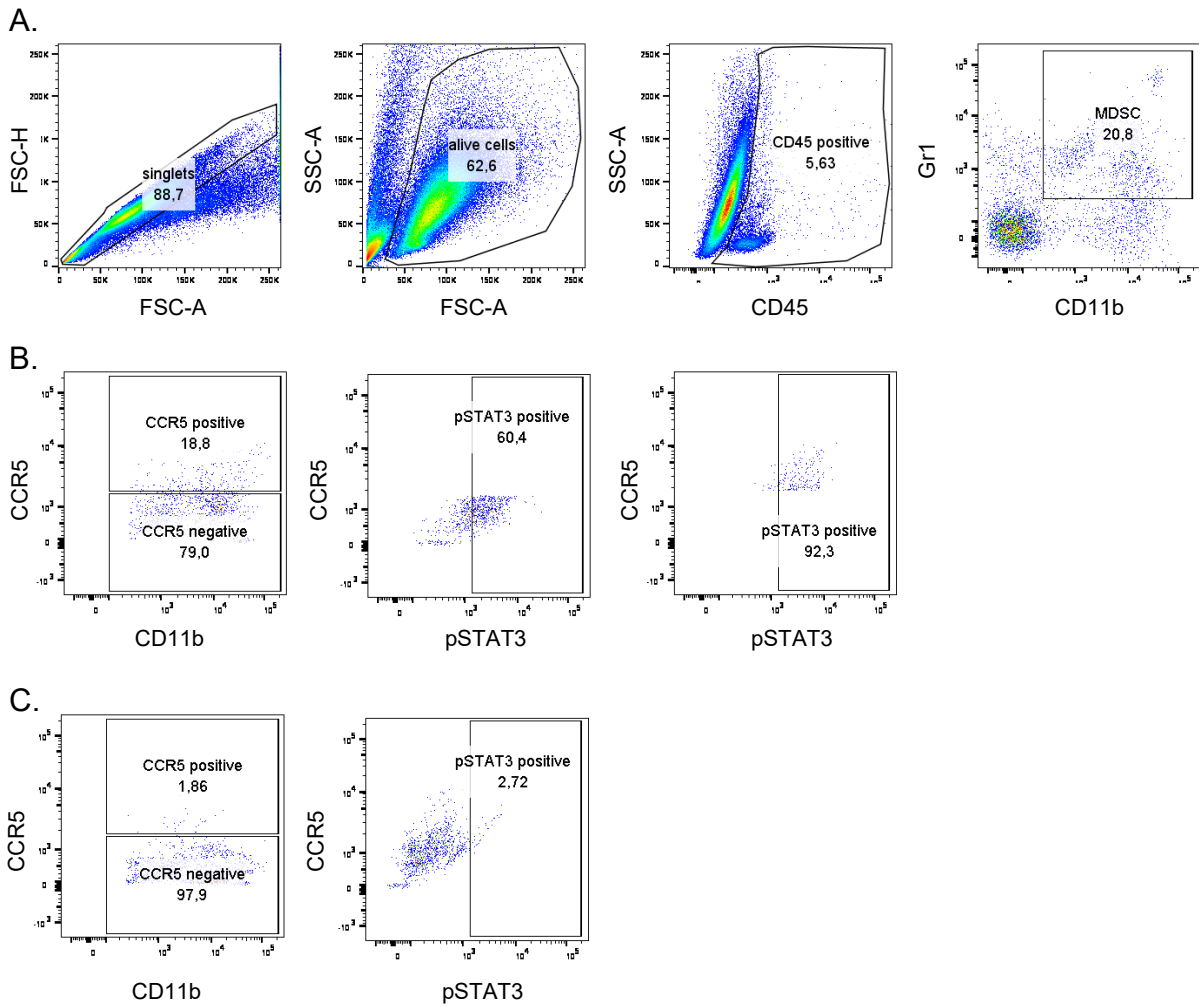

Supplementary Figure 1. Gating strategy for pSTAT3 in tumor-infiltrating MDSC.
Melanomas from *RET* transgenic mice were excised and single cell suspension was centrifuged over a Histopaque gradient for tumor-infiltrating leukocyte (TIL) enrichment. Enriched TIL were stained with fluorescently labelled antibodies and analyzed at the flow cytometer. A.) Duplets were excluded and alive cells were gated by excluding debris via FSC-A and SSC-A. As there was still contamination by tumor cells, $CD45^+$ cells were gated and then $CD11b^+Gr1^+$ MDSC. B.) After gating on $CCR5^+$ and $CCR5^-$ MDSC subpopulations, $pSTAT3^+$ cells were gated. C.) FMO control for CCR5 and isotype control for pSTAT3 on the $CD11b^+Gr1^+$ MDSC are shown. Gates were set according to the FMO and isotype control for CCR5 and pSTAT3.

GeneSymbol	GeneName	Fold change	Adjusted p-value
Cd207	CD207 antigen	0,09277142	0,0090757
Klk1b9	kallikrein 1-related peptidase b9	0,10763408	0,03202498
Itgae	integrin alpha E, epithelial-associated	0,11300339	0,00721917
Hepacam2	HEPACAM family member 2	0,11432416	0,0090757
Cd209a	CD209a antigen	0,1281702	0,00964232
Adam23	a disintegrin and metallopeptidase domain 23	0,13081433	0,00318537
Cd300e	CD300E molecule	0,13844189	0,01613617
Cd209c	CD209c antigen	0,14838281	0,01977314
Dscam	DS cell adhesion molecule	0,16198307	0,00752719
Sept3	septin 3	0,16684243	0,01157747
Ifi205	interferon activated gene 205	0,1721969	0,01777354
Trp53i11	transformation related protein 53 inducible protein 11	0,19478763	0,00374991
Adra2a	adrenergic receptor, alpha 2a	0,19735352	0,01261075
Rnase2a	ribonuclease, RNase A family, 2A (liver, eosinophil-derived neurotoxin)	0,20322047	0,00976968
Slc46a3	solute carrier family 46, member 3	0,20357997	0,00352665
Il2ra	interleukin 2 receptor, alpha chain	0,20374847	0,00721917
Tcea3	transcription elongation factor A (SII), 3	0,20496268	0,0090757
Hr	hairless	0,20759234	0,01007381
Aldh1a2	aldehyde dehydrogenase family 1, subfamily A2	0,2152803	0,0388911
Rtn1	reticulon 1	0,21884737	0,00721917
Mras	muscle and microspikes RAS	0,21991988	0,03604547
Gnb4	guanine nucleotide binding protein (G protein), beta 4	0,22323618	0,0117013
Slc27a3	solute carrier family 27 (fatty acid transporter), member 3	0,22423742	0,01329064
Adgrg6	adhesion G protein-coupled receptor G6	0,23082544	0,01407472
Serpinb6b	serine (or cysteine) peptidase inhibitor, clade B, member 6b	0,23171253	0,01872154
Fscn1	fascin actin-bundling protein 1	0,23283058	0,01729816
Mir155hg	Mir155 host gene (non-protein coding)	0,23613724	0,01129211
Nudt17	nudix (nucleoside diphosphate linked moiety X)-type motif 17	0,23910391	0,0303297
Strip2	striatin interacting protein 2	0,24274602	0,00976968
Gm11545	predicted gene 11545	0,24501129	0,00976968
Gfra2	glial cell line derived neurotrophic factor family receptor alpha 2	0,2452233	0,00916323
Aif1	allograft inflammatory factor 1	0,24562939	0,00981967
H2-Eb2	histocompatibility 2, class II antigen E beta2	0,24614721	0,03214069
Ciita	class II transactivator	0,2464158	0,00425583
Sema6d	sema domain, transmembrane domain (TM), and cytoplasmic domain, (semaphorin) 6D	0,2482481	0,00352665
Plek2	pleckstrin 2	0,2510835	0,03348868
Adgre4	adhesion G protein-coupled receptor E4	0,25452494	0,01389839

Dpp4	dipeptidylpeptidase 4	0,25699676	0,0090757
Lad1	ladinin	0,25707408	0,01714619
Tspan33	tetraspanin 33	0,25793593	0,01027859
P2ry10	purinergic receptor P2Y, G-protein coupled 10	0,2646965	0,01168719
Acot6	acyl-CoA thioesterase 6	0,26494547	0,010919
Asgr2	asialoglycoprotein receptor 2	0,26736763	0,01168719
Egfr	epidermal growth factor receptor	0,26876887	0,02611038
Nr4a3	nuclear receptor subfamily 4, group A, member 3	0,27076738	0,01060585
Cdh17	cadherin 17	0,27130759	0,00721917
Fndc5	fibronectin type III domain containing 5	0,27289362	0,02408874
Grap2	GRB2-related adaptor protein 2	0,27323249	0,01939392
Npr1	natriuretic peptide receptor 1	0,27655078	0,01977314
Fam49a	family with sequence similarity 49, member A	0,27779114	0,00932713
Myb	myeloblastosis oncogene	2,21957294	0,00880285
Nkg7	natural killer cell group 7 sequence	2,24289889	0,03400097
Aff2	AF4/FMR2 family, member 2	2,24467085	0,0181588
Rnf128	ring finger protein 128	2,24678214	0,01700318
Dnajc6	DnaJ heat shock protein family (Hsp40) member C6	2,24788081	0,02061768
Rgcc	regulator of cell cycle	2,2772347	0,02496048
Mpo	myeloperoxidase	2,28220706	0,00406529
Kcnk12	potassium channel, subfamily K, member 12	2,28521287	0,03446803
Mmp19	matrix metallopeptidase 19	2,30237846	0,03134275
Ms4a7	membrane-spanning 4-domains, subfamily A, member 7	2,31296578	0,00810542
Slc6a8	solute carrier family 6 (neurotransmitter transporter, creatine), member 8	2,32815002	0,0059042
Ms4a3	membrane-spanning 4-domains, subfamily A, member 3	2,33903177	0,0090757
Tm4sf19	transmembrane 4 L six family member 19	2,3698433	0,02641549
Prss57	protease, serine 57	2,38127809	0,04045276
Tfpi2	tissue factor pathway inhibitor 2	2,39366804	0,03231939
Igkc	immunoglobulin kappa constant	2,4237405	0,03374499
Ednrb	endothelin receptor type B	2,50934563	0,01700318
Plac8	placenta-specific 8	2,51340663	0,00976968
Gfi1	growth factor independent 1	2,55764797	0,01782451
Ada	adenosine deaminase	2,56458246	0,01119518
Eef1a2	eukaryotic translation elongation factor 1 alpha 2	2,58608237	0,0354977
Gria3	glutamate receptor, ionotropic, AMPA3 (alpha 3)	2,65206853	0,01168719
Prtn3	proteinase 3	2,67068385	0,01180423
Nxpe5	neurexophilin and PC-esterase domain family, member 5	2,69479547	0,0148192
Ctsg	cathepsin G	2,73450629	0,0121769

Ubash3a	ubiquitin associated and SH3 domain containing, A	2,73584345	0,02414497
Timp3	tissue inhibitor of metalloproteinase 3	2,75577213	0,01546694
Ctsl	cathepsin L	2,76116629	0,0050103
Gm5150	predicted gene 5150	2,76293206	0,03876117
Flrt2	fibronectin leucine rich transmembrane protein 2	2,78284875	0,04339092
Serpinb2	serine (or cysteine) peptidase inhibitor, clade B, member 2	2,79186329	0,02259377
Igf1	insulin-like growth factor 1	2,89634597	0,01721547
Serpina3b	serine (or cysteine) peptidase inhibitor, clade A, member 3B	2,9266742	0,04818576
Plppr3	phospholipid phosphatase related 3	3,03027057	0,010919
Ehd3	EH-domain containing 3	3,0967413	0,01427859
Fos	FBJ osteosarcoma oncogene	3,12458198	0,01811186
Muc13	mucin 13, epithelial transmembrane	3,37295894	0,0043277
Stfa2l1	stefin A2 like 1	3,53184149	0,0086817
Ly6a	lymphocyte antigen 6 complex, locus A	3,53556334	0,01977314
Glp1r	glucagon-like peptide 1 receptor	3,55142069	0,01237542
Ccl7	chemokine (C-C motif) ligand 7	3,60728012	0,01714619
BC117090	cDNA sequence BC1179090	4,05040566	0,0353952
Selp	selectin, platelet	4,57266064	0,00721917
Saa3	serum amyloid A 3	5,43252634	0,00721917
Pf4	platelet factor 4	5,60265676	0,00352665
Mmp13	matrix metallopeptidase 13	9,31119938	0,00352665
Stfa1	stefin A1	13,7955667	0,00721917
Stfa3	stefin A3	22,3030122	0,01367478
Ccl8	chemokine (C-C motif) ligand 8	23,2187417	0,01568624
Gm5416	predicted gene 5416	30,6179635	0,00444886

Supplementary Table 2. Differentially regulated genes between MDSC (IL-6, GM-CSF) and MDSC (GM-CSF).

The table shows the top 50 significantly down- and significantly upregulated genes (by fold change) in *in vitro* differentiated MDSC with IL-6 and GM-CSF for four days compared to MDSC differentiated by GM-CSF only by microarray analysis.